LA-UR-13-23269
Approved for public release; distribution is unlimited.

Title: Improving 6061-Al Grain Growth and Penetration across HIP-Bonded Clad Interfaces in Monolithic Fuel Plates: Initial Studies

Author(s): Hackenberg, Robert E.
McCabe, Rodney J.
Montalvo, Joel D.
Clarke, Kester D.
Dvornak, Matthew J.
Edwards, Randall L.
Crapps, Justin M.
Trujillo, R. Ralph
Aikin, Beverly
Vargas, Victor D.
Hollis, Kendall J.
Lienert, Thomas J.
Forsyth, Robert T.
Harada, Kiichi L.

Intended for: Report

Issued: 2013-05-06

Improving 6061-Al Grain Growth and Penetration across HIP-Bonded Clad Interfaces in Monolithic Fuel Plates: Initial Studies

Robert E. Hackenberg, Rodney J. McCabe, Joel D. Montalvo, Kester D. Clarke, Matthew J. Dvornak, Randall L. Edwards, Justin M. Crapps, Ralph R. Trujillo, Beverly Aikin, Victor D. Vargas, Kendall J. Hollis, Thomas J. Lienert, Robert T. Forsyth, and Kiichi L. Harada

Materials Technology: Metallurgy Group (MST-6)
Los Alamos National Laboratory

30 April 2013

Abstract

Grain penetration across aluminum-aluminum cladding interfaces in research reactor fuel plates is desirable and was obtained by a legacy roll-bonding process, which attained 20-80% grain penetration. Significant grain penetration in monolithic fuel plates produced by Hot Isostatic Press (HIP) fabrication processing is equally desirable but has yet to be attained. The goal of this study was to modify the 6061-Al in such a way as to promote a much greater extent of cross-interface grain penetration in monolithic fuel plates fabricated by the HIP process. This study documents the outcomes of several strategies attempted to attain this goal. The grain response was characterized using light optical microscopy (LOM) electron backscatter diffraction (EBSD) as a function of these prospective process modifications done to the aluminum prior to the HIP cycle. The strategies included (1) adding macroscopic gaps in the sandwiches to enhance Al flow, (2) adding engineering asperities to enhance Al flow, (3) adding stored energy (cold work), and (4) alternative cleaning and coating. Additionally, two aqueous cleaning methods were compared as baseline control conditions. The results of the preliminary scoping studies in all the categories are presented. In general, none of these approaches were able to obtain >10% grain penetration. Recommended future work includes further development of macroscopic grooving, transferred-arc cleaning, and combinations of these with one another and with other processes.

Outline

List of Symbols and Acronyms

Ac	Acetone
B&W	Babcock & Wilcox (Lynchburg, VA)
BB	Bead blasted
CR	Cold rolled
DI	Deionized (water)
DIC	Differential imaging contrast
EB	Electron beam
EBW	Electron beam welding
EBSD	Electron backscatter diffraction
ESD	Electro-spark deposition
FCC	Face-centered cubic
FEM	Finite-element modeling
GB	Grain Boundary
GTA	Gas-tungsten arc (welding)
HIP	Hot isostatic pressed
ID	Inner diameter (or identification)
INL	Idaho National Laboratory (Idaho Falls, ID)
IP	Isopropanol
IPF	Inverse pole figure
LANL	Los Alamos National Laboratory (Los Alamos, NM)
LOM	(Visible) light optical microscopy
OD	Outer diameter
RD	Rolling direction
SEM	Scanning electron microscopy
SB	Strongback
SW	Steel wool
TA	Transferred-arc (cleaning)
UG	Unique grain

1. INTRODUCTION

1.1. Purpose of this work

Grain penetration across aluminum cladding interfaces in research reactor fuel plates is desirable and was obtained by a legacy roll-bonding process, which attained 20-80% grain penetration[1]. Significant grain penetration in monolithic fuel plates produced by Hot Isostatic Press (HIP) fabrication processing is equally desirable but has yet to be attained. The monolithic fuel plate fabrication involves joining two 6061-Al plates to one another by HIPing. Hence, Al is bonding with Al.

The grain penetration is considered to result from the *growth* of Al grains (initially present or recrystallized) that originated from one of the Al mating surfaces. In a more general sense, this cross-interface penetration comes through the migration of the Al grain boundaries (GBs) irrespective of whether the individual grains undergo a net growth or shrinkage during the process.

The goal of this study was to modify the 6061-Al in such a way as to promote a much greater extent of cross-interface grain penetration in monolithic fuel plates fabricated by the HIP process.

Three baseline conditions were be examined as controls. These involved Al that was cleaned by one of three methods, but with the Al metal otherwise unaltered. These baseline results were be compared against process improvement results obtained after modifying the Al prior to the HIP cycle.

1.2. Background

The Al-Al cladding bond in plate-type fuels provides for primary containment of fission products and is therefore important in safety analyses. The amount of grain penetration observed across the Al-Al cladding interface in dispersion fuel plates fabricated by the roll bonding process has been a long-standing criteria used in manufacturing process qualification and periodic process inspection. The acceptance criteria for fuel plates manufactured by the roll bonding process varies from reactor to reactor, but in general, the metallurgical bonding requirement has historically been associated with the observation of anywhere from 20% to 80% grain penetration across the bond line length [1967erw], as determined by detailed light optical microscopy (LOM) examination of etched plate cross-sections that were rotated under polarized light illumination [2005ken]. These interface grain penetration levels are routinely achieved when proper Al cleaning procedures are followed and sufficient thickness reduction ratios are employed in the roll bonding process [1967erw, 1969erw, 2005 ken].

Monolithic fuels fabricated by the HIP bonding process have a significantly different thermomechanical history compared to roll-bonded dispersion fuels. Specifically, during HIP bonding there is no large-scale thickness reduction to drive recrystallization and grain growth, and metallurgical bonding occurs primarily via diffusion-mediated mechanisms such as creep.

[1] Historically, the term "grain growth" was used [1967erw, 1969erw, 2005ken]. In this report we use the more precise term "grain penetration," which recognizes the fact – observed for example in the bead blasting studies in [2011bur] and the present work – that grains can grow to larger sizes on both sides of the bonding interface without actually penetrating across the interface to give the desired metallurgical bonding.

As might be expected, preliminary characterization of the Al-Al clad interface in HIP bonded fuel plates has shown that substantially less interface grain penetration occurs compared to roll-bonded fuel plates[2]. In fact, the observed grain penetration is typically close to zero. However, it is expected that the amount of interface grain penetration observed in HIP bonded fuel plates can be improved by manipulating a number of process variables that have not yet been optimized or exploited. This is the goal of this research.

1.3. Scope of this work

LANL was tasked with fabricating a series of blank (i.e. no fuel or surrogate fuel) 6061 Al clad fuel plates using the existing LANL HIP process, and then doing detailed microstructural examinations of the Al-Al interfacial regions to quantitatively characterize the extent of grain penetration *across* the bond line length. This was conducted using LOM and electron backscatter diffraction (EBSD), with the latter being considered the gold standard, and LOM serving as a supplemental method, useful for the initial survey of large regions. Results obtained from examination of a long stretch of bond line length, in the range of 7–26 mm, constituted a reasonable statistical survey to support the conclusions drawn.

This work was divided into two major tasks:

A. **Baseline studies.** Two LANL-made HIP blanks, one with the LANL cleaning process and another with the Babcock & Wilcox (B&W) cleaning processes were characterized as controls for comparison with the outcomes of the process improvement studies. These are both aqueous cleaning methods. A third condition, involving minimal cleaning with a simple acetone + isopropanol wipe, was also examined.
B. **Process improvement studies.** A variety of LANL-made HIP blanks were subjected to prospective process modifications to increase the cross-interface grain penetration. Four general strategies were considered:
    1. Enhancing Al metal flow from engineered **macroscopic gaps.**
    2. Enhancing Al metal flow from **engineered asperities.**
    3. Enhancing Al recrystallization and grain growth from **stored energy** imparted prior to the HIP run.
    4. **Alternative cleaning and coating** of the Al.

These four strategies are summarized in Table 1.1, along with a listing of specific processes that were considered for each strategy.

Section 2 covers the experimental details common to both the baseline and the process improvement studies. Section 3 presents and discusses the results from the baseline studies. The rationale and experimental details particular to the various process improvement studies (Section 4) precede the results and discussion from the same, grouped by the four general strategies (Sections 5-8). General conclusions (Section 9), tables, figures, and several appendices follow.

[2] In addition, since there is no apparent recrystallization taking place in the HIP cycle, the Al grain size remains largely the same as what it was prior to the HIP cycle. In this study, the grain size remains 20-30 micron, which is a factor of ten or more lower than the 250-500 micron grain sizes evaluated a transverse section of a roll-bonded fuel plate [2005ken].

2. EXPERIMENTAL

2.1. Material

The material configuration in all studies was the simplest possible one: Al-on-Al sandwiches. There was no real or surrogate fuel, diffusion barrier, or other additional materials in these sandwiches. The same pedigree of commercially-procured 6061 Al sheet used in other ongoing LANL studies in the CONVERT program was used throughout. The as-received condition was the T651 temper, which is a solution anneal + quench + 1% stretch.

Several starting sheet thicknesses were available, ranging from 0.030″ to 0.090″ (30 to 90 mills = 0.762 to 2.286 mm). Blanks of Al were cut to size by one of three methods:

1. machined (in the case of 24″ long rectangular specimens),
2. electro-discharge machined out of the sheet (for circular specimens), or
3. sheared along orthogonal axes (for canless squares).

The specific details of the additional material processing (e.g., bead blasting, macroscopic grooving) will be described in Section 4.

2.2. Cleaning processes

After any processing of the Al (e.g., rolling, bead blasting) and before the vacuum-enclosing step, all Al specimens were cleaned. Except where the alternative transferred-arc (TA) cleaning or simple acetone + isopropanol wipe cleaning was used (this will be noted in due course), all cleaning of aluminum was done with one of two aqueous processes: LANL or B&W. All other materials in the vacuum enclosure (cans, lids, strongbacks, evacuation tube, etc.) were cleaned with a different process appropriate for these other metals (usually steel). These are summarized as follows.

2.2.1. LANL cleaning process for Al

1. 40% nitric acid plus 1% ammonium bifluoride: soak 1 minute at room temperature.
2. Rinse in deionized (DI) water.
3. Hot caustic etch (20% sodium hydroxide) for 30 seconds at 80ºC.
4. Rinse in DI water.
5. Desmut with 40% nitric acid plus 1% ammonium bifluoride for 1 minute at room temperature.
6. Rinse in DI water.
7. 40% nitric acid: soak 1 minute at room temperature.
8. Rinse in DI water.
9. Dry with clean compressed air or nitrogen.

2.2.2. B&W cleaning process for Al

1. The cladding material was degreased to remove any grease, grit, and dirt.
2. Roughening/abrading was done on the to-be-bonded surfaces of each cladding set using a coarse stainless steel wire brush.
3. Cladding sheets were cleaned with Proceco cleaning solution (0.5 gallon of Triton DF-16 detergent (Dow Chemical) mixed into 250 gallon of DI water), rinsed in hot DI water, then wiped with isopropyl alcohol until all dirt and debris were removed.

4. The cladding received an additional chemical cleaning step in a pickling solution made up of 32.5 gallon of nitric acid (70% concentration) and 4 gallon of hydrofluoric acid (49% concentration) in 130 gallon of DI water. This was followed by a hot water rinse.

Step 2 was omitted in this study, since the surface preparation was the main variable being examined.

2.2.3. Cleaning process for all other materials (mainly steel)

1. Ultrasonic clean in aqueous solution of Blue Gold degreaser for about 5 minutes at 60ºC.
2. Rinse in DI water.
3. Caustic etch of 10% sodium hydroxide for about 5 minutes at 70ºC.
4. Rinse in DI water.
5. If there is still rust, 10% sulfuric acid etch for about 30 seconds at room temperature.
6. Rinse in DI water.

2.3. Hermetically-sealed enclosures

One of the premises of the HIP process is that the parts to be consolidated are enclosed in an evacuated and hermetically-sealed enclosure. This allows the imposed hydrostatic pressure to work on the parts to its maximum effect since there is no counterpressure from entrapped gas inside the enclosure. There are a variety of ways of accomplishing the vacuum evacuation and seal. There were three types of hermetically sealed enclosures used in this study:

1. **Long Can –** canned in a long, pre-welded rectangular box approximately 24″ x 3″ x 1.6″,
2. **Round Can –** canned in a round deep-drawn cup, 3.875″ inner diameter and ~1.05″ inner height, with a round flat top lid, or
3. **Canless –** canless squares of Al, 3.75″ on a side, electron-beam welded (EBW'd) to one another.

Examples of these are given in Figures 2.1 and 2.2 (long can), 2.3 (round can), and 2.4 (canless). The long can is the same size as that used in related CONVERT-program studies at LANL in the [2011kat]. The round can is a more recent development, described in [2012cla]. The canless approach is likewise described elsewhere [2011bur, 2012cla]. The results of this work and other CONVERT-program studies at LANL did not give any indications that these three enclosure types yielded different bonding outcomes (when executed properly). So to first approximation they are interchangeable from a Al-Al bonding perspective.

Several Al-Al stack-ups (which for n Al layers provide n-1 bonding-pair sandwiches) were accommodated in each *canned* enclosure and were separated from one another by hardened steel strongbacks (SBs) 0.125″, 0.25″ or 0.375″ thick. The Al-Al and Al-SB interface planes were all parallel to one another. Strongbacks previously used in other LANL cans that remained sufficiently flat were re-used after being re-cleaned by the normal process (Section 2.2.3).

Either Neolube or molybdenum disulfide lubricant/parting agent was liberally applied to all surfaces of the strongbacks. The stackups of alternating Al and strongbacks fit snugly within the cans; any gaps were typically <0.025″; the largest gap was usually in the vertical direction (i.e., that of the stack-up thickness) and this did not exceed 0.1″.

The long can was made out of 304L stainless steel. The bottom plate and 4 sidewalls were first gas-tungsten-arc (GTA) welded together to form an open box. This subassembly and evacuation tube (about 36″ long, 0.125″ OD, 0.055″ ID) were cleaned. The evacuation tube was then GTA welded into the hole in the top end of the can. The weld seam forms the seal on the inside of the can.

After loading the sandwiches and strongbacks, the lid was GTA welded onto the subassembly[3]. The can was then evacuated with a scroll pump to a vacuum of ~50 micron Hg (at the gauge), which is equivalent to about 55-65 micron at positions internal to the can. It is simultaneously baked out at 315ºC. This combined pump + bake-out operation lasted at least one day and sometimes went as long as 3 or 4 days for reasons of operational convenience. A valve at the end of the tube was shut, after which the tube was crimped and welded shut at a point much closer to the can. The excess tube was then cut off. Small fins were welded on the outside of the can bottom to give the can better support for standing upright in the HIP chamber.

The round cans were made of 1018 steel. After loading the sandwiches and strongbacks, the can was evacuated inside an EBW chamber to a vacuum of 3×10^{-5} torr. During the same operation the round lid was electron-beam (EB) welded around its circumference to seal it shut. The process parameters were as follows: 110 kV, 12.0 mA, Sharp Focus + 10, 40″/minute travel speed, working distance = 14.75″.

The canless squares were likewise evacuated and EB welded shut inside the EBW chamber to similar vacuum levels as the round cans. This canless process is described in more detail by Burgardt et al. [2011bur, 2012cla]. A square weld pattern was imparted. The process parameters were as follows: 100 kV, 6.3 mA, Sharp Focus, 78″/minute travel speed, working distance = 13″.

Several canless sandwiches were stacked in a simple graphite crucible and were separated from each other by hardened steel strongbacks either 0.125″ or 0.25″ thick (including one at the very top, which were lubricated with molybdenum disulfide. This stacking sequence provided a similar configuration of deadweight mass to that in the canned enclosures. To get them to fit, about 0.25″ around the perimeter of the as-welded squares was sheared off, which left about 0.25″ or more remnant material outside the weld line.

2.4. Hot isostatic pressing

The primary HIP variables of temperature, hold time and cooling rate were held constant in this study. The HIP cycle was as follows: it was heated to 560ºC with simultaneous pressurizing with a gas, held for 90 minutes at a pressure of 15,000 psi, then free cooled to 300ºC and vented down to 60 psi.

For purposes of orienting the samples relative to the can, the “top or valve end” was the highest point the hermetically sealed enclosure in the HIP chamber (above the chamber floor); the

[3] Welding the lid imparted considerable heat to the entire can, as evidenced by it being warm to the touch 1-2 hours after completion of the weld. The effect of this pre-evacuation/pre-HIP heating on the sandwich microstructure may be important (e.g., annealing out the stored energy from Al process modifications). These potential effects were not further examined in this work but should be considered in the future.

"bottom or base end" is the surface on which the can sat at the bottom of the HIP chamber. The long cans sat upright in the HIP chamber; the top end was where the crimped and sealed valve end stuck out. The round cans and canless sandwiches sat squat.

The "top face"/"bottom face" designated the outer surface of the plates (when seen in plan view) that were closer/further away to the lid of the canned enclosures or, in the instance of the canless enclosures, that which was situated closer/further away to the top of the HIP chamber.

After removal from the HIP chamber the hermetically-sealed enclosures were cut open and the specimens separated from the container and strongbacks. Photographs were usually taken before and/or after the HIP cycle.

It should be noted that a single HIP cycle usually processed more than one hermetically sealed enclosure. Furthermore, each *canned* enclosure contained multiple sandwiches. Each *canless* enclosure constituted a self-contained sandwich in and of itself. The breakdown of HIP cycles, vacuum enclosures, surface modification methods, and Al-Al sandwich details are found in Tables 2.1 and 2.2. The listing is in chronological order.

The materials were not given a post-HIP heat treatment. Given the high temperature of the HIP cycle, the post-HIP Al microstructures are expected to be well-annealed, strain-free, equiaxed grains. Given the relatively slow cooling rate from 560ºC, we expect any second-phase particles that were fully or partially dissolved at 560ºC (dispersoids, precipitates) to re-precipitate out on cooling with a relatively coarse length scale, on the order of 0.1–1 micron

2.5. Metallographic preparation, imaging and analysis

2.5.1. Mounting, grinding, and polishing

Each metallographic specimen was assigned a unique job number in the LANL MST-6 Materials Characterization Team Database. Each specimen may contain one or more Al-Al bonding pairs, called sandwiches. All specimens were mounted in cross-section; specimens from orthogonal cross-sectional views were mounted. For specimens extracted from 24″ long-can plates, the standard nomenclature on location and cross-sectional view is shown in Figure 2.5.

The samples were mounted, usually in cross-section, using ten parts EPON 815C epoxy to one part diethylenetriamine and cured for at least 6 hours in a pressure vessel at 600-1,000 psi.

The first step was to grind the surface reasonably parallel starting with 320 grit. The process advanced through 400, 600 grit, and 800 grit. This could be done by hand or by an automated grinder/polisher. Depending on sample thickness, the time spent on each grit ranged from 5-second passes with 90° rotations and 30-second passes with 90° rotations. After completing 800 grit grinding, the sample was rinsed in water and wiped with a wet cotton ball.

The polishing process began with counter-rotation using 3 μm polycrystalline diamond suspension on a Struers MD-Mol cloth for 9 minute at 20 N with a lubricant of 75% DI water and 25% propylene glycol solution. This process was repeated in co-rotation. The sample was then rinsed in water and wiped with a wet cotton ball.

The second step in the polishing process began with counter-rotation using 1μm polycrystalline diamond suspension on a Struers MD-Mol cloth for 9 minutes at 15 N with a lubricant of 75% DI water and 25% propylene glycol solution. This process was repeated in co-rotation. The sample was then rinsed in water and wiped with a wet cotton ball.

For the final polishing step, counter-rotation was used with 1 μm polycrystalline diamond suspension on a Struers MD-Nap cloth for 9 minute at 20 N and used a lubricant of 75% DI water and 25% Propylene Glycol solution. This process was repeated in co-rotation. The sample was then rinsed in water and wiped with a wet cotton ball. A final rinse with isopropyl alcohol and blow dry concluded the grinding and polishing process.

Imaging by light optical microscopy (LOM) was done after etching in one of two ways. In the LOM results that follow, the regular etch is assumed unless stated otherwise.

2.5.2. Acid etch

The regular acid etch used the following etchants:

- Boss's Etchant: 100 mL DI H_2O, 10 mL HCl, 10 mL HF
- 6061 Aluminum Etchant: 85 mL DI H_2O, 10 mL H_2SO_4, 10 mL HF

The etching sequences were as follows:

- Step 1- Immerse sample and agitate in Boss's Etchant for about 20 seconds then rinse under running water. Use isopropanol alcohol under a blow dryer to remove any water markings.
- Step 2- Immerse sample and agitate in 6061 Aluminum Etchant for about 20 seconds then rinse under running water. Use isopropanol alcohol under a blow dryer to remove any water markings.
- Step 3- Immerse sample and agitate in Boss's Etchant for about 20 seconds then rinse under running water. Use isopropanol alcohol under a blow dryer to remove any water markings.

The specific immersion times were adjusted depending on the sample size.

2.5.3. New caustic etch

A new caustic etching approach was developed partway through this project. It provides a much clearer view of the microstructure than the regular acid etch. This consisted of electro-etching in 1% NaOH in water at 3-5 V for 15-60 seconds. This was sometimes preceded by immersion in the same solution (no current applied) for up to 10 minutes.

2.5.4. Electron backscatter diffraction

A subset of the LOM samples were examined by electron backscatter diffraction (EBSD). EBSD is a more accurate method of discerning whether grain penetration is taking place across the bond line interface. All scans were run on the metallographically polished surface (unetched) as described earlier. A large number of fields of view were taken, on the order of a few thousand microns (= a few mm).

EBSD was done using scanning electron microscopy (SEM). The SEM electron beam interacted with the sample surface tilted at 70 degrees to the beam, resulting in the formation of electron

backscatter patterns on a phosphor screen in close proximity to the sample. The instruments used were an FEI FEG XL30 (field emission gun SEM) and an FEI INSPECT-F30 FEG-SEM outfitted with EDAX/TSL OIM hardware and software. The scans were collected at 20 kV and a final aperture of 100 microns. The spot size was chosen to optimize the pattern intensity. Step sizes were typically 0.5–2.0 microns. A clean-up routine was applied to the raw data in order to remove spurious single data points.

The EBSD patterns were indexed to specific crystal orientations by the data collection software. The beam was rastered over a user defined area with a user-defined step size with the crystal orientation being determined at each raster point. The analytical software was used to calculate the texture (a representation of the distribution of all individual orientations) and to evaluate microstructure (grains, grain boundaries, defects, second phases, etc.) The texture was not of interest and was not reported here.

The microstructural features in this study that were actually measured by EBSD were the face-centered cubic (FCC)-Al grains and grain boundaries. (The intermetallic second phases which occur along the bond line were too small and/or not well-retained by the preparation to be measurable.) The grain structure was usually presented as a colored inverse pole figure (IPF) map where the colors represented the crystal direction in the direction normal to the plane of polish. The IPF maps here were correlated with crystal directions corresponding to the FCC-Al standard triangle (the standard triangle color-legend was the same for all IPF map as it is in Figure 3.2.)

Within the displayed IPFs, grains with the same color represent the same crystallographic normal of the grain with respect to the plane of polish but not necessarily the same absolute orientation, since similarly-colored grains have an additional degree of freedom in this software reconstruction: they are free to rotate about their common plane-of-polish-normal crystallographic direction. Grain boundaries (GBs) were established between grain triple points using a 5 degree minimum point-to-point misorientation criterion. They are displayed as thin black lines on IPF maps and the breaks in color on UG maps.

2.5.5. Presentation of LOM and EBSD images.

A large number of fields of view were imaged by both LOM and EBSD for each sandwich. A typical LOM series included up to 32 consecutive montage images at 100x or 200x, as well as a lesser number of 50x and 500x images. A typical EBSD series consisted of 15 consecutive maps that were about 1000 micron across.

The images presented through this report are samplings of this large image data set. Images in a given figure should not be construed to be consecutive montage images unless called out as such. As a general rule, the bond line passes through the center region of a given image. The bond line runs top-bottom in portrait-oriented images and it runs left-right in landscape-oriented images.

2.6. Criteria for grain penetration

Since observing grain penetration across the interface is the major goal of this characterization, it is important to explicitly call out the criteria for deciding whether a given bond line region exhibits grain penetration. For grains to be considered as candidates for grain penetration, they

had to be contiguous across the bond line, i.e., share a common segment of the bond line, at least as viewed in the 2D planes of polish in this work[4]. These will be termed "facing grains."

LOM was useful for this only insofar as it *indirectly* provided signs of grain penetration. The following are indicators of grain penetration:

1. GB contact angles with respect to the bond line were equal or nearly equal coming from the facing grains (i.e., parallel GB segments suggest the lack of an intervening GB within the bond line, on an interfacial force-balance argument).
2. The facing grains were noticeably larger near the bond line than in regions removed from the bond line (suggestive of grain growth).

Indicator #1 is somewhat more useful than indicator #2 since (as will be seen in Section 7.2), bead blasting gave a lot of grain growth without penetrating the bond line.

Quantification of LOM results was not done since assessment by LOM was very indirect (it provided no direct crystallographic orientation data), especially in the absence of polarized light imaging with a rotating stage [2005ken]. Furthermore, LOM imaging varied a lot depending on the intrinsic variability in surface preparation and appearance compared to EBSD.

As a general observation, all of the bond lines examined (baseline and process improvement) showed little indication of grain penetration by LOM. Indeed, in the vast majority of the hundreds of images taken in this work, it was quite obvious where the bond line was for the very reason that the grains did *not* penetrate. If success were to be obtained with penetration of most or all the grains, the initial bond line could likely fade from view or disappear entirely. There were suggestions of this 'fading from view' only in some regions of the TA+ESD sandwiches.

EBSD was considered the gold standard for such measurements. Ideally the definition of grain penetration is defined as:

1. the facing grains have the same orientation, and
2. the facing grains have no GB line between them.

Theoretically, these two statements are tautological; they say the same thing in different ways. They are listed separately to allow a clearer consideration of the issues with actual EBSD data.

Knowing whether facing grains have the same orientation (#1) is not as clear-cut in IPF maps as one would first imagine it to be. Two grains having a similar color is a necessary but not sufficient condition for a common grain orientation (the color only indicates parallelism of one direction, not all directions.)

This is where the demarcation of the GB lines (#2) by the EBSD software becomes important. Ideally, all the thin black lines in an IPF map are true grain boundaries that separate grains that differ in orientation by 5º or more. When looking at the contiguous, facing grains, a dark line between them on the bond line has a potentially ambiguous meaning:

- either a "true-positive" – it is a true grain boundary (in which case there is no grain penetration),

[4] Measurements in 3D would be ideal, since it would reveal grain connectivity outside the plane of polish. However, 3D methods are very time-consuming and only 2D measurements were justified in this scoping study.

- or a “false-positive” – it is break in the EBSD pattern not due to any GB but rather due to microscopic intermetallic particles, etch-pits, defects, or other irregularities at the bond line itself.

The false-positive result could happen even when the particles, etc. at the bond line are invisible in images of this magnification since these features they could still be sufficiently large to be detected by the EBSD scan, and, not being indexed as FCC, force the software to color these pixels black (meaning data that are indeterminate, bad, or non-FCC), which results in the same appearance as a GB line.

This ambiguity was dealt with by defining strict and loose practical definitions of grain penetration:

- strict: facing grains must satisfy #1 and #2 above, i.e., must have the same color and have no dark line between them.
- loose definition: facing grains must only satisfy #1 above, i.e., they only need to have the same color.

The loose definition was used for all analyses since the occurrence of these similarly-colored grains (#1) was so infrequent (usually 5% or less of the total bond length), observations of common color-orientation were assumed to be true grain penetrations (which assumed that any dark lines between the grains were false-positives). This give the most liberal estimate of grain penetration. **Unless stated otherwise, all grain penetration percent values discussed in these results are based on the loose definition.**

One standard deviation of this measurement based on the best judgment of the analyst (REH) is estimated to be about 2% absolute. (This implies that two measurements differing by less than 1.96 standard deviations = 4% absolute are not statistically significant on the basis of 95% confidence.) This is the error solely due to the analyst deciding which grains met the loose definition (above and beyond any upstream errors attributable to the EBSD software or specimen preparation). Due to the large number of images and conditions that were examined, this entailed a higher-than-ideal speed of ‘eyeball’ scanning that on occasion missed qualifying regions.

It should be recognized that a significant over-estimation of grain penetration could result from using the loose definition. In the few instances in this study where both strict and loose values were determined, the ratio of loose-to-strict ranged from 4 to 7.

In a few instances unique grain (UG) maps were also generated, which helped with the identification of grain penetration on the strict definition. Individual grains in UG maps were represented by individual non-specific colors. Such maps resolve the ambiguities in absolute orientation (#1) but would still suffer from bond-line irregularities (#2). Unlike the IPF maps, the color differences in UG maps did not indicate the relative difference in orientation between any pairs of grains.

3. RESULTS AND DISCUSSION – BASELINE STUDIES

3.1. Overview

Baseline studies were used to document the Al grain penetration response when no additional process modification steps were done to the Al. As controls, these Al-Al sandwiches were fabricated using the existing LANL fabrication process (i.e. as currently practiced, including Al stock material, cleaning, HIP can geometry, and HIP cycle.).

The importance of surface cleaning of the Al plates prior to bonding has been widely recognized. It is also known that B&W was using a substantially different cleaning procedure from that used at LANL (which furthermore is also different from that used by INL). The LANL cleaning was used prior to the start of this project in February 2012. At the request of INL, the B&W cleaning was provisionally designated as the new preferred cleaning process for the process improvement studies in this project.

Therefore, an apples-to-apples comparison of the B&W cleaning procedure against the LANL cleaning procedure was done. A third condition generated as a byproduct in this project also presented an opportunity, which was a superficial cleaning with common solvents. Therefore, three conditions were examined:

1. 24″ plates with the LANL cleaning (leftover specimens from HIP cycle 246)
2. 24″ plates with the B&W cleaning process (HIP cycle 254)
3. 3.875″ diameter discs with cleaned only by wiping them with acetone (Ac) and then isopropanol (IP) (HIP cycle 258)

The Al surface was not deliberately altered in any other way on either sandwich. Neither did they have any LEU-Mo or surrogate fuel inside the sandwich. All other known process parameters (e.g., HIP cycle) were held constant.

Results from these three baseline conditions will now be elaborated.

3.2. LANL cleaning

The LANL cleaning condition that was selected for interrogation came was run in HIP cycle 246, prior to initiation of this project. LOM was carried out on both the longitudinal and transverse cross-sections-1T1 from the base end (see Figure 2.5). A montage containing the bond line was generated from 32 fields taken at 200x. Each image was 450 microns wide, giving a total of 14,400 micron (14.4 mm) scanned. None of these areas showed evidence of cross-interface grain penetration. Some higher-magnification images were taken periodically; all these 500x micrographs confirmed the conclusions based on the 200x micrographs. Figure 3.1 shows representative images. The complete LOM and EBSD scans for the 1L orientation are captured in Appendix 1. This gives an idea of the length of bond line examined by both methods. (Note that we were unable to correlate specific points/featured on the LOM and EBSD scans.)

EBSD was then undertaken to get a more accurate assessment. A total of 27 fields of view were examined (split between two sections, 1yT1 and 1yL). Each image was 400 microns across, giving a total of 9,900 micron (9.9 mm). Figure 3.2 gives an example of a regions with a somewhat higher-than-average grain penetration. The IPF map (left side) gave numerous areas in this and other images, with 6.0% grain penetration on the loose definition. Only two regions

were found showing penetration on the strict definition; one of these is boxed in the UG map shown on the right side. The total grain penetration on the strict definition came to a much lower value, 0.08%.

These results confirm more definitively the prior understanding that HIP'd Al-Al bonding surfaces experience grain penetrations that range from small (loose definition) to negligible (strict definition.)

3.3. B&W cleaning

The B&W cleaning specimens were selected from the long can run in HIP cycle 254 run as part of this project. EBSD was run on specimens taken from the center of the plate (2L and 2T1 positions; see Figure 2.5).

Grain penetration on the loose definition was 7.9%, which was based on 20 images (2T1 orientation) totaling 19.8 mm in length.

Grain penetration on the strict definition totaled 1.84%, which was derived from 18 images (2L orientation). About half of the 18 images looked similar to the three shown in Figure 3.3, with a small amount of grain penetration. The other images showed no grain penetration.

3.4. Acetone + isopropanol cleaning

These regions were from areas A, B, and C in the TA-ESD discs (HIP run 258, Figures 3.4-3.5) that were far removed from the roughly-square patches altered by the TA-ESD treatment. The only cleaning these regions experienced was a manual wiping with acetone and then isopropanol to remove any residue remaining on the sheared Al discs. Otherwise, the bonding configuration was bare Al contacting bare Al, with milling lines, scratches and all else intact.

Only region 12718-B was examined and selected EBSD results are in Figure 3.6. A total of 3.1% of the 15.6 mm of bond line length surveyed showed grain penetration (loose definition).

3.5. Baseline studies – discussion

Overall, grain penetrations were somewhat higher for the B&W cleaned condition than for the LANL cleaned condition, though they probably are not statistically significant. Still, this does indicate that at a minimum, the B&W cleaning generates as good or better results vs. the LANL cleaning. It can be said with somewhat greater confidence that both LANL and B&W cleanings give better outcomes than a simple acetone+isopropanol wipe of the surface.

The foregoing show that neither the LANL nor the B&W cleaning process by itself is sufficient to promote grain penetration. At best, these processes remove second phase impediments to grain penetration and thereby are enablers for success engendered by more deliberate process modifications. Having said that, there is no direct evidence at present to support the supposition that cleaning actually removes second phase particles.

4. PROCESS IMPROVEMENT STUDIES – OVERVIEW AND EXPERIMENTAL

4.1. Rationale

Given the small if practically nonexistent amounts of grain penetration observed in both baseline conditions, process improvement studies were undertaken. The technical rationale will be presently described.

There are two driving forces for grain boundary (GB) migration that would assist in obtaining cross-interface grain penetration:

1. reduction of interfacial area and energy (the local driving force is proportional to the local curvature of the GB segment)
2. relief of energy stored as remnant elastic and plastic deformation (released during recovery and/or recrystallization processes)

The first of these provides very little driving force in the conditions being examined, and represents conventional grain coarsening. Hence there is the necessity of augmenting the driving force with the second of these, stored energy in the microstructure.

Stored energy can be imparted prior to the HIP process (cold rolling, bead blasting), or activated during the HIP process by geometric modifications that promoting metal flow under HIP conditions (grooving, knurling, steel wool abrasion).

The restraining forces for GB migration include at least these three factors:

1. dissolved solute that segregates and slows any GB that tries to migrate (solute drag)
2. particles that pin grain boundaries (Zener pinning)
3. surface oxide that prevents the facing metal grains from touching to begin with.

Adding a cleaner interlayer would help reduce solute drag. Better cleaning might reduce the interfacial particles and their pinning in addition to possibly removing some of the oxide. Finally, engineered asperities (knurling, steel wool abrasion) would allow pre-existing oxide layers to be scraped off as the metal flows during the HIP cycle. All three

The experimental matrix focused was on process modifications that covered as many of the scientific issues mentioned above while also being practical and economical in a production environment. A diversity of overall strategies and particular processes (Table 1.1) were pursued.

All enclosure types were employed: large can, round can, and canless. This was done for practical reasons since the time and expense of preparing the latter two types of enclosures were lower than those of the large can. Except in instances where the Al cleaning was done by transferred-arc (TA) cleaning, all surface cleaning for the process improvement work used the B&W process; the LANL cleaning process and Ac + IP wiping were not employed further.

All four strategies in Table 1.1 were considered and investigated, as described below. (The experimental runs, results and discussion for each will be given in Sections 5, 6, 7, and 8.)

4.2. Macroscopic gaps

In the first strategy, it is desirable to increase the deformation occurring at/near the bond line during HIP bonding through the use of macroscopic gaps.

One approach is to engineer large-scale gaps in the HIP can itself, which gives room for the Al sandwich to squeeze out into. This would allow in-situ thickness reductions of the Al. This would most likely require redesign of the canned enclosure itself, as the currently used long can has substantial rigidity that would have to be modified, probably in the direction of less rigidity.

The simpler approach undertaken here was to focus on engineering macroscopic features in the Al plates themselves, while leaving the long can and strongback configuration the same.

Machining macroscopic, rectangular grooves in the Al plates was the strategy selected. A variety of trial designs were run through finite-element modeling (FEM) simulations to arrive at promising combinations of groove depths and widths. The FEM modeling process and results are captured in Appendix 2. Practical designs which showed the most shear strain (as calculated from the relative displacements of the mating surfaces) were pursued. The three sandwich designs all had a grooved plate overlaid on a flat plate. The three grooved designs are shown in Figure 4.1.

The longitudinal axes of the plates (24″ length) were the same the rolling direction during manufacture. Grooves running the entire longitudinal direction were machined. The grooved plates used in sandwiches 1, 2, and 3 are shown in Figure 4.2.

Running from top to bottom, the stacking sequence of Al-Al sandwiches and steel strongbacks (SBs) in the long can (and Characterization job #s 12xxx) were as follows:

- Top of can (lid cover GTA welded on after loading the can)
- SB 5
- Sandwich 2.1a4 – flat / flat – job 12701
- SB 4
- Sandwich 2.1a3 – flat / grooved (10 mil deep, 15 mil wide) – job 12700
- SB 3
- Sandwich 2.1a2 – flat / grooved (10 mil deep, 10 mil wide) – job 12699
- SB 2
- Sandwich 2.1a1 – flat / grooved (5 mil deep, 15 mil wide) – job 12698
- SB 1
- Bottom of can (cover pre-welded to the 4 sides and tube)

The grooved plates in sandwiches 2.1a1, 2.1a2, and 2.1a3 were situated on the bottom with its flat counterpart situated on the top. We did not expect a substantially different loading response from the interior sandwiches (2.1a2 and 2.1a3) relative to the sandwiches closest to the bottom and top of the can (sandwiches 2.1a1 and 2.1a4).

Sandwich 4, the baseline B&W cleaned condition was reported in Section 3.3. Sandwiches 1, 2, and 3 contain progressively wider and deeper grooves and will be reported in Section 5.

4.3. Engineered asperities

In the second strategy, it is desirable to promote a large amount of highly localized shear deformation across the bond line (even in the presence of the quasi-uniaxial loading provided by the HIP can with strongback configuration) by modifying the surface geometry. Specifically,

the goal is to generate a significant number of engineered asperities that undergo intense shear as they are squeezed together during the HIP cycle. This material flow scrapes off or at least thin the native oxide, surface debris, and second phase particles – exposing more fresh metal – while at the same time generating stored energy that might assist recrystallization and grain growth across the interface (a dynamic but admittedly short-lived process at the 560ºC HIP temperature). This strategy can be implemented on a microscopic or macroscopic scale, as will be discussed presently.

4.3.1. Knurling

Macroscopic asperities could be achieved by machining patterns in the plate surfaces, knurling, engraving, laser sculpting, or coarse sanding. Engraving and laser sculpting are more involved than the present study would allow. In earlier work, Lienert [2011bur] tried coarse sanding with 180 grit paper and found no effect on the grain penetration, so this approach was not pursued further. Machining patterns was not explored but offers a lot of possibilities, especially in combination with optimization by FEM. Because of its relative simplicity, **knurling was the approach taken to alter macroscopic asperities**. A relatively coarse pattern was imparted (Figure 4.3). The plate tended to curl during the processing. When the opposite side was knurled, most of the curl went away. This behavior is promising in the sense that it indicated that residual stresses and stored energy were imparted. For producing flat, reproducible plates in a production environment, this warpage might turn out to be more problematic. The knurling specifics are as follows:

- The knurling tool had single set of parallel grooves. So two passes per line were needed to create a diagonal tread pattern .
- Depth ≈ 20 mil = 0.5 mm.
- Spacing = 67 mil = 1.7 mm.
- The tread pattern lines were angled about 60 degrees off the direction of travel.
- The pressure applied by the machinist's manual downforce on the lever of the mill was moderate to heavy.

Although the plate was supported during knurling, it deflected down beneath the local tread line when the knurling tool pressure was removed. The deflection extended to the entire plate in proportion to the fraction of the plate area that had been knurled at any given point in time.

The deflection Δz was about 6 mm when only one side was knurled; relaxed to <0.5 mm after both sides were treated. The opposite side had ~85% coverage; the machinist did only what was needed to reflatten the plates. Therefore, the knurling of the opposite faces involved considerable flattening pressure (from the mill's lever arm) on the knurled faces that will be bonded together.

4.3.2. Steel wool abrasion

Microscopic asperities could include methods such as severe etching (for grain relief), wire brushing, or rubbing with steel wool. Severe etching would require some amount of trial and error and has the downside of generating more contaminants (e.g., re-depositing and hence concentrating the unhelpful insoluble second phase particles in the Al). Wire brushing suffers from the issues of cross-contamination. Roll bonding experience with other materials at LANL indicated that improved bonds were realized with steel wool rubbing or wire brushing.

Rubbing with steel wool (grade 0) was the approach taken to create the microscopic asperities. Rubbing was done back and forth along only a single axis, the rolling direction of the as-received plate. The rubbing was done until the side was fully burnished. The metal surface developed a hazy sheen after all visible artifacts (scratches, etc.) of the original surface had been rubbed away or otherwise obscured. Each face required a few minutes of rubbing.

4.4. Stored energy

In a third strategy, it is desirable to increase the amount of stored energy in the form of cold work within the plates prior to HIP. Stored energy as a result of deformation provides the driving force for recrystallization and grain growth. The energy can be stored either locally at the mating surfaces of the plates (e.g. by laser or shot peening, grit blasting, etc.), or in the bulk of the Al, for example, when it is in a heavily cold worked condition.

4.4.1. Bead blasting

Earlier work by Lienert [2011bur] showed that bead blasting gave the most promising results, as the Al grains grew larger in the vicinity of the interface, even though they did not cross the bond line itself. Lienert noted that the Al plates noticeably bent during the bead blast, which testifies to the significant amount of stored energy in the material. Similar bending behavior was observed when thin (31 mil thick) Al plates were used.

Bead blasting was carried out with the following parameters:

- equipment = Zero Blast-N-Peen
- pressure = 80 psi
- flow rate = constant
- bead size = very fine, about a few mills
- angle of impact = either 90º (head-on) or 45^{o}
- travel direction = up and down 3 times
- travel speed = constant (~30 seconds each side)
- The deflection Δz was about 2 mm when only one side was blasted; this relaxed to <0.2 mm after both sides had been blasted.

The geometry of deflection is depicted in Figure 4.4.

4.4.2. Cold rolling

Cold working was also pursued. Al sheet 87 mil initial thickness was cold rolled down to 32 mil thickness, a 63% reduction, over a number of passes but with no annealing between passes.

4.5. Alternative cleaning and coating

Alternative surface cleaning treatments (including chemical, electrical, plasma methods, etc.) were also considered. These can potentially reduce the continuity, thickness or growth rate of the native oxide layer that is present on the Al surfaces prior to HIP. Two of these were examined: transferred-arc (TA) cleaning, and TA cleaning in combination with electro-spark deposition (ESD) of a pure Al layer. Previous work has shown that TA removes a significant amount of oxide layer thickness and other surface debris. The addition of ESD of Al further minimizes the potentially inhibiting role of second phase particles, particularly those large

dispersoids and precipitates that reduce the metal-metal contact area as well as pin grain boundary (GB) lines, triple junctions, and corners.

The preliminary work used 4″ squares for the bonding surfaces. It was carried out in an argon environment. Prior to treatment, each sample was wiped with acetone and then wiped by isopropanol. Only the top half of each square was altered by TA+ESD (which were the bond mating surfaces). Two sandwiches were prepared as follows:

- Sandwich 2.4a1 (Figure 4.5). The top half of each square was TA cleaned only, while the bottom half continued arcing until roughened .
- Sandwich 2.4a2 (Figure 4.6). The top half of each square has ESD deposition of 99.5+% Al onto the Al sheet at 100 microF. The top strip used 50V, the middle strip used 100V, and the bottom strip used 150V. The bottom half was left untreated.

These preliminary canless squares did not survive handling to the point of being HIP'd, so no further results on these will be discussed.

Later on, a second attempt was made with somewhat different geometry. Circular specimens meant for round HIP cans were subjected to TA+ESD treatments in localized areas according to the scheme shown in Figures 3.4 and 3.5 and detailed in Table 4.1. Due to time and funding limitations only regions B and E of the argon-processed sandwich were characterized.

4.6. Process improvement studies – preliminary work

As a control, the B&W cleaning process was exclusively used to clean the Al in the process improvement studies; the LANL cleaning process was not used. Neither of these aqueous cleaning processes were used in instances where the cleaning was done by transferred-arc (TA) cleaning.

The initial survey of a number of these strategies relied on canless HIP squares. All of these failed to give the desired bonding (see bottom of Tables 2.1 and 2.2). Three of the 8 sandwiches failed before they made it into the HIP:

- One of these (knurled parallel) did not weld correctly based on visual inspection. The fact that the knurling pattern overlapped on the weld line did not help, which is an item to note for the future.
- Two of these (TA cleaned, ESD) snapped open when their remnant edge sections (well removed of the weld line) were deliberately sheared off to reduce their size, indicating the weld did not have sufficient strength (assuming it was leaktight to begin with).

Another one of these (bead blast, head-on) obviously failed during the HIP cycle, as it puffed up like a pillow.

Of the four remaining canless squares that appeared intact after the HIP cycle (Figure 2.4), none of them bonded correctly, as seen by LOM in Figure 4.7. The mating surfaces failed to touch and bond, presumably because they contained residual gas that prevented their collapse into one another during the HIP cycle. The EBW process had not been fully optimized at this point in the program, so a failure to create sound welds is the most probable root cause that could result in one or more of the following secondary causes of failure:

1. the weld was leaktight but had entrapped gases,

2. the weld was leaktight to begin with but was punctured during the shearing, or
3. the weld was not leaktight to begin with.

An alternative or contributing cause could include the B&W cleaning process (which might evolve trapped hydrogen), but this is considered more of a long-shot hypothesis in the absence of more direct evidence. Ultrasonic scans (not reported here) on these sandwiches were consistent with these outcomes. Since these early trials of the EBW process, the process has been improved, as evidenced by success in other projects in this program.

Of the process modifications that failed in this first attempt, all were retried with the exception of knurling. The results and discussion from the process developments were successfully sealed and HIP'd follow in Sections 5, 6, 7, and 8.

For ease of reference, Table 4.2 provides a succinct summary of the % grain penetration results for the various baseline and process improvement conditions examined.

5. RESULTS AND DISCUSSION – MACROSCOPIC GAPS

EBSD scans along the bondline from the dead center (2L) of all 3 macroscopically grooved sandwiches revealed 5-9% grain penetration (loose definition). The specific values are as follows:

- 5.2% for sandwich 2.1a1 (5 mil deep, 15 mil wide grooves)
- 8.9% for sandwich 2.1a2 (10 mil deep, 10 mil wide grooves)
- 4.9% for sandwich 2.1a3 (10 mil deep, 15 mil wide grooves)

These data indicate that the 10 mil deep grooves were more effective at promoting grain penetration than the shallower 5 mil deep grooves.

Figure 5.1 shows representative fields of view from all three sandwiches. Figure 5.2 shows the complete image series from sandwich 2.1a1. The other two sandwiches looked similar in this orientation.

Figure 5.3 shows the transverse 2T1 orientation. The two images shown are where the bond line direction changes abruptly. These are most likely the regions near the corners of the original grooves. What is interesting is that even in this region where the shear stresses and other local forces would be at their maximum, the grain size and penetration changed little; they merely rotated without changing shape (i.e., they preserved their aspect ratio with respect to the local orientation of the bond line.)

Given that these grain penetration values are comparable to that of the baseline B&W cleaning by itself (7.9%) and that the grains did not penetrate any differently in the regions of maximum stress, the conclusion for the present time is that macroscopic grooving is ineffective or only marginally effective in promoting grain penetration.

6. RESULTS AND DISCUSSION – ENGINEERED ASPERITIES

6.1. Knurling

The canless sandwich representing the initial attempts at engineering asperities by knurling and steel wool rubbing failed to bond, probably due to their welds not being leaktight (Figures 2.4b and 4.5).

Knurling is a more involved process requiring more time and expert judgment to get right. Due to the time constraints in this phase of the project, knurling was not pursued further. However, there is no technical reason known at the present time to rule this out as a viable option.

6.2. Steel wool abrasion

A steel wool / steel wool sandwich was prepared successfully with a round can (sandwich 3a1), but was not characterized due to time and funding limitations. The steel wool / bead blasted sandwiches (3b2b and 3c2b) were examined and are presented in Section 7.5.

7. RESULTS AND DISCUSSION – STORED ENERGY

7.1. Overview

The canless sandwich representing the initial attempt at imparting stored energy by bead blasting failed to bond, probably due to it not being leaktight (Figure 4.7).

The bead blasting and cold rolling strategies were tested again with round cans. A number of bonding combinations were tried, and 75% of these characterized by EBSD. Each stack-up in the round HIP cans consisted of 3 Al plates = 2 bonding pairs. Figure 7.1 shows typical low-magnification cross-section images of one of these configurations. The differing appearances in this example are due solely to the as-polished (unetched) vs. acid-etched preparation; the underlying microstructure looks the same from these orthogonal directions.

The following nomenclature will be used throughout:

- BB90 = bead blasted at a 90 degree angle to surface (i.e., head-on impact)
- BB45 = bead blasted at a 45 degree angle
- CR in plane = cold rolled, RD in the plane of polish
- CR normal = cold rolled, RD normal to the plane of polish
- SW = abraded with steel wool

The specific bonding combinations will now be considered in turn.

7.2. Cold rolling

Two CR/CR sandwiches were run in the HIP: with rolling directions (RD) oriented perpendicular (sandwich 3b1a) and parallel (sandwich 3c1a). The RD orientation did not alter the LOM results, so only microstructures from the perpendicular RD orientation (sandwich 3b1a) will be shown.

Figure 7.2 shows the as-polished condition. This reveals inclusion content instead of grain structure. The continuity of the matrix phase (light blue) across the bond line is seen: this is a necessary but not sufficient condition for good bonding. The etched microstructures (Figure 7.3)

reveal the grain structure. In several places the grains appear to penetrate the bond line (black arrows), but this was not widespread. EBSD (Figure 7.4) confirms these results that indicate only sporadic cross-interface penetration (boxes): the amount was 3.6%. Some fields of view such as Figure 7.4c showed no such regions.

7.3. Hybrid sandwich: bead blasting / cold rolling

Several hybrid sandwiches were run, which examined the effect of bonding two dissimilarly-processed surfaces. The first of these was a BB (90º)/CR sandwich (3b1b). Figure 7.5 shows the as-polished LOM condition, which is comparable to the CR/CR images (Figure 7.2), though with slightly more inclusion content. The greater local waviness of the bond line could be attributed to the bead blasting process. The etched images (Figure 7.6) showed less apparent bond line grain penetration than in the CR/CR sandwich. The EBSD results (Figure 7.7) confirm these findings, with only 2.4% of cross-interface grain penetration.

7.4. Bead blasting

Two BB/BB sandwiches were run:

- BB (90º)/BB (90º) – sandwich 3b2a
- BB (45º)/BB (45º) – sandwich 3c2a

Recall that the angle is with respect to the plate surface, so 90º means head-on impact by the beads. Both of these gave similar outcomes.

The BB90/BB90 sandwich showed some occasional signs of grain penetration that could be seen by LOM (Figure 7.8) following the caustic etch. A large number of oversize grains in the immediate vicinity of the bond line were found. EBSD results (Figure 7.9) confirmed these findings. The larger grains had the same appearance as the bead blasted bonding interfaces examined in earlier work in this program [2011bur]. There were also a number of finer grains, which are best seen in the magnified EBSD images (Figure 7.10). They could have arisen from recrystallization of the surface regions that were most intensely cold-worked by bead blasting. Although both the oversize and fine grains contributed to the 4.2% grain penetration, the fine grains may have contributed more to the total percent.

The B45/BB45 sandwich showed similar results (Figures 7.11-7.12) as the BB90/BB90 sandwich and gave 2.9% grain penetration. It is interesting that large portions of the bond line in the BB/BB sandwiches did not resolve by EBSD (hence, rendered as black) and also showed gaps in the LOM. This suggests a higher than normal level of intermetallics at the interface, which would preferentially dissolve (explaining the LOM results) or not be indexed as FCC (explaining the EBSD results). The contamination from the bead blasting could be responsible for this, either via direct transfer of the bead material to the Al, or transfer by cross-contamination of foreign matter picked up by the beads in prior use of the bead blasting equipment. The observation that smaller though noticeable bond line areas are black in the sandwiches where only one face was bead blasted (see Section 7.5) lends some credence to this hypothesis.

7.5. Hybrid sandwich: bead blasting / steel wool

Bead blasting in combination with steel wool rubbing gave the same behavior as the BB/BB sandwiches on the side of the bond that had experienced BB, but not the other side that saw SW rubbing. The BB90/SW outcome was 1.5% grain penetration and is in Figures 7.13-7.14. The BB45/SW outcome was higher at 4.5% grain penetration and is in Figures 7.15-7.16. These results are just on the threshold of statistical significance.

8. ALTERNATIVE CLEANING

An alternative cleaning and surface preparation method was examined, based on transferred-arc (TA) cleaning, which was combined with subsequent electro-spark deposition (ESD) of a thin layer of Al. This was done in LANL's plasma-spray unit, which is being used for other efforts in the larger program. TA cleaning is known to remove a large amount of surface contamination and probably the second-phase particles that are thought to hinder grain growth. So this was tried out in lieu of the LANL or B&W aqueous cleaning processes. The ESD Al is purer than the base metal, which can furthermore promote grain penetration since fewer growth-inhibiting impurities are present.

The initial attempt to examine this cleaning method did not succeed because of the problems with the leaktightness of the canless square sandwiches (sandwiches 2.4a1 and 2.4a2). A second effort to test TA+ESD processing was done successfully with round HIP cans. Bonding sandwiches were prepared in both argon and nitrogen atmospheres according to the schemes in Figures 3.4 and 3.5, respectively. The specific conditions for each of the regions (A-I) are in Table 4.1.

Due to time and funding constraints, only regions B and E in both TA+ESD sandwiches were characterized. Neither of the surfaces in region B were altered by TA+ESD; they only saw the acetone + isopropanol cleaning and the results were described in Section 3.4 (Figure 3.6). Region E represented the condition of two TA+ESD surfaces contacting one another (100 volt condition)

Figures 8.1 and 8.2 show representative LOM images for the argon-processed and nitrogen-processed sandwiches, respectively. The images run in sequence but are not a montage series.

These LOM images show regions of Al deposition up to 50 micron thick, though 20-30 micron was more typical. The Al deposition regions are only partly-connected. The grain structure of the deposited Al was not well revealed by etching response, and the black regions are not well characterized (e.g., bona fide voids vs. regions formerly inhabited by intermetallics). In light of these issues, conclusions could not be drawn on the efficacy of cross-interface grain penetration from LOM by itself.

EBSD was done on the argon-processed sandwich with selected results in Figure 8.3. Only a few of the regions (of the 15 total surveyed by EBSD) showed the enlarged grains suggestive of Al deposits and these are what are displayed. Regions where the bond line appears to split into two are boxed in. Such regions were counted as cross-interface penetration, giving a total of 2.6% (counted over all 15 images) or 10.7% (if only the three images shown in Figure 8.3 are used in the statistics). Cross-interface penetration in the regions not having notably oversized

grains (the tops of all three images) was not apparent. These results suggest that the ESD Al grains grow to large sizes and presumably bond well with the original 6061-Al surfaces. The problem in the present results is that the ESD Al grain coverage was incomplete. One could envision further TA-ESD process development that would improve ESD Al grain coverage. This should prompt further consideration of what is our working definition of cross-interface penetration when an interlayer of Al is present. For example, the bond line splits and soon becomes hard to recognize in the bottom half of Figure 8.3c; this appears to be a sign of the good bonding that is desired.

9. CONCLUSIONS

1. A new caustic etch provided better LOM imaging than a traditional combination acid etch.
2. EBSD continues to be a useful way of measuring the cross-interface grain penetration at Al-Al bondlines. It was used to examine 7–26 mm lengths of bond line in a variety of sandwiches.
3. Baseline (cleaning only) and process improvement bonding sandwiches all exhibited <10% grain penetration, on a loose definition. These values are far away from the 20–80% grain penetration that is desired. Most of the differences among specific methods are not statistically significant.
4. For the baseline studies, cleaning Al with the B&W method resulted in marginal improvements in cross-interface grain penetration relative to the LANL method used for LANL HIP studies up until the present time. Both were better than a simple wiping with acetone and isopropanol.
5. The best process improvement outcomes came from macroscopic grooving (5-15 mil depth and width).
6. Other process improvement work did not show any improvement vs. the LANL or B&W cleaning:
    a. imparting stored energy (cold rolling, bead blasting),
    b. creating engineering asperities (steel wool rubbing), and
    c. transferred-arc cleaning with electro-spark deposition.
7. Of these other process developments, the TA+ESD was the least mature, and provides the most room for future improvement. Macroscopic grooving, giving good results, also presents opportunities for further development.
8. Other combinations of multiple processes, including processes considered but not tested, present additional opportunities for future work.

ACKNOWLEDGEMENTS

We thank Dave Alexander, Tim Beard, Don Bucholz, Paul Burgardt, Carl Cross, Dave Dombrowski, Andy Duffield, Bob Field, Nate Mara, Deb Summa, and Richard Weinberg for assistance during this work. The authors would like to acknowledge the financial support of the US Department of Energy Global Threat Reduction Initiative Reactor Convert program. Los Alamos National Laboratory is operated by Los Alamos National Security, LLC, for the National Nuclear Security Administration of the U.S. Department of Energy under contract DE-AC52-06NA25396.

REFERENCES

1967erw J.H. Erwin, "Bonding of Type 1100 to Type 6061 Aluminum," Oak Ridge National Laboratory report ORNL-4170, "Metals and Ceramics Division Annual Progress Report for Period Ending June 30, 1967," pp. 179-181, (November 1967).

1969erw J.H. Erwin, "Roll Bonding of Unclad 6061 Aluminum," Oak Ridge National Laboratory report ORNL-4470, "Metals and Ceramics Division Annual Progress Report for Period Ending June 30, 1969," p. 122, (October 1969).

2005ken E.A. Kenik, T.J. Huxford, J.R. Mayotte, T.S. Nedkova, and J.D. Sease, "Evaluation of Grain Growth and Bonding in Roll Bonded Aluminum Alloy Plates," *Microscopy and Microanalysis* **11**, Suppl. 2, pp. 1840-1841 (2005).

2011bur P. Burgardt, K.D. Clarke, R.T. Forsyth, A.N. Duffield, P.A. Papin, B. Aikin, T.N. Claytor, V.D. Vargas, D.W. Bucholz, T.J. Lienert, C.E. Cross, "Canless HIP Approach to Al Cladding of LEU Fuel Foils Using Electron Beam Welding," Los Alamos National Laboratory, report LA-UR-11-05598 (29 September 2011).

2011kat J. Katz, K. Clarke, B. Mihaila, J. Crapps, B. Aikin, V. Vargas, R. Weinberg, A. Duffield and D. Dombrowski, "Scale-Up of the HIP Bonding Process for Aluminum Clad LEU Reactor Fuel," Proceedings of RERTR 2011, held 23-27 October 2011, Santiago, Chile. Also published as Los Alamos National Laboratory report LA-UR-11-06029 (20 October 2011).

2012cla K.D. Clarke, C.E. Cross, R.E. Hackenberg, R.J. McCabe, J.D. Montalvo, M.J. Dvornak, R.L. Edwards, J.M. Crapps, R.R. Trujillo, B. Aikin, V.D. Vargas, K.J. Hollis, B. Mihaila, D.L. Hammon, R.W. Hudson, T.J. Tucker, J.E. Scott, A.N. Duffield, R.Y. Weinberg, D.E. Dombrowski, "Development of Aluminum-Clad Fuel Plate Processing Through Canned and Canless Hot Isostatic Pressing (HIP), and Studies of Aluminum Cladding Grain Growth during HIP," Proceedings of RERTR 2012, held 14-17 October 2012, Warsaw, Poland. Also published as Los Alamos National Laboratory report LA-UR-12-25123 (October 2012).

Table 1.1. PROCESS IMPROVEMENT STRATEGIES AND PROCESSES. The general strategy is in the top row, with specific process examples in the rows beneath. The ones in bold italics were experimentally tested in this work.

1. Aluminum metal flow into **macroscopic gaps** (breaks up oxides; deforms Al)	2. Aluminum metal flow at contact points of **engineered asperities**	3. Aluminum re-crystallization and grain growth from **stored energy** imparted prior to HIP run.	4. **Alternative cleaning and coating**
Machine channels in Al plates at strategic locations	***Knurling***	***Cold rolling***	***Transferred-arc (TA) cleaning***
	Steel wool abrasion	***Bead blasting (glass)***	***Electro-spark deposition (ESD) of pure Al***
	Machined grooves	Grit blasting (silica)	Al foil interlayer
	Engraving / laser sculpting		
	Wire brushing		
	Coarse sanding		
	Severe etching (grain relief)		

Table 2.1. HIP CYCLE AND ENCLOSURE DETAILS. Each HIP cycle could hold more than one enclosure; only those enclosures relevant to this study are listed. Each enclosure could have more than one stack-up, which in turn could have 1 or more Al-Al bonding sandwiches.

Successful sealing and HIP bonding

HIP run		Enclosure	Parting	Vacuum pulled		Sand-	Al thick-	Aluminum	
cycle #	Date	type and ID	agent	How	Date	wich ID	ness (mill)	Cleaning Type	Date
246	1-Apr-11	Long can 7	Neolube	SS tube	not known	1	32+37	LANL	not known
254	7-Jun-12	Long can	MoS2	SS tube	16-May-12	2.1a1	31+31	B&W	11-May-12
						2.1a2	31+31	B&W	11-May-12
						2.1a3	31+31	B&W	11-May-12
						2.1a4	31+31	B&W	11-May-12
258*	16-Aug-12	Round can	MoS2	EBW unit	8-Aug-12	3a1	32+32	B&W	18-Jul-12
		3a				3a2	48+48	TA	18-Jul-12
						3a2	48+48	Ac+IP	18-Jul-12
						3a3	48+48	TA	25-Jul-12
						3a3	48+48	Ac+IP	25-Jul-12
259	17-Sep-12	Round can	MoS2	EBW unit	10-Sep-12	3b1a	32+32	B&W	4-Sep-12
		3b				3b1b	32+48	B&W	4-Sep-12
						3b2a	48+48	B&W	4-Sep-12
						3b2b	48+32	B&W	4-Sep-12
259	17-Sep-12	Round can	MoS2	EBW unit	10-Sep-12	3c1a	32+32	B&W	4-Sep-12
		3c				3c1b	32+48	B&W	4-Sep-12
						3c2a	48+48	B&W	4-Sep-12
						3c2b	48+32	B&W	4-Sep-12

*Cycle 258 ran for the expected time-temperature profile, with a 90 minute hold at 560ºC. However, due to a low gas supply pressure, the peak pressure of 15 ksi was not attained until 30 minutes into the hold. So the parts did experience 60 minutes at 15 ksi and 560ºC. The cans looks like they were well squeezed, so at first glance this anomaly did not seem to affect the outcome.

Unsuccessful sealing and/or HIP bonding

HIP run		Enclosure	Parting	Vacuum pulled		Sand-	Al thick-	Aluminum	
cycle #	Date	type and ID	agent	How	Date	wich ID	ness (mill)	Cleaning Type	Date
253	24-May-12	Canless	MoS2	EBW unit	11-May-12	2.2a1	37+37	B&W	10-May-12
						2.2a2	37+37	B&W	10-May-12
						2.3a1	37+37	B&W	10-May-12
						2.3a2	37+37	B&W	10-May-12
						2.3b1	37+37	B&W	10-May-12
						2.3b2	37+37	B&W	10-May-12
						2.4a1	37+37	B&W	9-May-12
						2.4a2	37+37	B&W	9-May-12

Table 2.2. PROCESS MODIFICATIONS AND RESULTS ON HIP'D SANDWICHES. The line length is the bond line length scanned by EBSD for the loose grain penetration measurement.

Successful sealing and HIP bonding								
HIP cycle #	Sand-wich ID	Aluminum process modification (mating surfaces)	MST-6 Char. Job #	Line length mm	% Al grain penetration strict	% Al grain penetration loose	Comments	Sand-wich ID
246	1	flat/flat	12556	9.9	0.08	6.0	LANL clean	1
254	2.1a1	flat/grooved (5 deep, 15 wide)	12698	13.0		5.2		2.1a1
254	2.1a2	flat/grooved (10 deep, 10 wide)	12699	15.1		8.9		2.1a2
254	2.1a3	flat/grooved (10 deep, 15 wide)	12700	26.0		4.9		2.1a3
254	2.1a4	flat/flat	12701	19.8	1.84	7.9	B&W clean	2.1a4
258	3a1	steel wool, lines perpendicular	12717				not characterized	3a1
258	3a2	TA+ESD/TA+ESD in argon	12718	7.3		2.6		3a2
258	3a2	flat/flat	12718	15.6		3.1	AC+IP wipe	3a2
258	3a3	TA+ESD/TA+ESD in nitrogen	12719				not characterized	3a3
258	3a3	flat/flat	12719				not characterized	3a3
259	3b1a	63% CR/63% CR, perpendicular	12761	15.6		3.6		3b1a
259	3b1b	63% CR/bead blast (90*)	12761	15.6		2.4		3b1b
259	3b2a	bead blast (90*)/bead blast (90*)	12761	15.6		4.2		3b2a
259	3b2b	bead blast (90*)/steel wool	12761	15.1		1.5		3b2b
259	3c1a	63% CR/63% CR, parallel	12761				not characterized	3c1a
259	3c1b	63% CR/bead blast (45*)	12761				not characterized	3c1b
259	3c2a	bead blast (45*)/bead blast (45*)	12761	14.8		2.9		3c2a
259	3c2b	bead blast (45*)/steel wool	12761	14.8		4.5		3c2b

Unsuccessful sealing and/or HIP bonding							
HIP cycle #	Sand-wich ID	Aluminum process modification (mating surfaces)	MST-6 Char. Job #	Line length mm	% Al grain growt	% Al grain growth	Comments
253	2.2a1	bead blast (90*)/bead blast (90*)	na				failed; not leaktight
253	2.2a2	bead blast (45*)/bead blast (45*)	12667				failed; not leaktight
253	2.3a1	steel wool/steel wool, parallel	12668				failed; not leaktight
253	2.3a2	steel wool/steel wool, perpendicular	12669				failed; not leaktight
na	2.3b1	knurled, parallel	na				failed when welded
253	2.3b2	knurled, perpendicular	12666				failed; not leaktight
na	2.4a1	TA cleaned/TA cleaned	na				failed when sheared
na	2.4a2	TA cleaned + ESD/TA cleaned	na				failed when sheared

Table 4.1. TRANFERRED ARC SPECIMEN CONDITIONS. Figures 3.4 and 3.5 provide the map of the lettered regions.

Region	Mating surfaces	Voltage
A	acetone+isopropanol / acetone+isopropanol	na
B	acetone+isopropanol / acetone+isopropanol	na
C	acetone+isopropanol / acetone+isopropanol	na
D	TA+ESD / TA+ESD	50
E	TA+ESD / TA+ESD	100
F	TA+ESD / TA+ESD	150
G	TA+ESD / acetone+ethanol	50
H	TA+ESD / acetone+ethanol	100
I	TA+ESD / acetone+ethanol	150

Table 4.2. SUMMARY OF ALUMINUM GRAIN PENETRATION VS PROCESS. The values were determined on the loose definition.

Strategy	Process	% Al grain penetration
Baseline (no modification)	acetone + isopropanol wipe	3.1
	LANL aqueous cleaning	6.0*
	B&W aqueous cleaning	7.9**
Macroscopic gaps	grooving (5 deep, 15 wide)	5.2
	grooving (10 deep, 10 wide)	8.9
	grooving (10 deep, 15 wide)	4.9
Engineered asperities	steel wool / bead blast (90*)	1.5
	steel wool / bead blast (45*)	4.5
Stored energy	cold roll / cold roll	3.6
	cold roll / bead blast (90*)	2.4
	bead blast (90*) / bead blast (90*)	4.2
	bead blast (45*) / bead blast (45*)	2.9
Alternative cleaning and coating	TA cleaning + ESD / TA cleaning + ESD (both 100 volts)	2.6

* strict definition value = 0.08%

** strict definition value = 1.84%

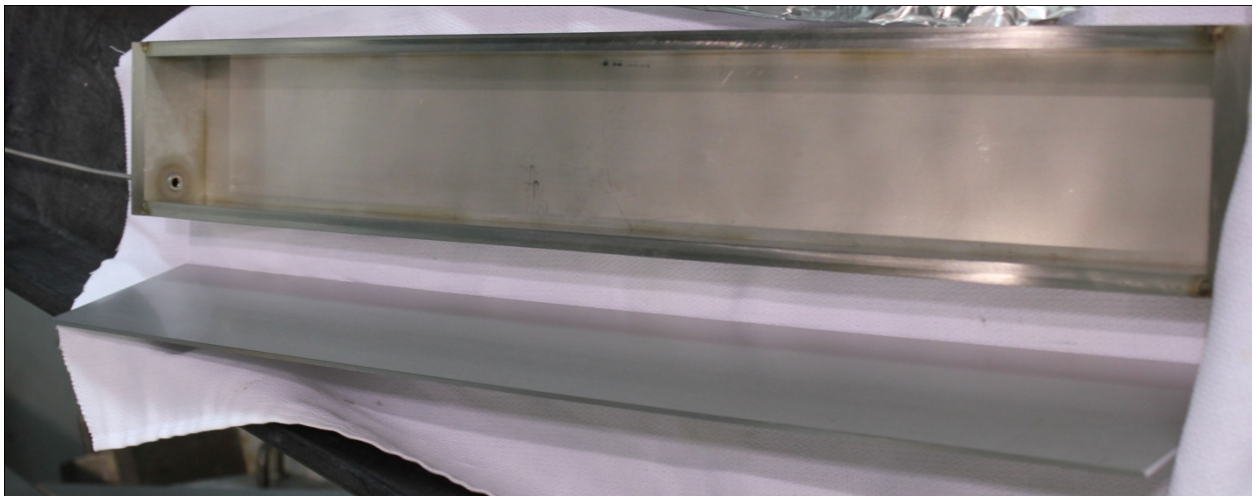

(a)

(b)

Figure 2.1. Long can hermetically sealed enclosure, run in HIP cycle 254. (a) Entire empty can prior to loading; the top lid (shown here resting nearly upright) is welded on after loading. The evacuation tube and hole are seen on the left (= "top side") (b) Four Al sandwiches after HIP cycle. Their left-right orientation is the same as in (a). Plate 1 has been cut up according to the scheme in Figure 2.5. The other 3 plates were cut up in the same fashion soon after this photo was taken. Plate 2 was bent because it stuck to the strongback more than normal and needed additional force to pry apart. (All specimens were extracted from regions well removed from the bent region seen here.)

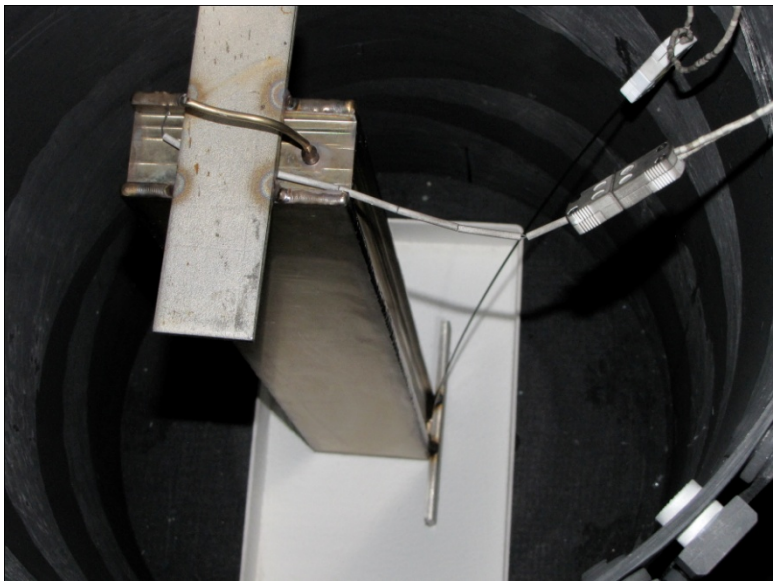

(a)

(b) *(c)* *(d)* *(e)*

Figure 2.2. Evacuated and sealed long can for HIP cycle 254. (a) Loaded into HIP chamber before the HIP run. (b, c, d, e) Appearance after HIP run.

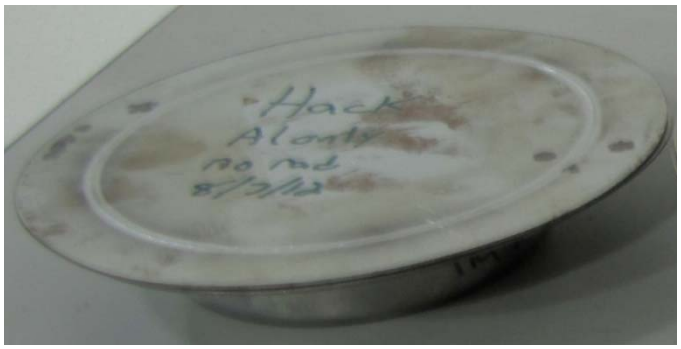

(a)

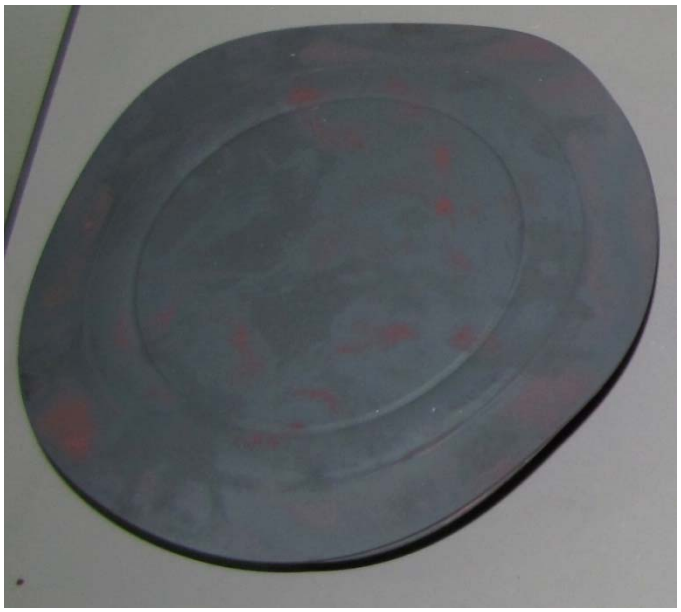

(b)

(c)

Figure 2.3. Round can hermetically sealed enclosure, run in HIP cycle 258. (a) Before HIP cycle. (b, c) After HIP cycle. The warpage around the lip probably resulted from the suction of the body of the can pulling in the outer extremities. The body of the can did not appear warped.

(a)

(b)

Figure 2.4. Canless hermetically sealed squares, run in HIP cycle 253. (a) As stacked in graphite container for HIP run. Al sandwiches were alternated with tool steel strongbacks; only the top sandwich is visible. (b) Four Al sandwiches after HIP cycle.

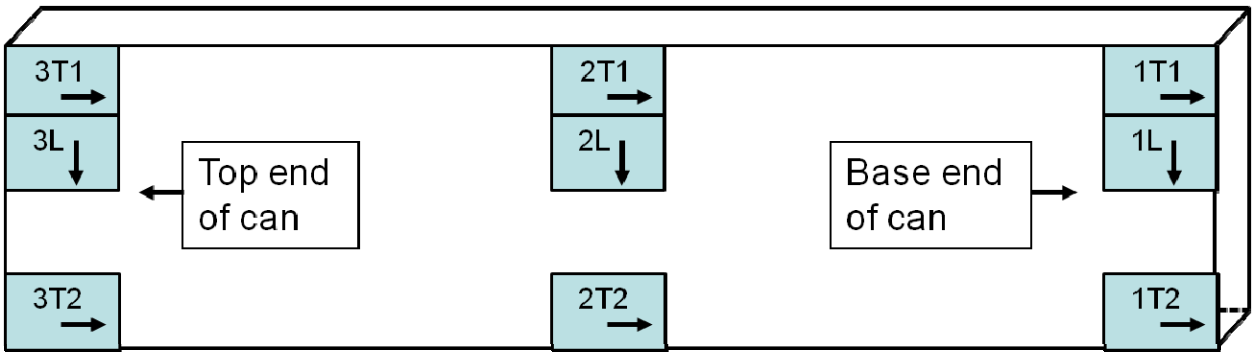

Figure 2.5. Schematic of specimen locations and orientations used in metallographic job numbering scheme for plates in the 24″ long can. The arrow indicates which cross-sectional surface is revealed.

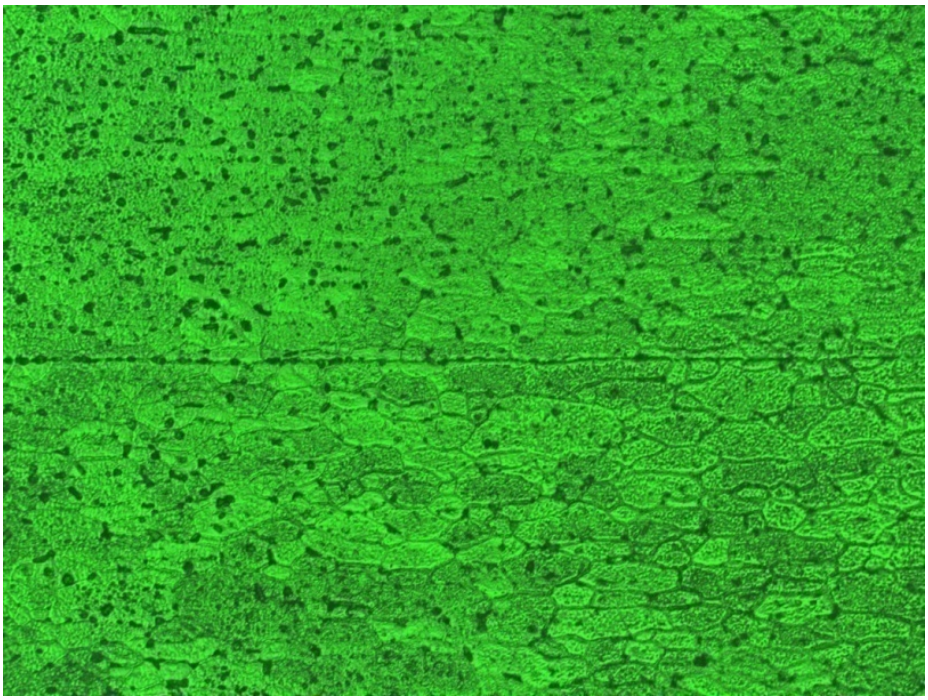

(a)

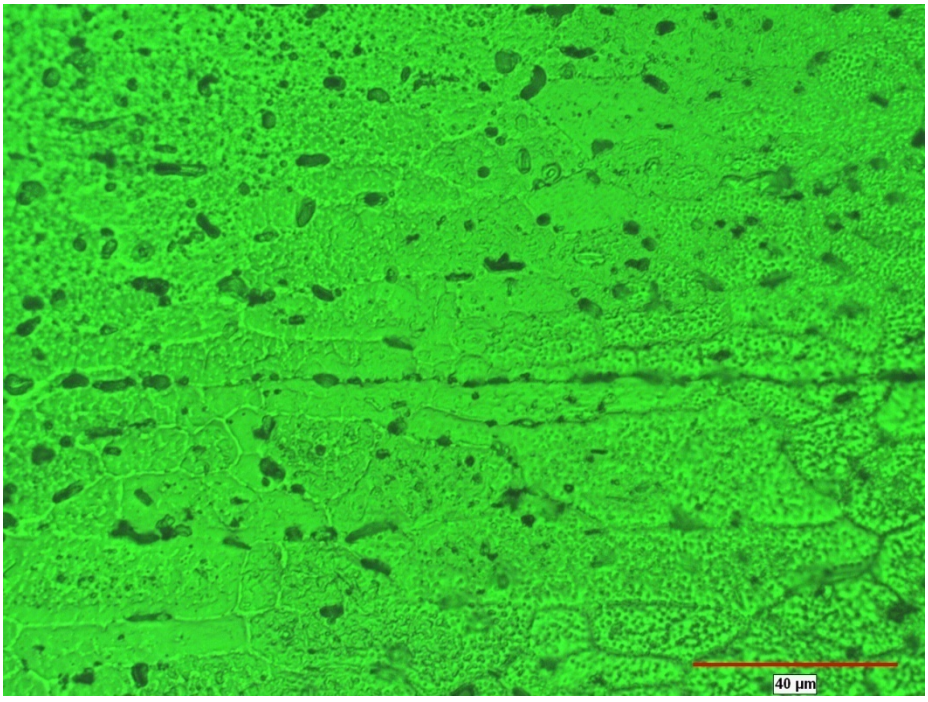

(b)

Figure 3.1. LOM of baseline condition with LANL cleaning (sandwich 1, job 12556-5-1T1). (a) Representative lower-magnification image (450 micron wide), one out of 32 images in the montage. (b) Higher-magnification image (180 micron wide) of a different area. The bond line runs horizontally across the center of both images, and is decorated by second-phase particles. No grain penetration either across or in the vicinity of the bond line is evident. Acid etched.

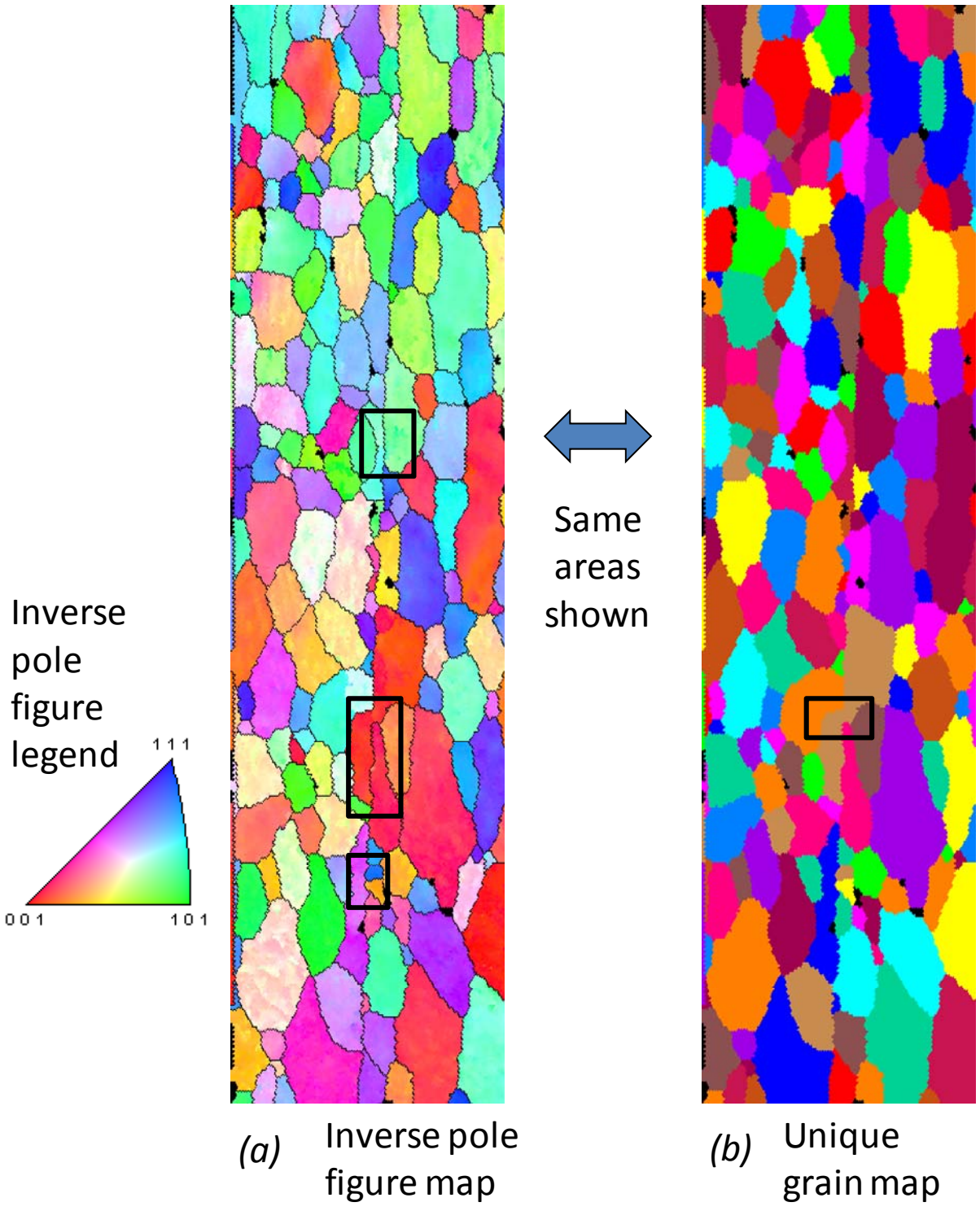

Figure 3.2. EBSD of baseline condition with LANL cleaning (sandwich 1, job 12556-5-1yT1). The images are 400 × 100 micron. The region shown here has a higher than normal amount of grain penetration (boxed regions). The boxed regions in the IPF map would be counted on the loose definition only; the single box on the UG map would be counted on both strict and loose definitions. (A total of 27 EBSD images examined for sandwich 1).

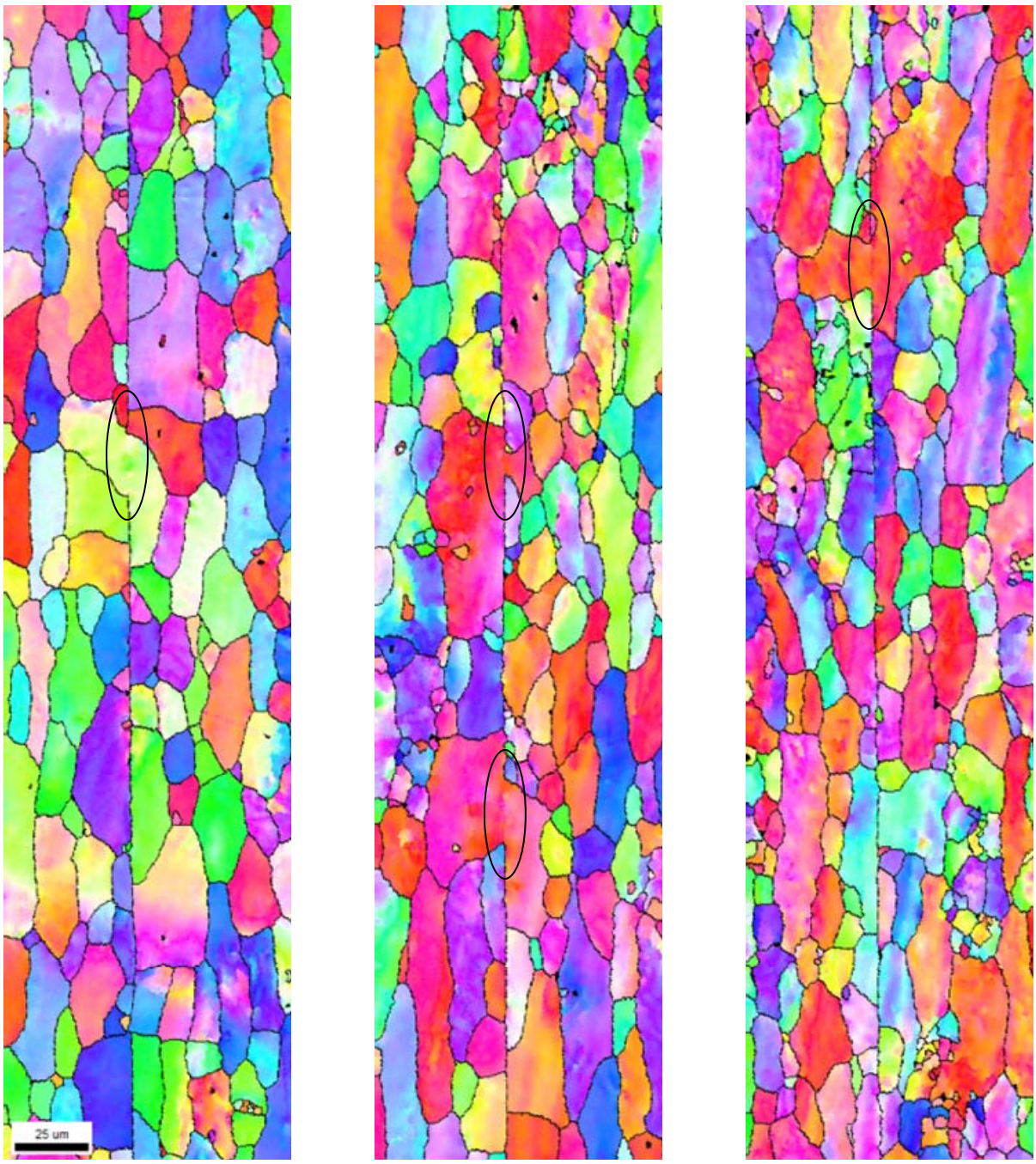

(a) *(b)* *(c)*

Figure 3.3. EBSD of baseline condition with B&W cleaning (sandwich 2.1a4, job 12701-2L.) The images are all 365 × 92 micron. Regions of grain penetration that met the strict definition are circled in these images.

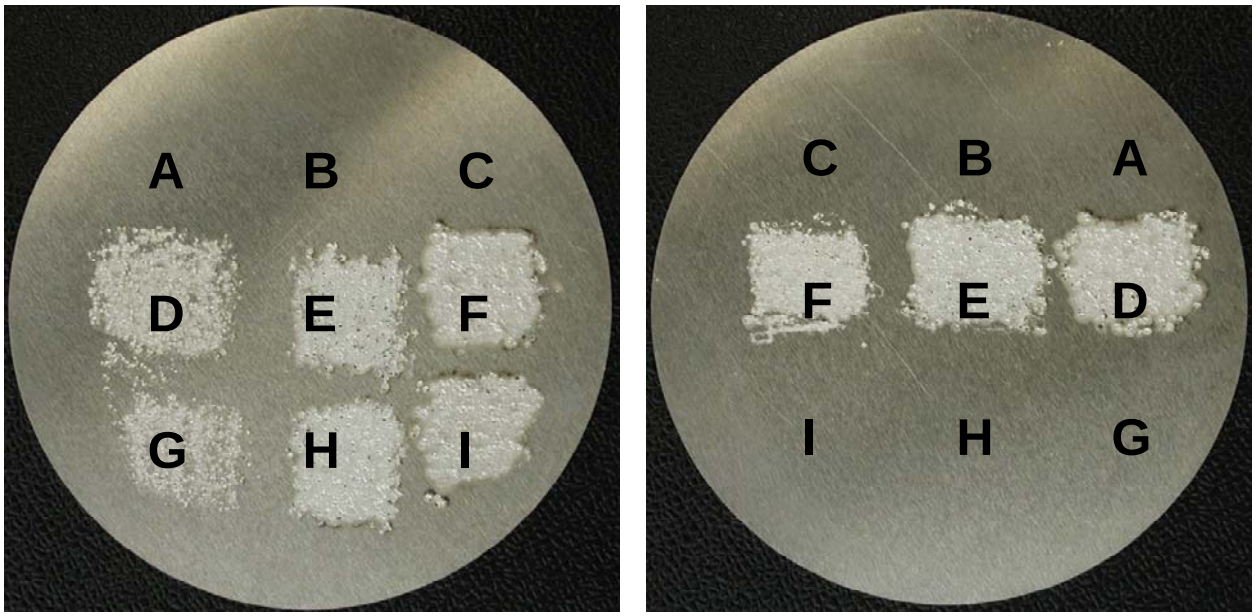

Figure 3.4. Sandwich 3a2 (HIP run 258), with mating surfaces shown prior to loading the round can. Areas D-I (left disc) and D-F (right disc) were the patches subject to transferred-arc-cleaning + electrospark deposition of pure Al. Unaffected Ac+IP cleaned regions were A-C. The TA-ESD was done in argon. Job 12718. Images reduced in size about 20%.

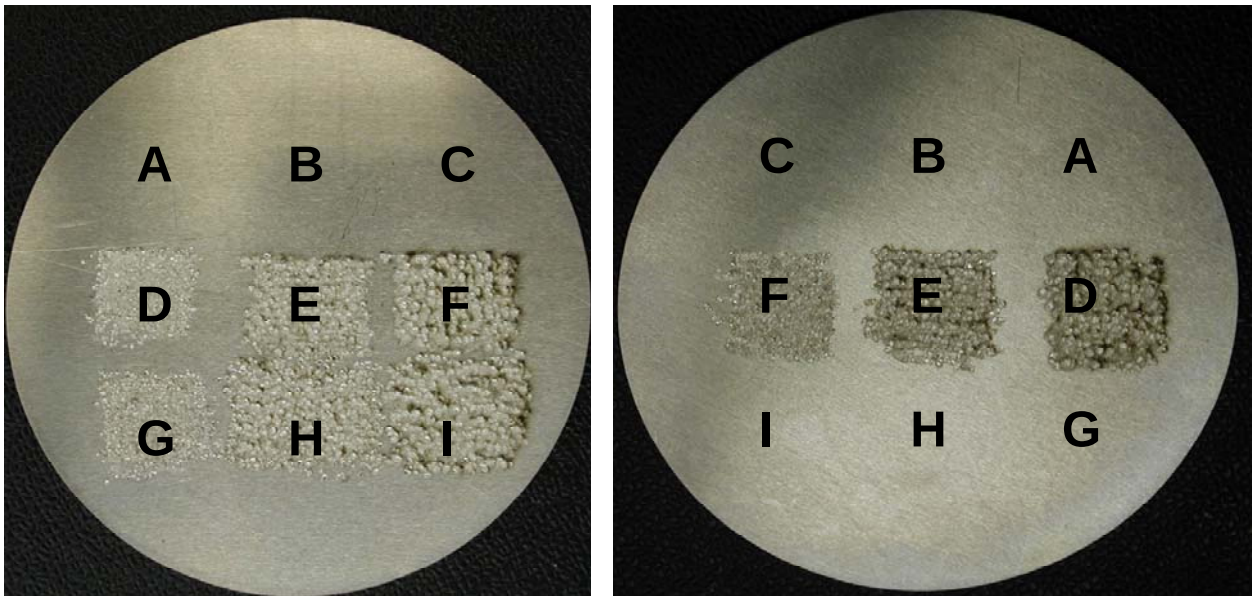

Figure 3.5. Sandwich 3a3 (HIP run 258). The labeling scheme, orientations, and magnifications are the same as in Figure 3.4 except the TA-ESD was done in nitrogen and the job is 12719.

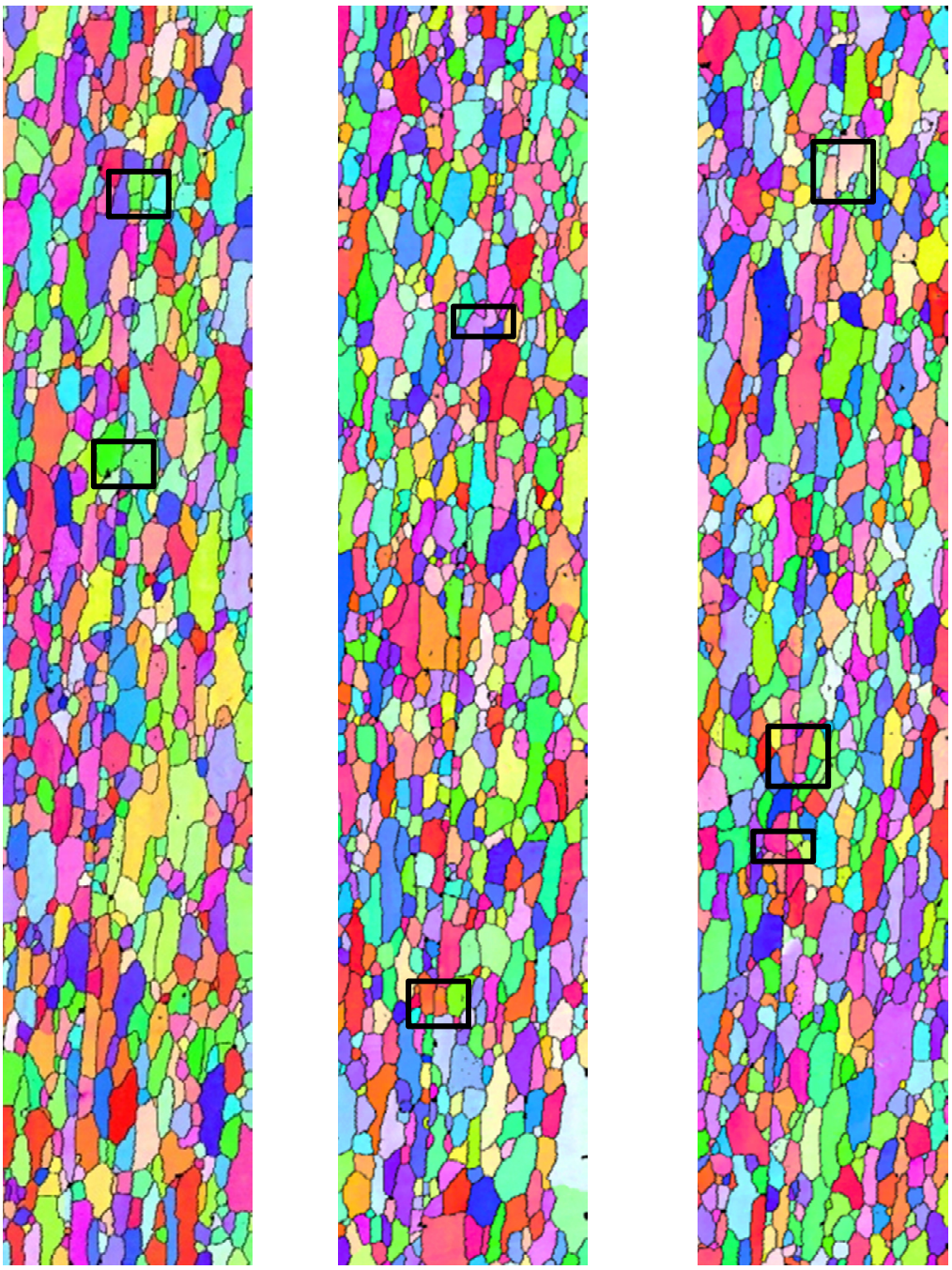

(a) *(b)* *(c)*

Figure 3.6. EBSD of baseline condition with acetone+isopropanol cleaning (sandwich 3a2, job 12718-B). Areas of grain penetration, all on the loose definition, are boxed. Images are 1000 × 200 micron.

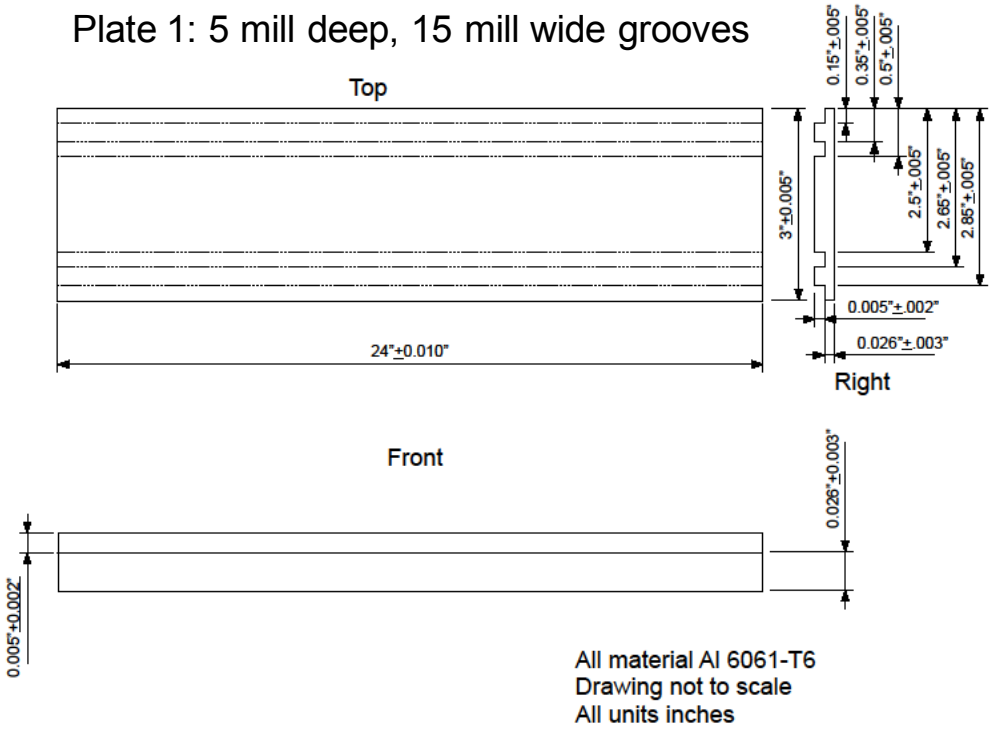

(a)

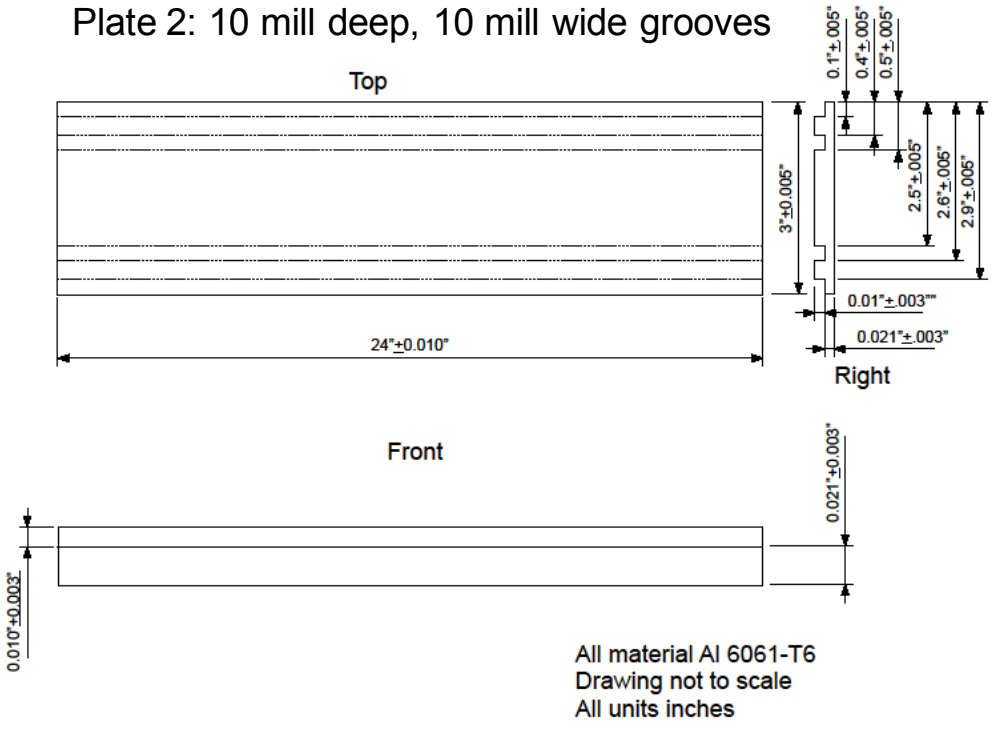

(b)

Figure 4.1. Schematic drawings of macroscopically grooved plates.

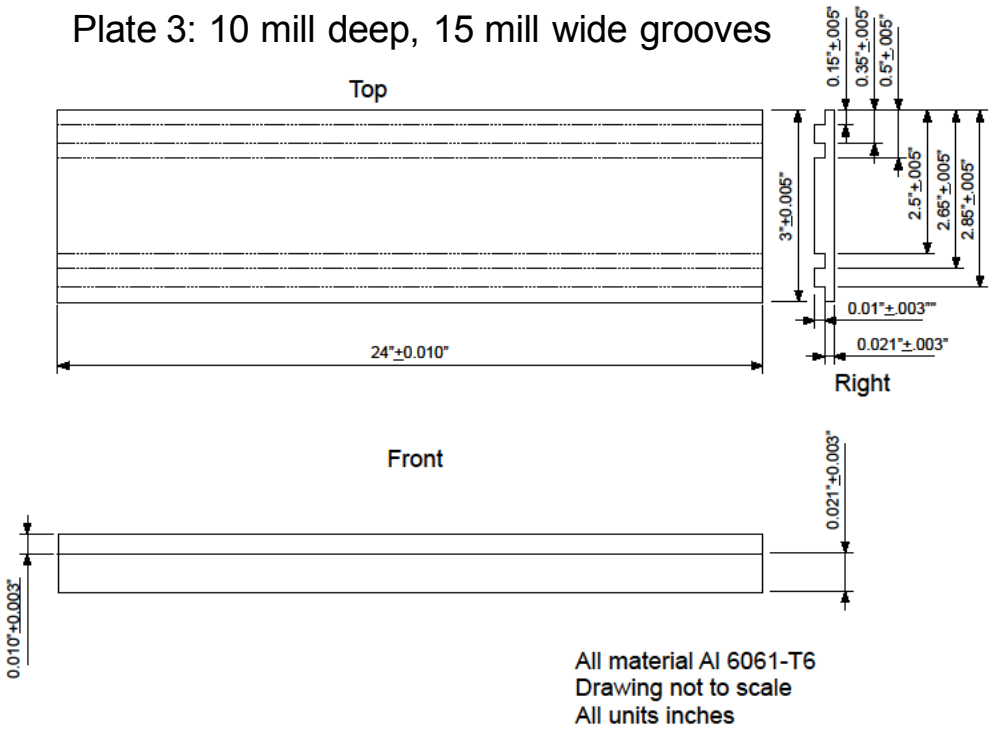

(c)

Figure 4.1. Schematic drawings of macroscopically grooved plates (cont'd).

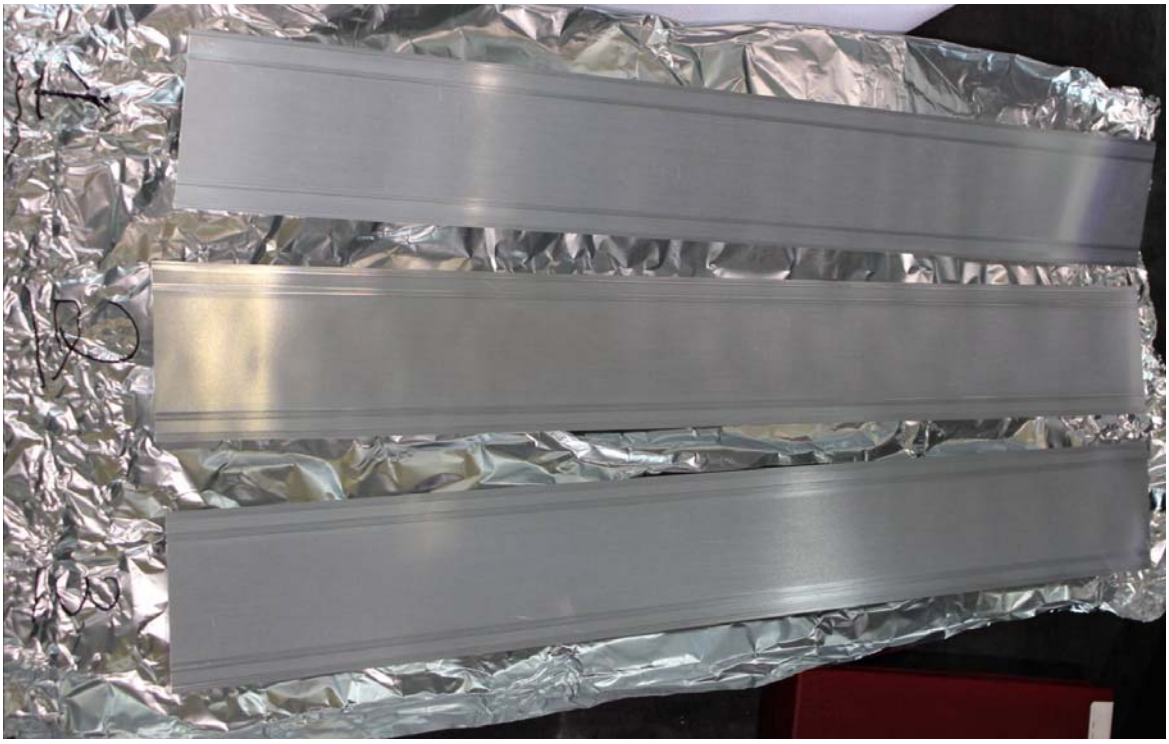

Figure 4.2. The as-cleaned grooved plates used in sandwiches 1, 2, and 3 in HIP cycle 254.

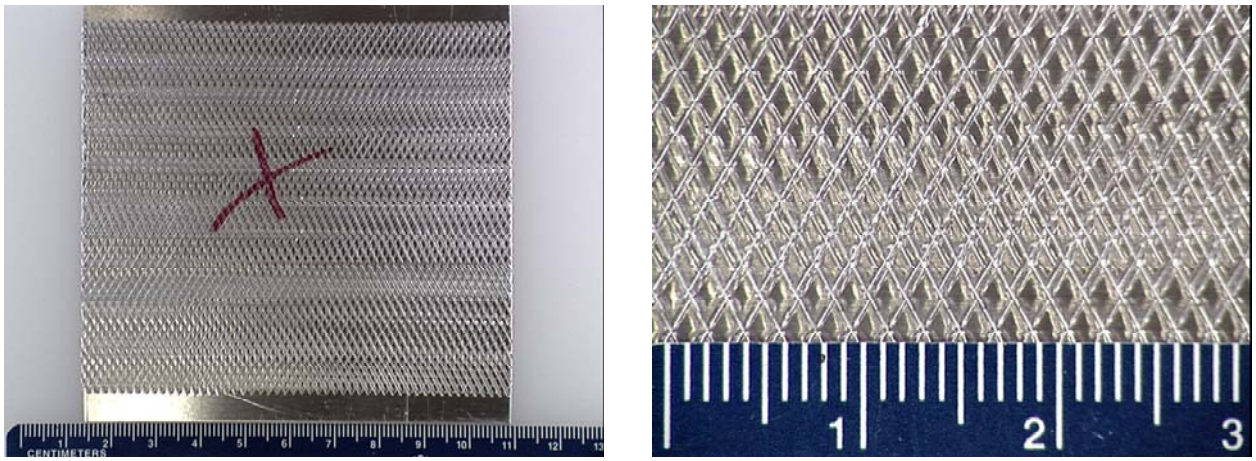

Figure 4.3. Knurled specimens prior to bonding.

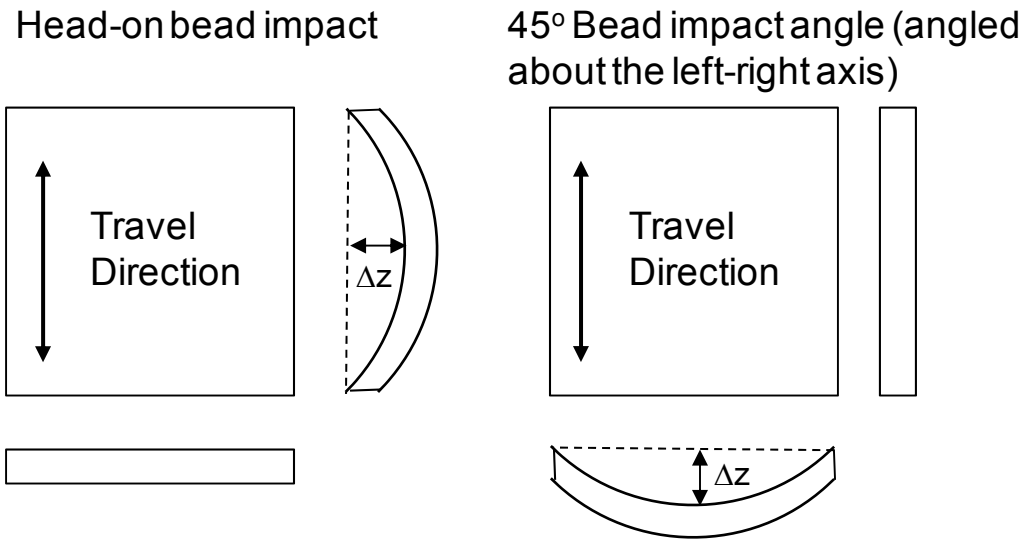

Figure 4.4. How the Al squared deflected during bead blasting 3.75″ wide, 32 mil thick squares. The deflection was far less pronounced when the 3.875″ diameter, 48 mil thick circles were blasted under otherwise identical conditions.

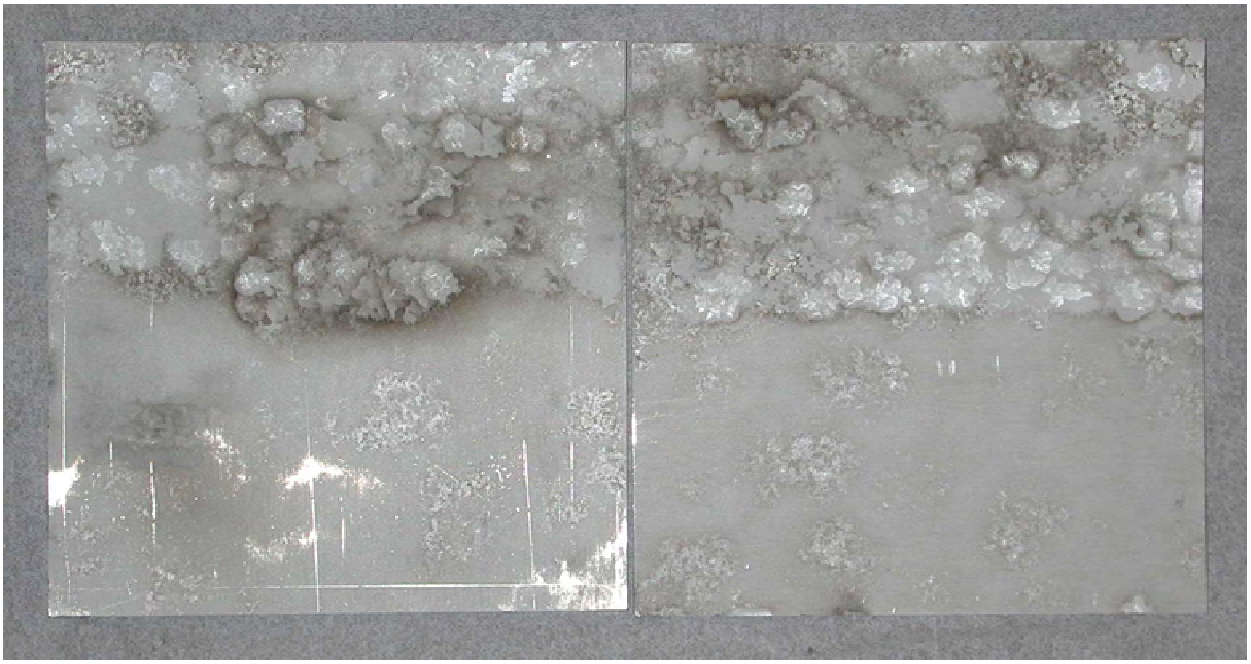

Figure 4.5. Sandwich 2.4a1. The top half of each square was TA cleaned and the bottom half continued arcing until roughened. This was not HIP'd due to EB weld failure during handling after welding.

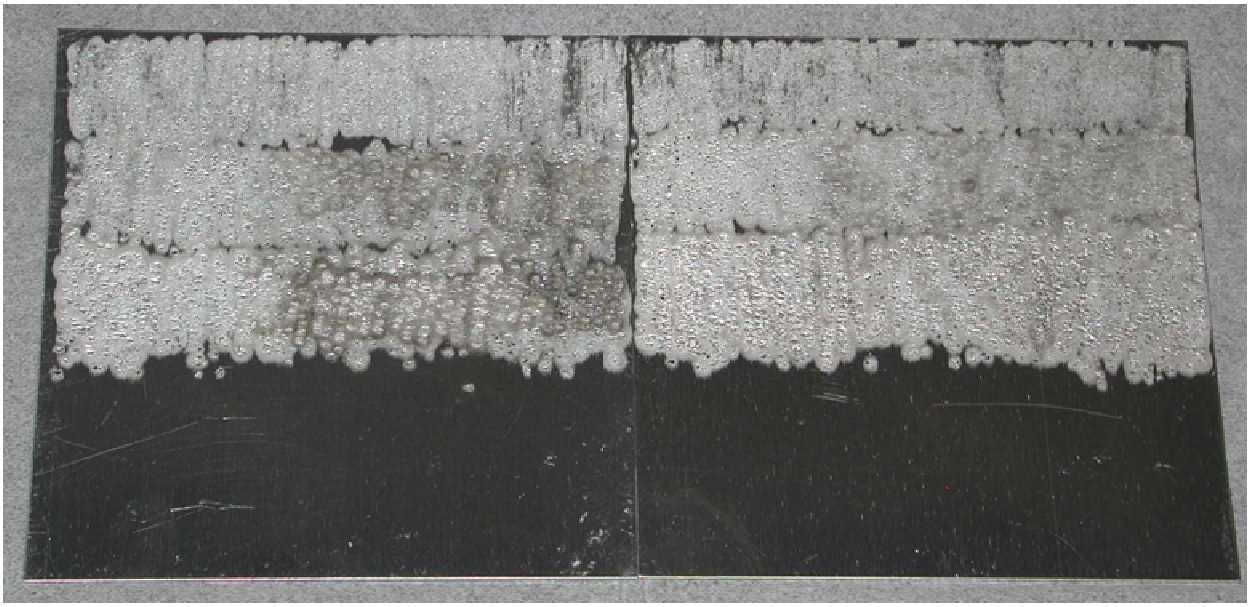

Figure 4.6. Sandwich 2.4a2. The top half of each square was subject to electrospark deposition of 99.5+% pure Al at 100 microF. The three strips of Al were deposited at 50, 100, and 150 V going top to middle, respectively. This was not HIP'd due to EB weld failure during handling after welding.

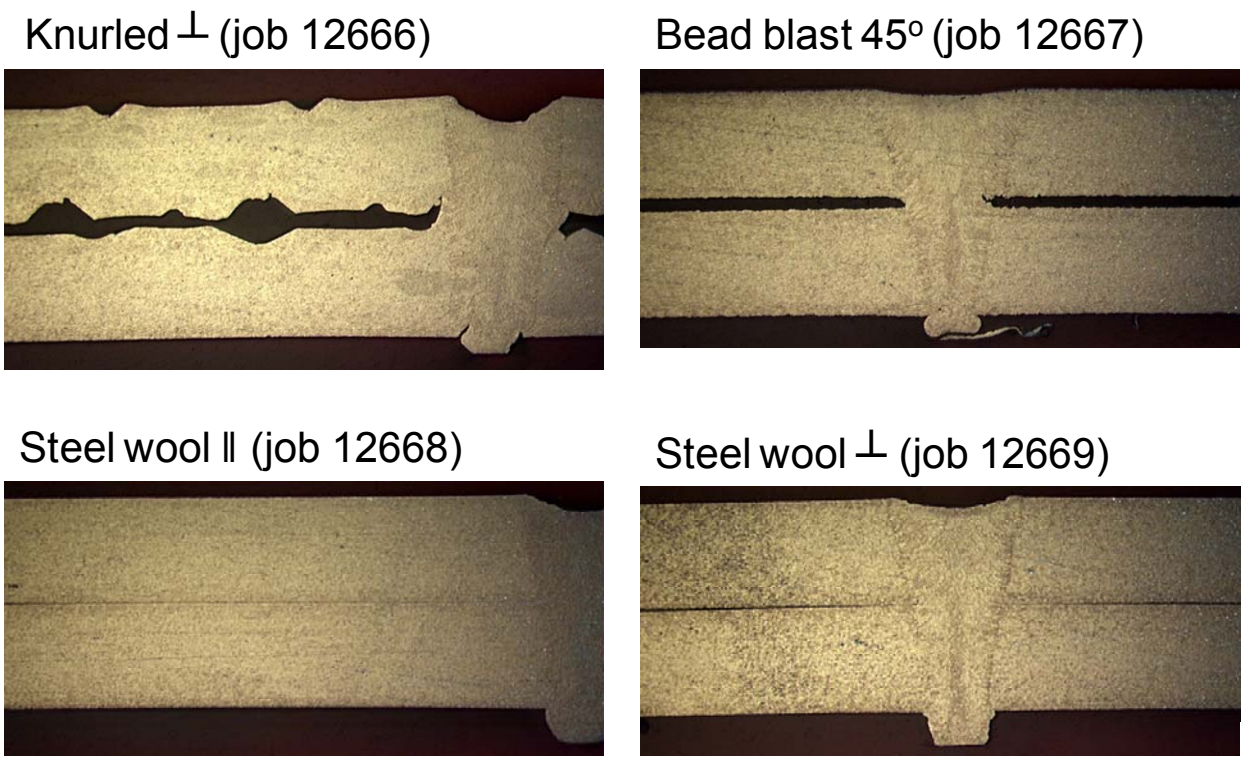

Figure 4.7. Low-magnification LOM of canless HIP cycle 253 showing the welds. The mating surfaces failed to touch and bond, presumably because they contained residual gas that prevented their collapse into one another during the HIP cycle. A few marks of the knurling pattern are apparent in the top left image.

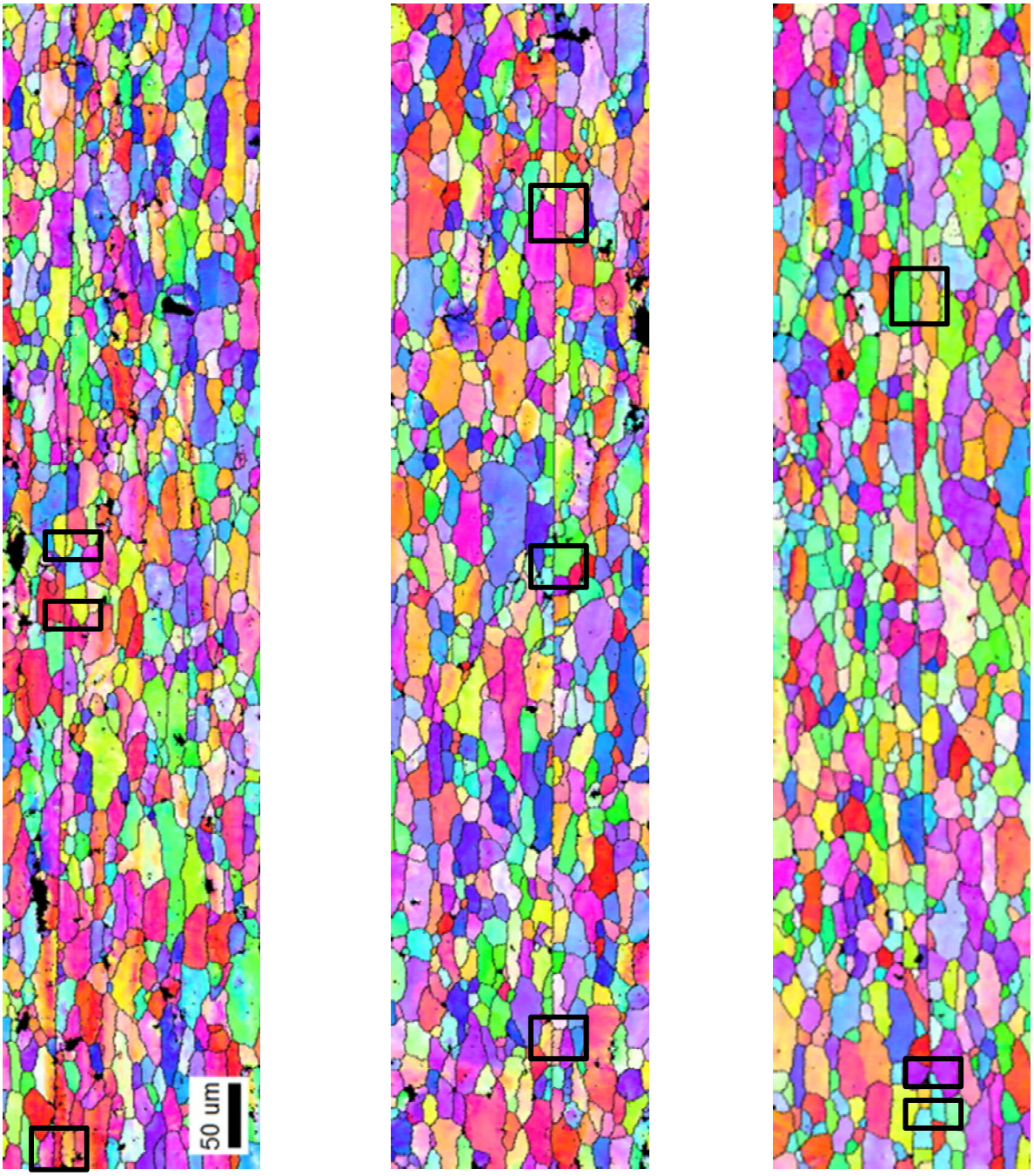

Figure 5.1. EBSD of the three macroscopically grooved sandwiches. (a) Sandwich 2.1a1, job 12698-2L. (b) Sandwich 2.1a2, job 12699-2L. (c) Sandwich 2.1a3, job 12700-2L. The boxed regions are areas of grain penetration (counted on the loose definition only).

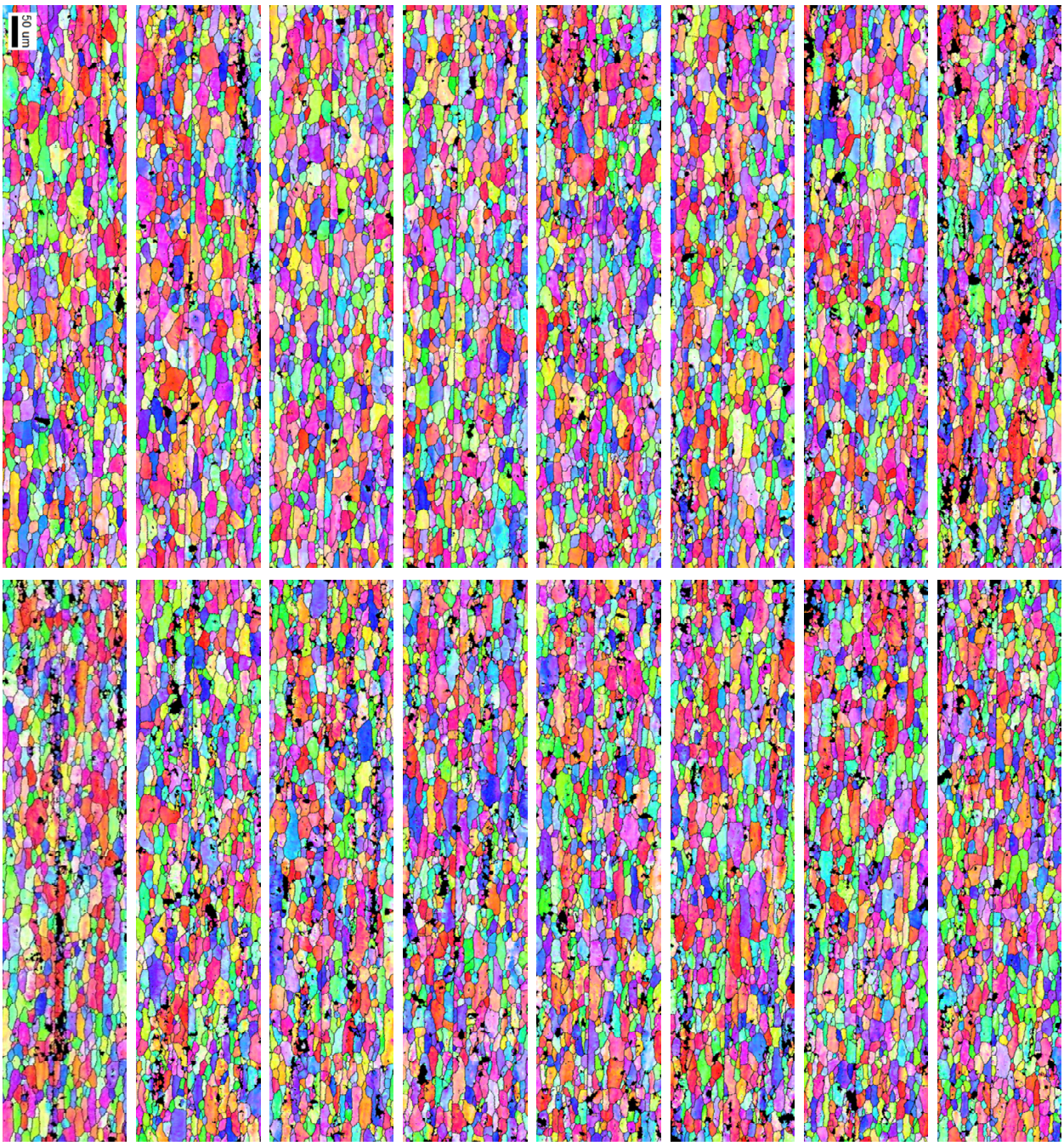

Figure 5.2. EBSD of macroscopically grooved plate, sandwich 2.1a1, job 12698-2L. All but the last image in the total montage are shown. Each image overlaps with about 5% of the preceding image. The relative order of images along the bond line runs left to right and then top to bottom. Specific regions of grain penetration are not called out. Images are 800 × 175 micron.

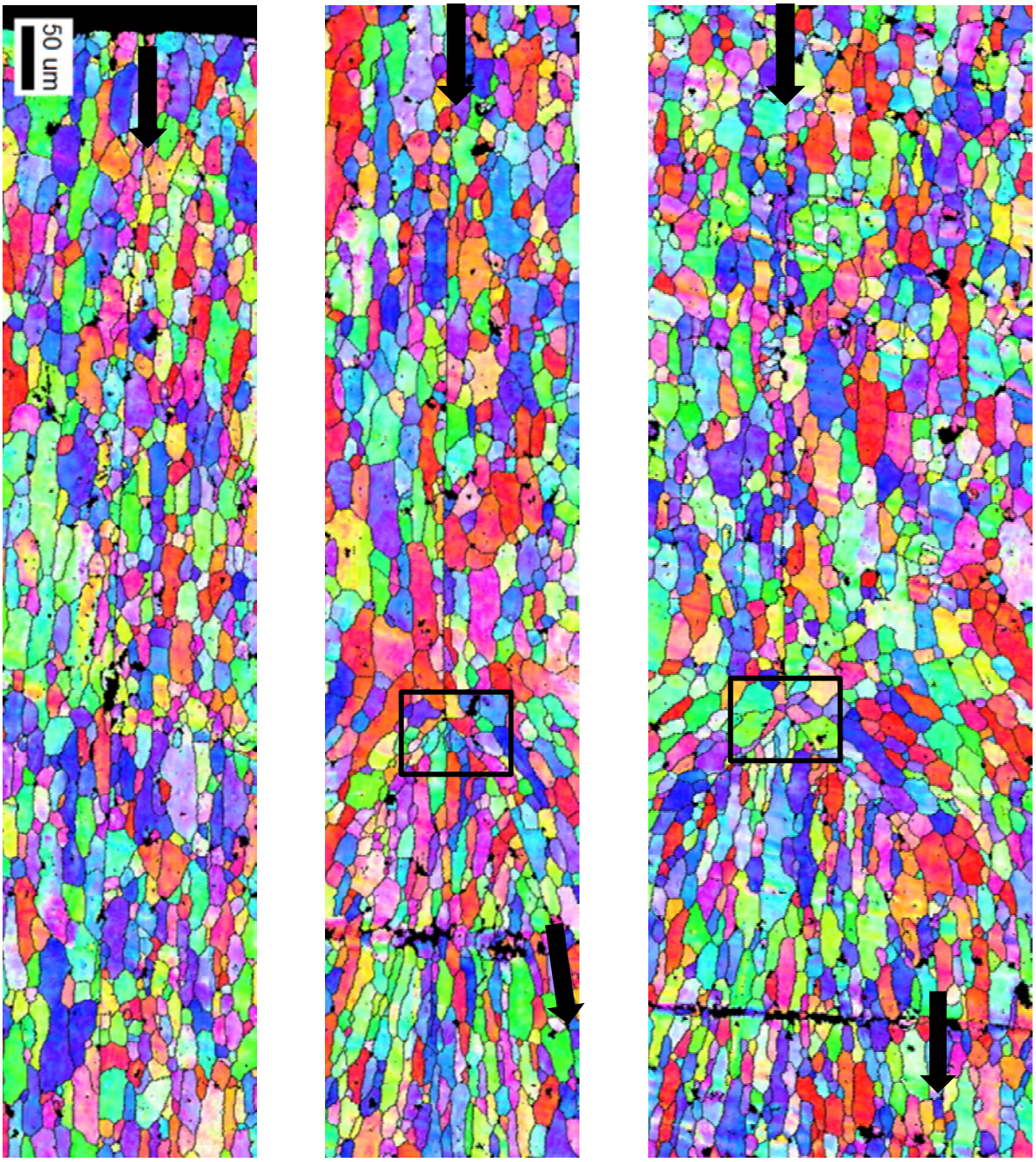

Figure 5.3. EBSD of macroscopically grooved plate, sandwich 2.1a3, job 12700-2T1. (a) region where the bond line is straight. (b,c) regions where the bond line orientation changes dramatically (boxed). The arrows indicate the bond line. It was unclear as to which side of the bond line the grooved plate was located with respect to these EBSD images. The images have the same magnification but are not contiguous. Images are 900 × 200 micron.

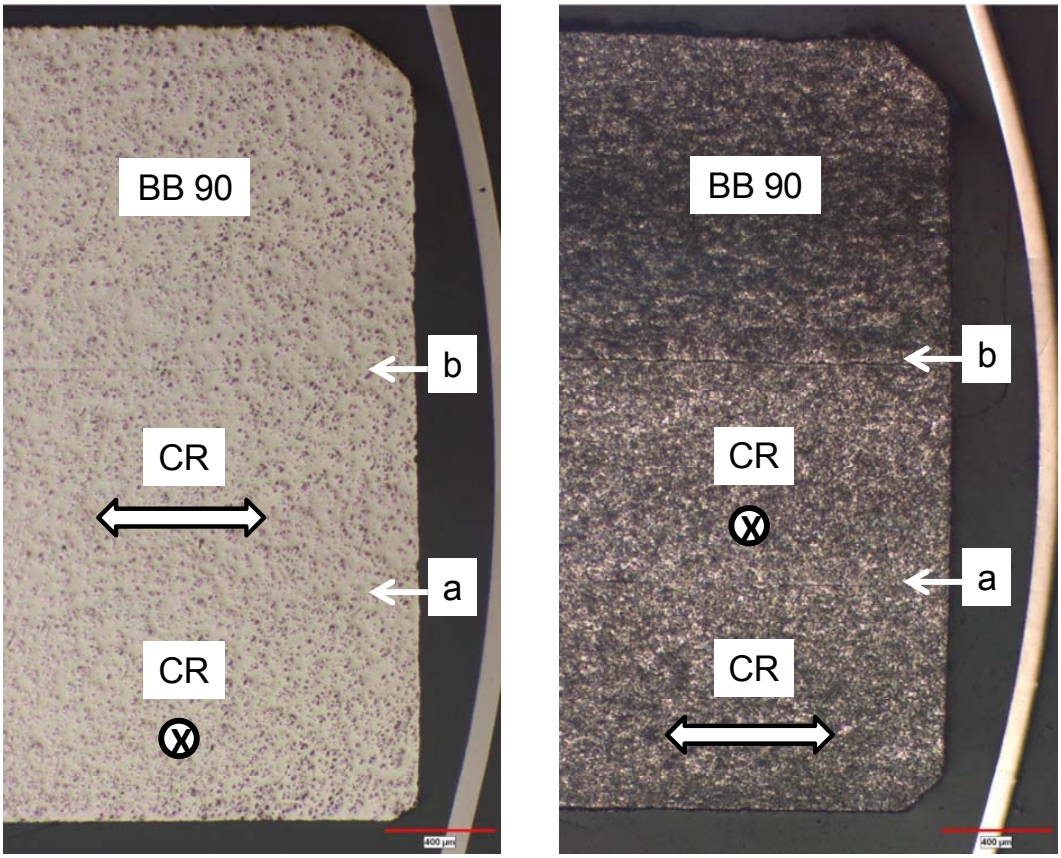

(a) *(b)*

Figure 7.1. Log-magnification images of bonding stackup 3b1. The letters indicate the bond line (a or b), which keys to the sandwich ID (3b1a, 3b1b). (a) and (b) show the orthogonal planes of polish (east and north, respectively). (a) was as-polished; (b) was acid etched. Job 12761.

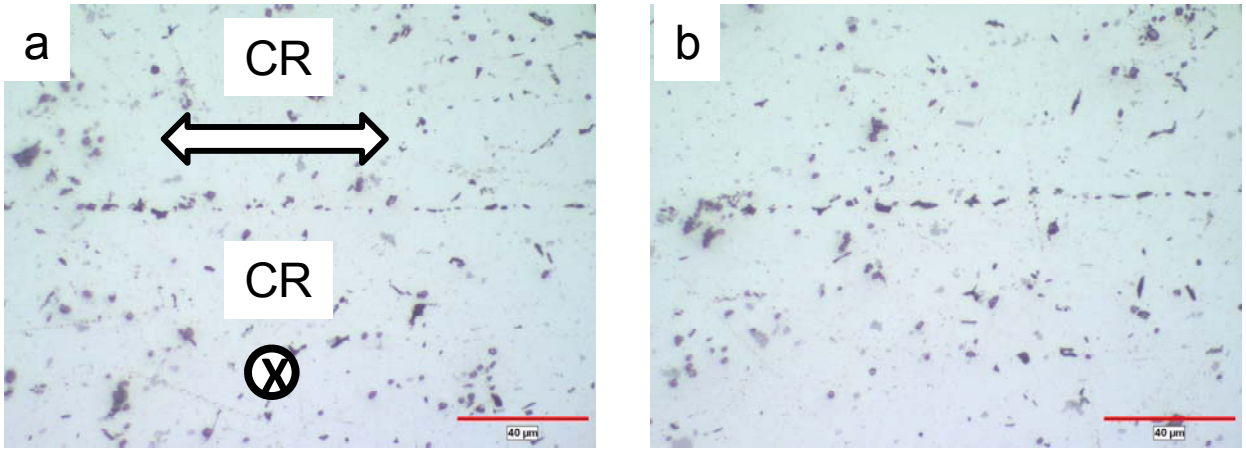

Figure 7.2. LOM images of sandwich 3b1a (cold rolled / cold rolled, RD oriented perpendicular) in the as-polished condition. Job 12761, east plane of polish.

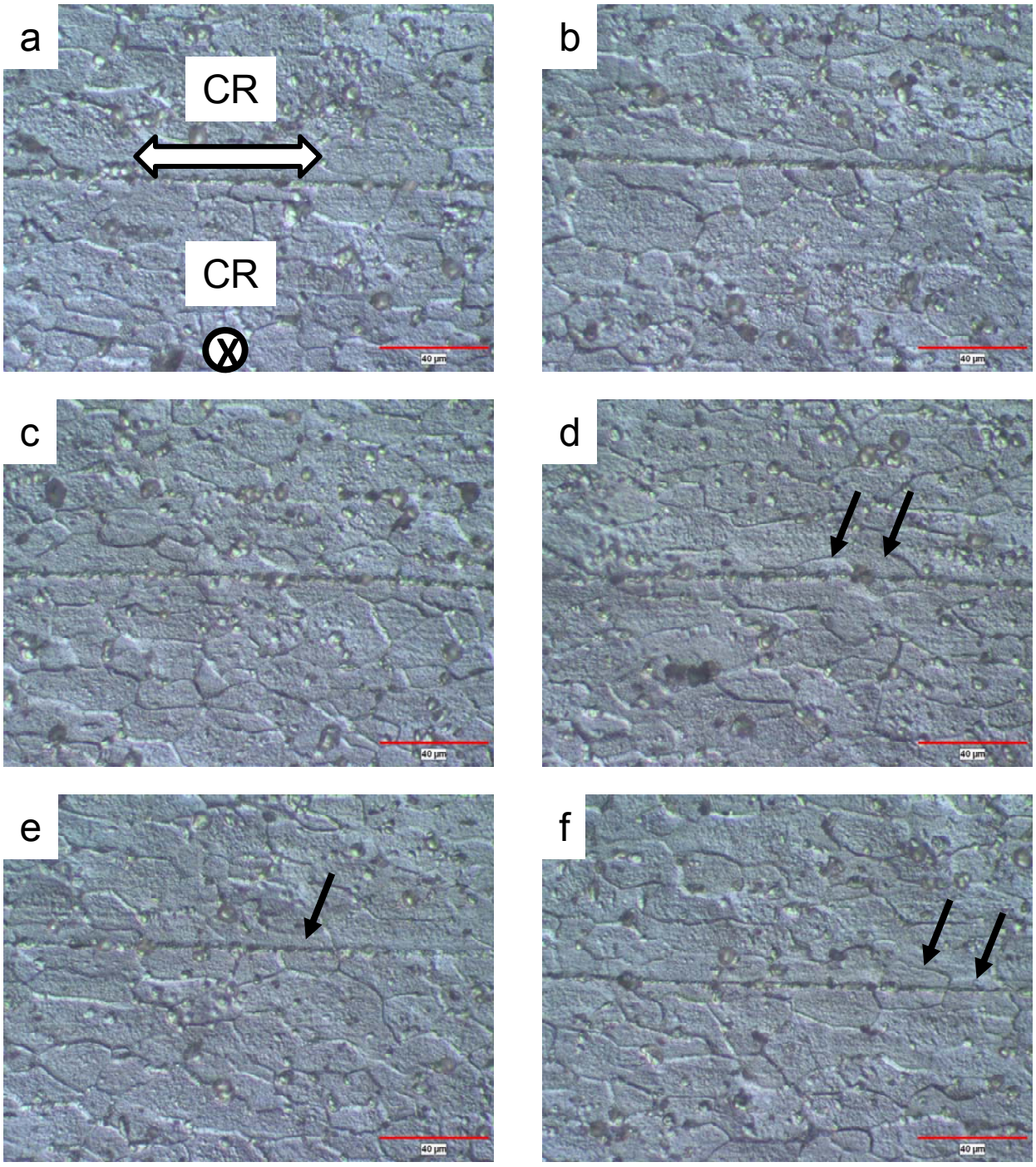

Figure 7.3. LOM images of sandwich 3b1a (cold rolled / cold rolled, RD oriented perpendicular) in the caustic etched condition (3 V, 15 seconds). Arrows indicate grains that may have penetrated the bond line. Job 12761, east plane of polish.

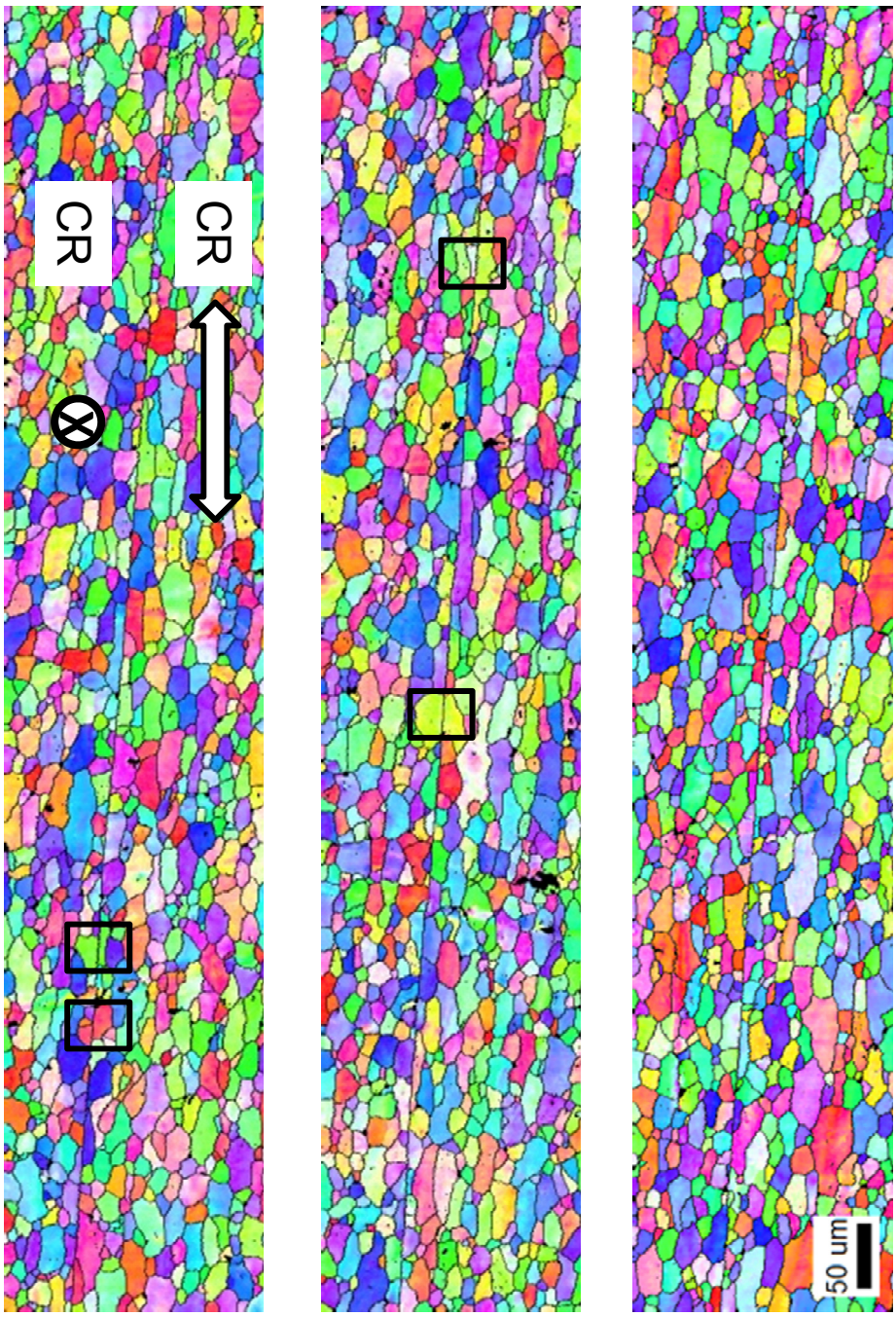

(a) *(b)* *(c)*

Figure 7.4. EBSD images of sandwich 3b1a (cold rolled / cold rolled, RD oriented perpendicular). The boxed regions are areas of grain penetration (counted on the loose definition only). Images are 1000 × 200 micron. Job 12761, north plane of polish.

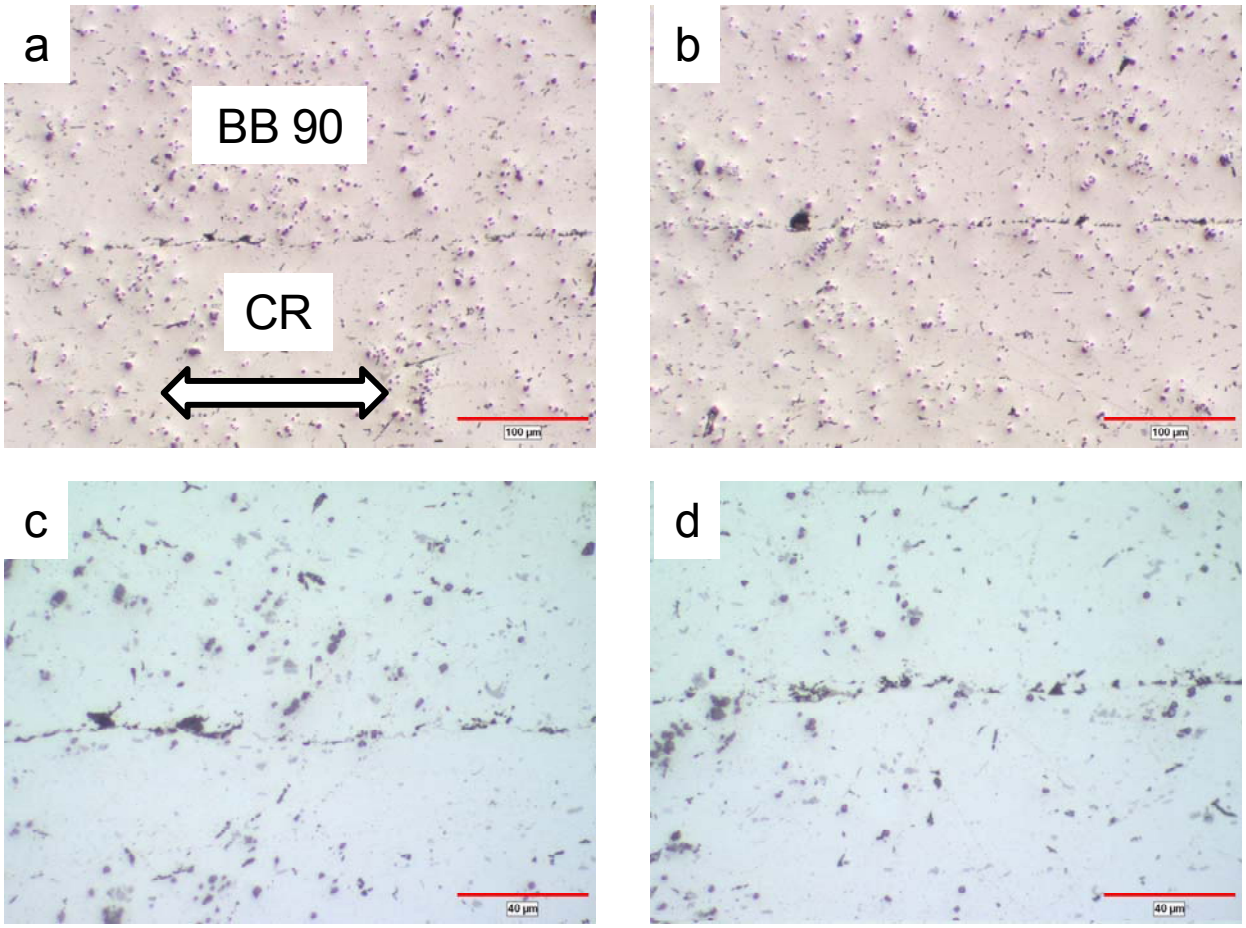

Figure 7.5. LOM images of sandwich 3b1b (bead blasted 90º / cold rolled) in the as polished condition. Job 12761, east plane of polish.

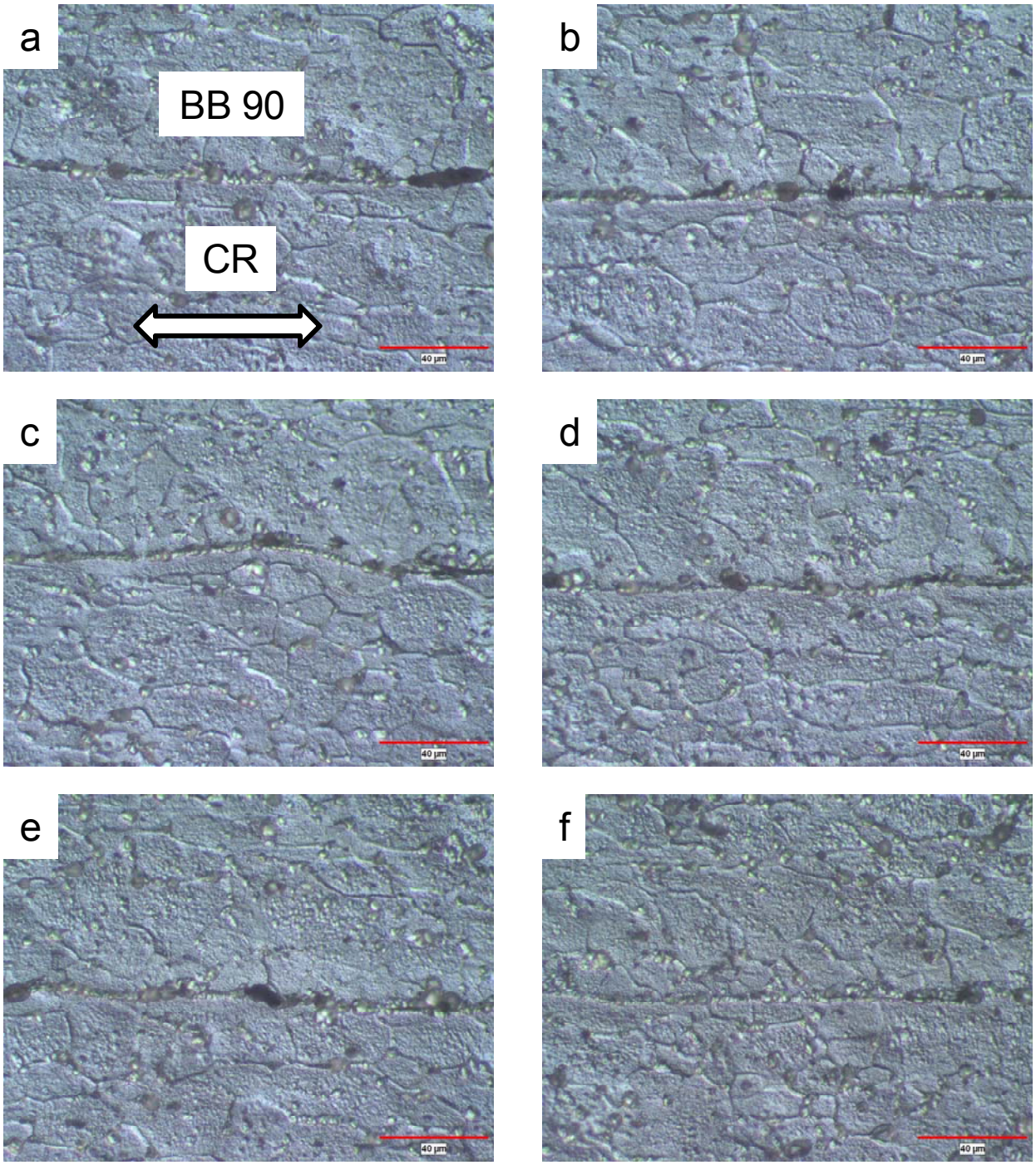

Figure 7.6. LOM images of sandwich 3b1b (bead blasted 90º / cold rolled) in the caustic etched condition (3 V, 15 seconds). These images show no indications of grains that penetrated the bond line. Job 12761, east plane of polish.

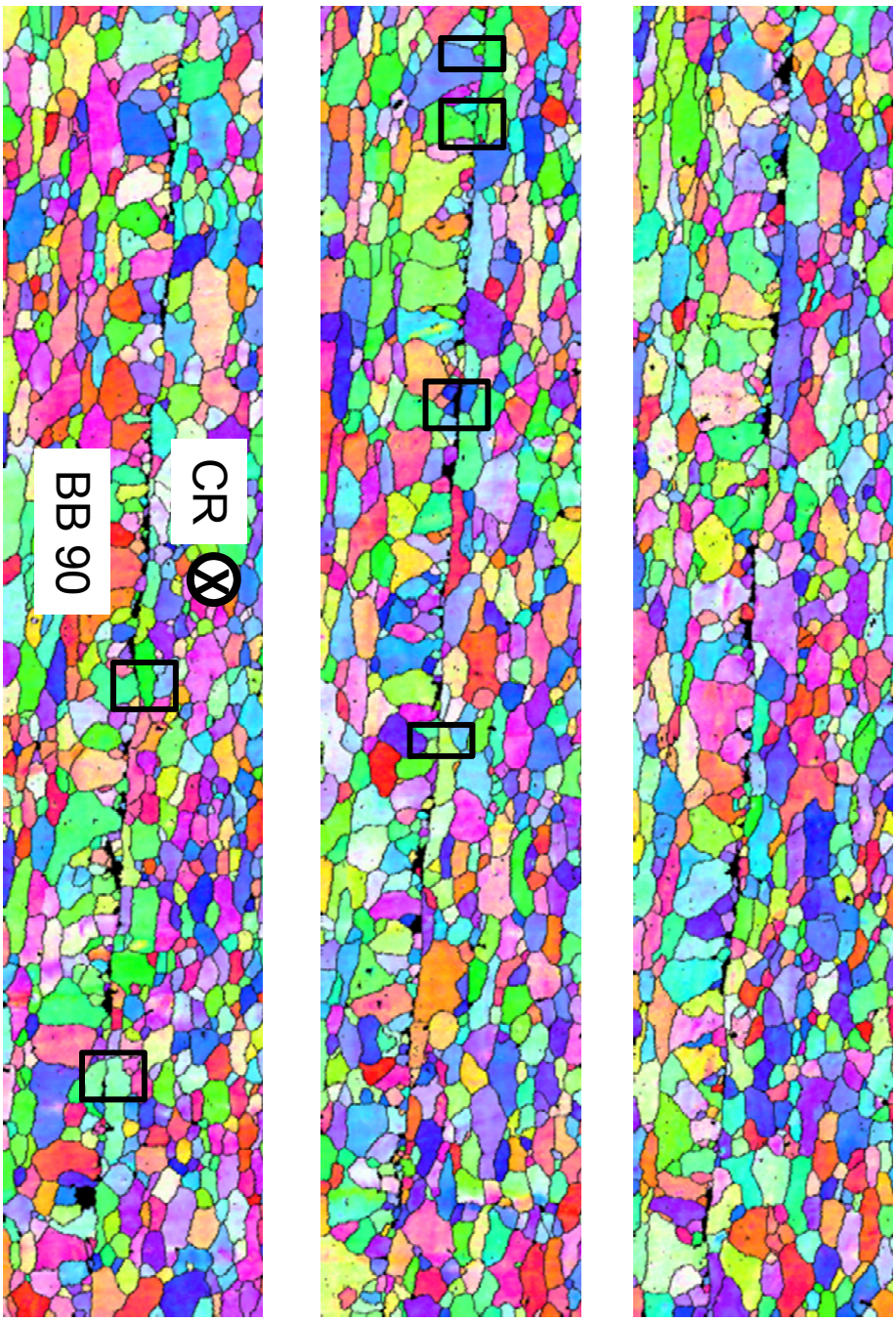

(a) *(b)* *(c)*

Figure 7.7. EBSD images of sandwich 3b1b (bead blasted 90º / cold rolled). The boxed regions are areas of grain penetration (counted on the loose definition only). Images are 1000 × 200 micron. Job 12761, north plane of polish.

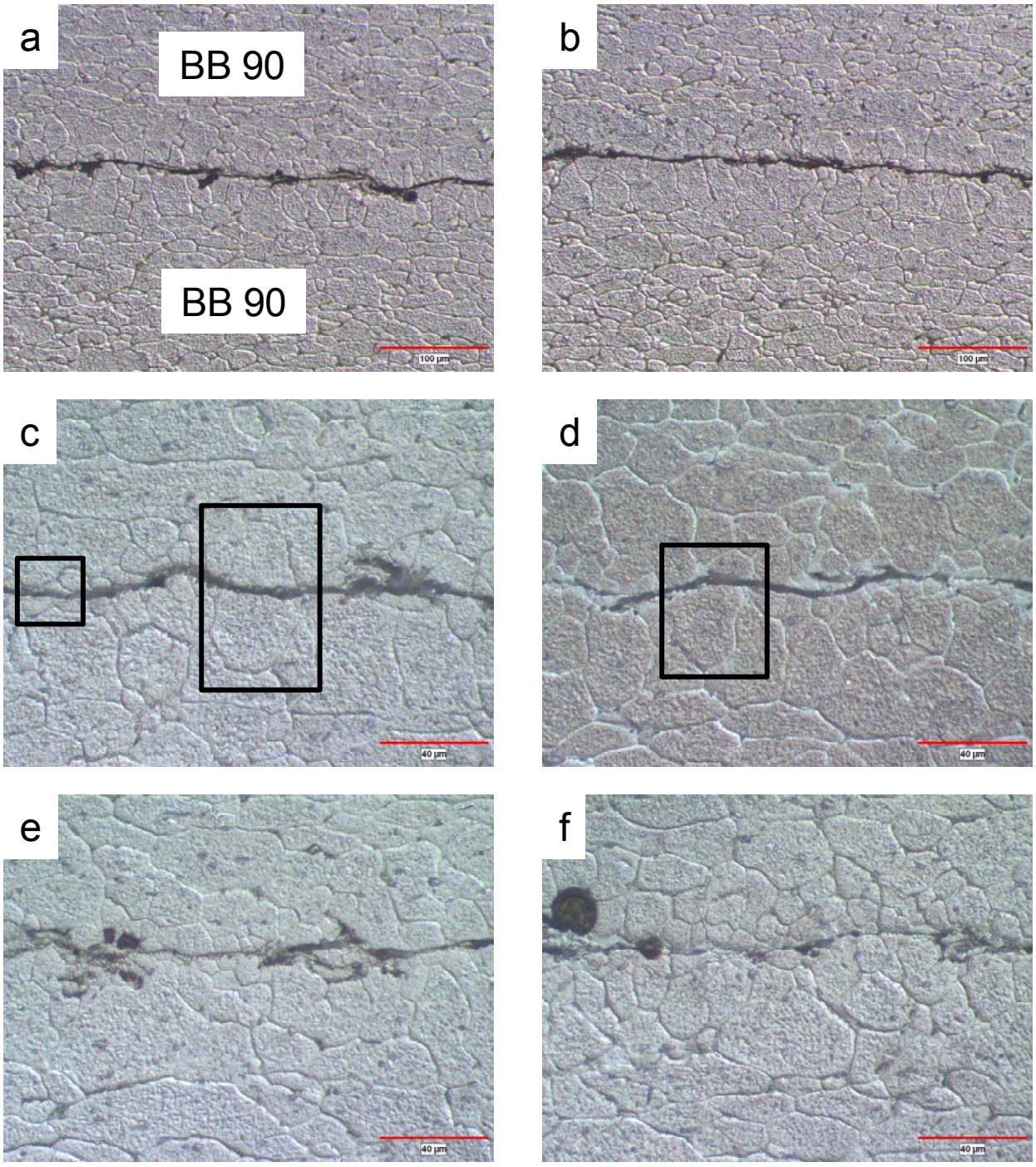

Figure 7.8. LOM images of sandwich 3b2a (bead blasted 90º / bead blasted 90º) in the caustic etched condition (1% NaOH immersion for 5 minutes + 1% NaOH at 4 V for 30 seconds). The boxed regions in (c)-(f) are areas of possible grain penetration (identified on the contact-angle criterion). Job 12761, east plane of polish.

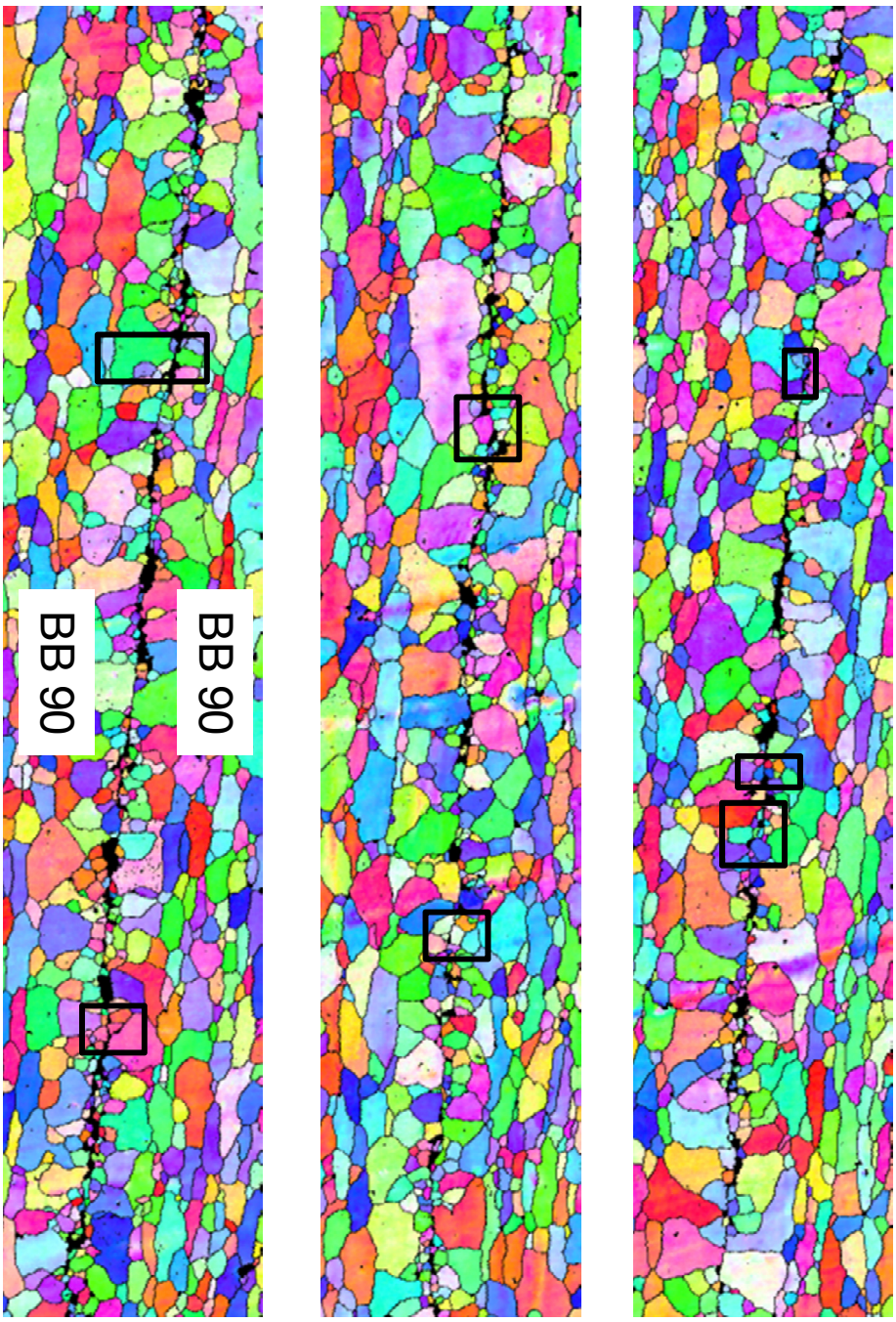

Figure 7.9. EBSD images of sandwich 3b2a (bead blasted 90º / bead blasted 90º). The boxed regions are areas of grain penetration (counted on the loose definition only). Images are 1000 × 200 micron. Job 12761, east plane of polish.

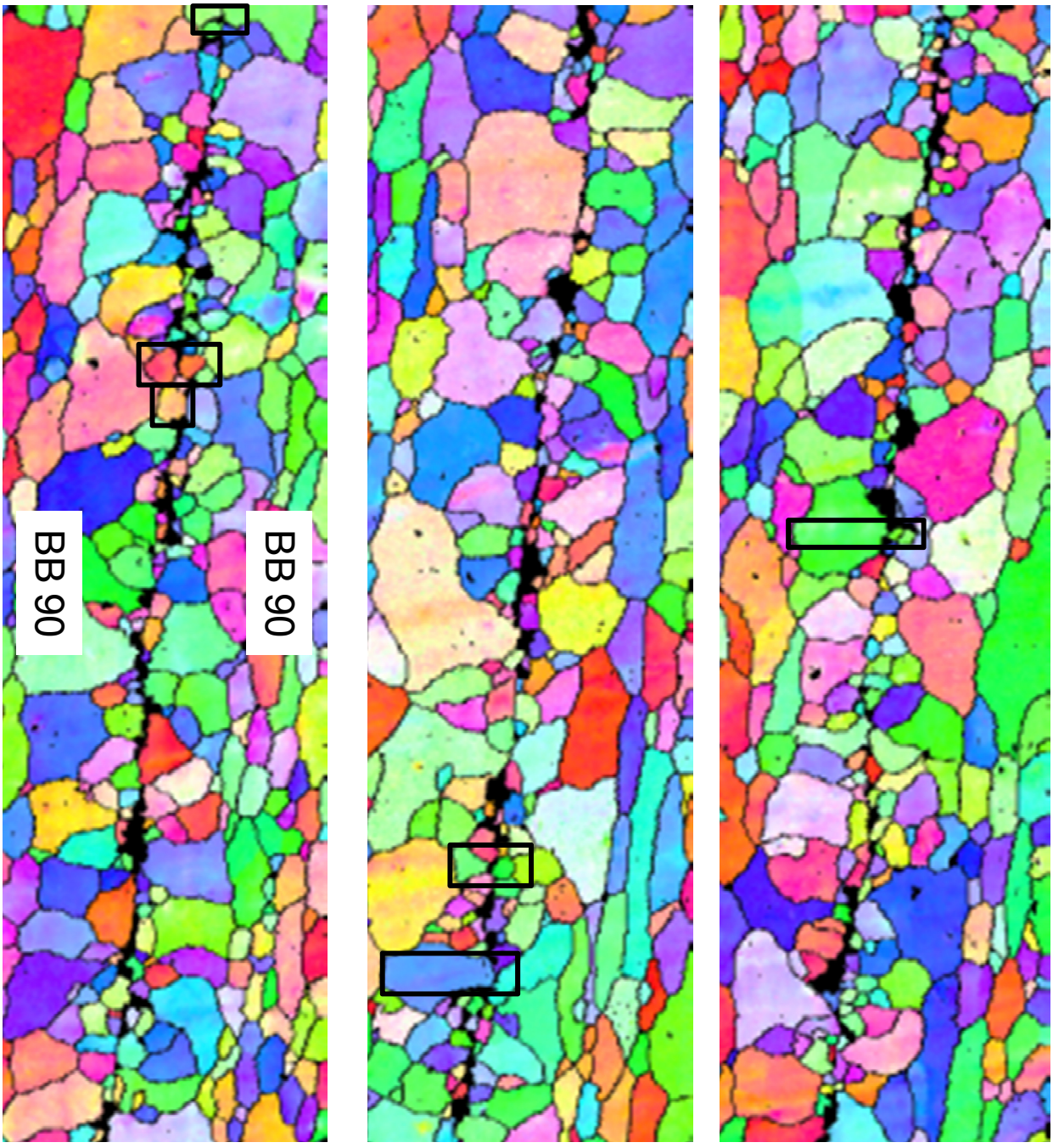

(a) *(b)* *(c)*

Figure 7.10. EBSD images of sandwich 3b2a (bead blasted 90º / bead blasted 90º). The boxed regions are areas of grain penetration (counted on the loose definition only). Images (different regions than those in Figure 7.9) have been magnified to twice the usual magnification. They have been cropped to 500 × 75 micron in this view. Job 12761, east plane of polish.

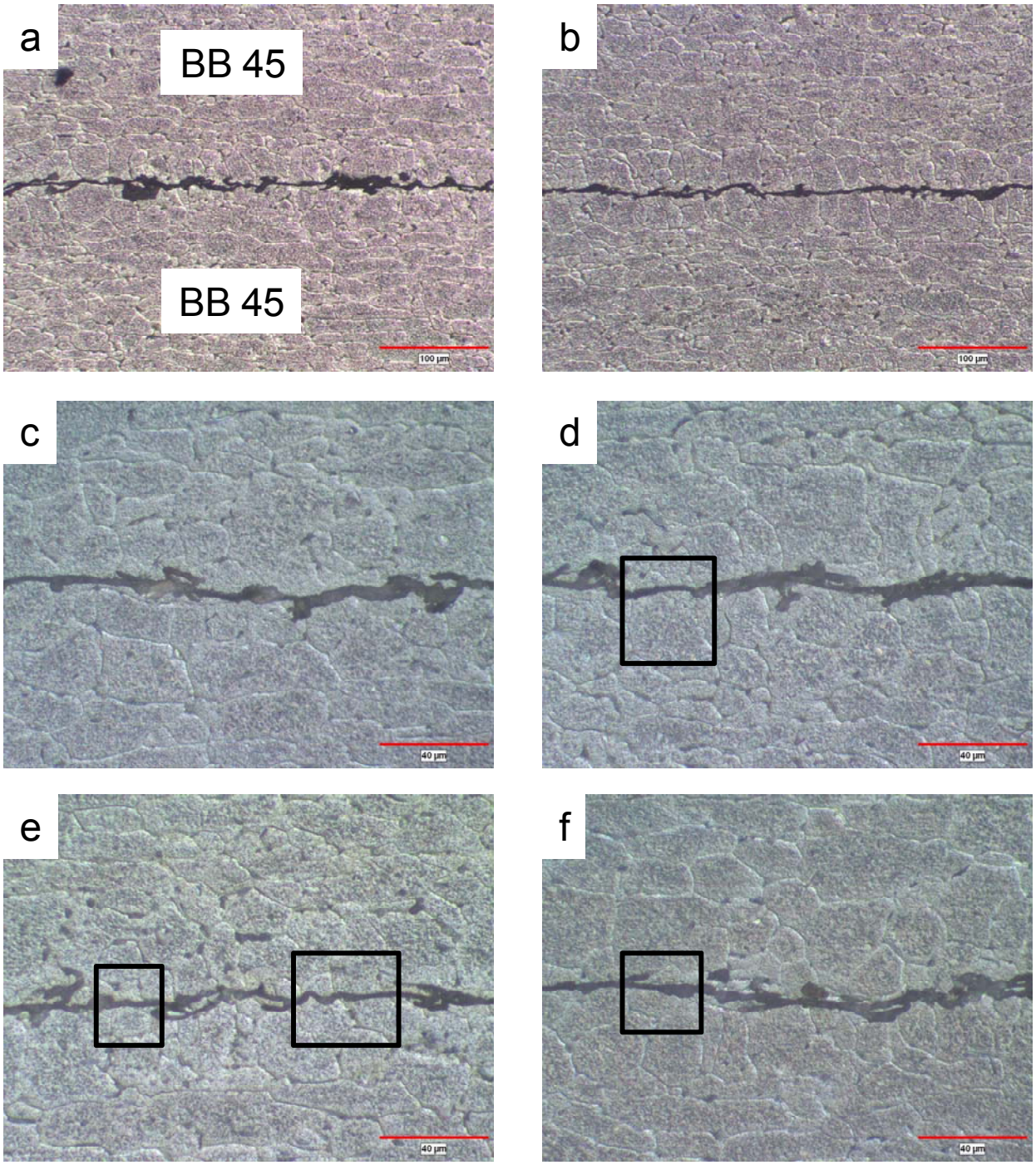

Figure 7.11. LOM images of sandwich 3c2a (bead blasted 45º / bead blasted 45º) in the caustic etched condition (1% NaOH immersion for 7 minutes + 1% NaOH at 4 V for 30 seconds). The boxed regions in (c)-(f) are areas of possible grain penetration (identified on the contact-angle criterion). Job 12761, east plane of polish.

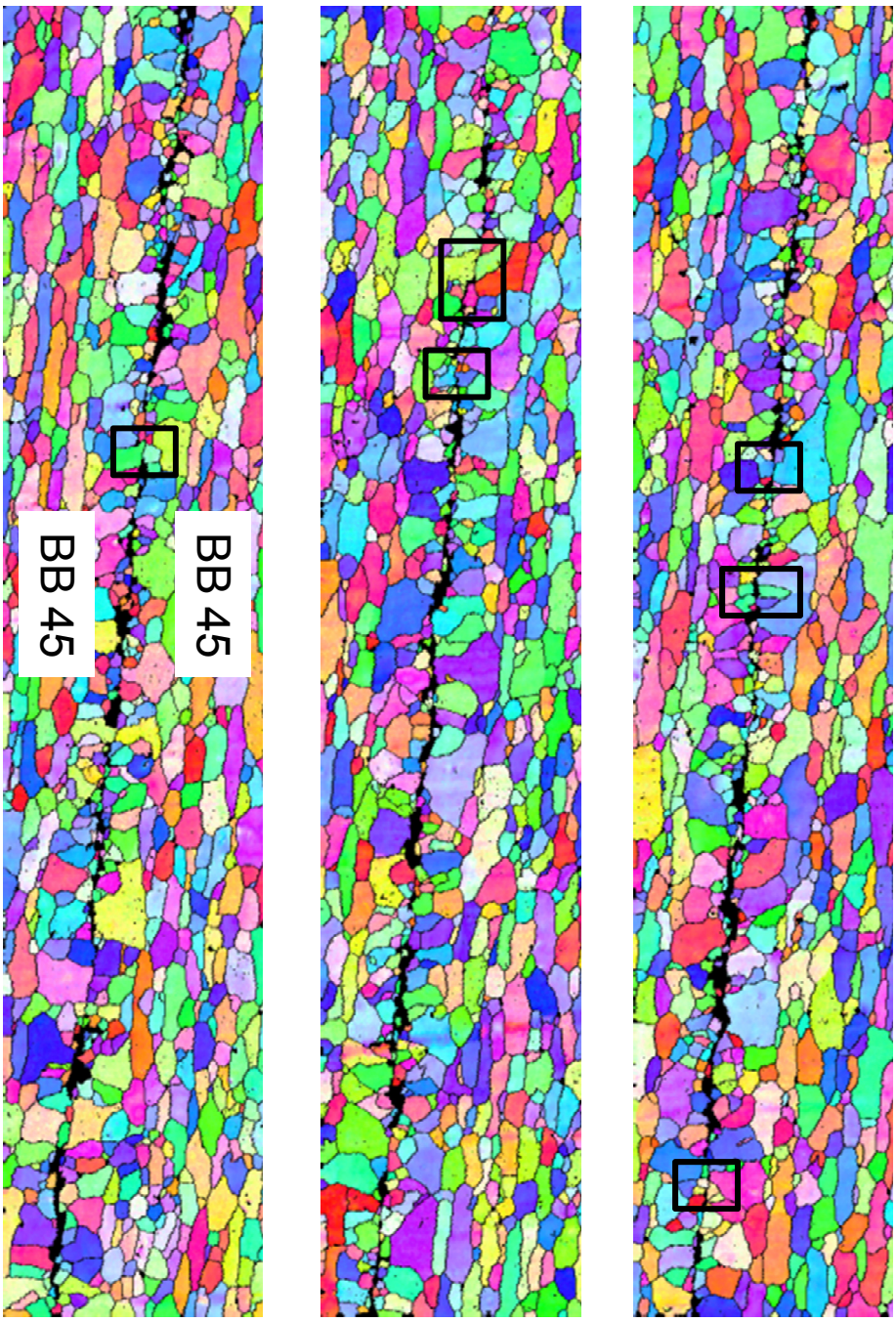

Figure 7.12. EBSD images of sandwich 3c2a (bead blasted 45º / bead blasted 45º). The boxed regions are areas of grain penetration (counted on the loose definition only). Images are 1000 × 200 micron. Job 12761, east plane of polish.

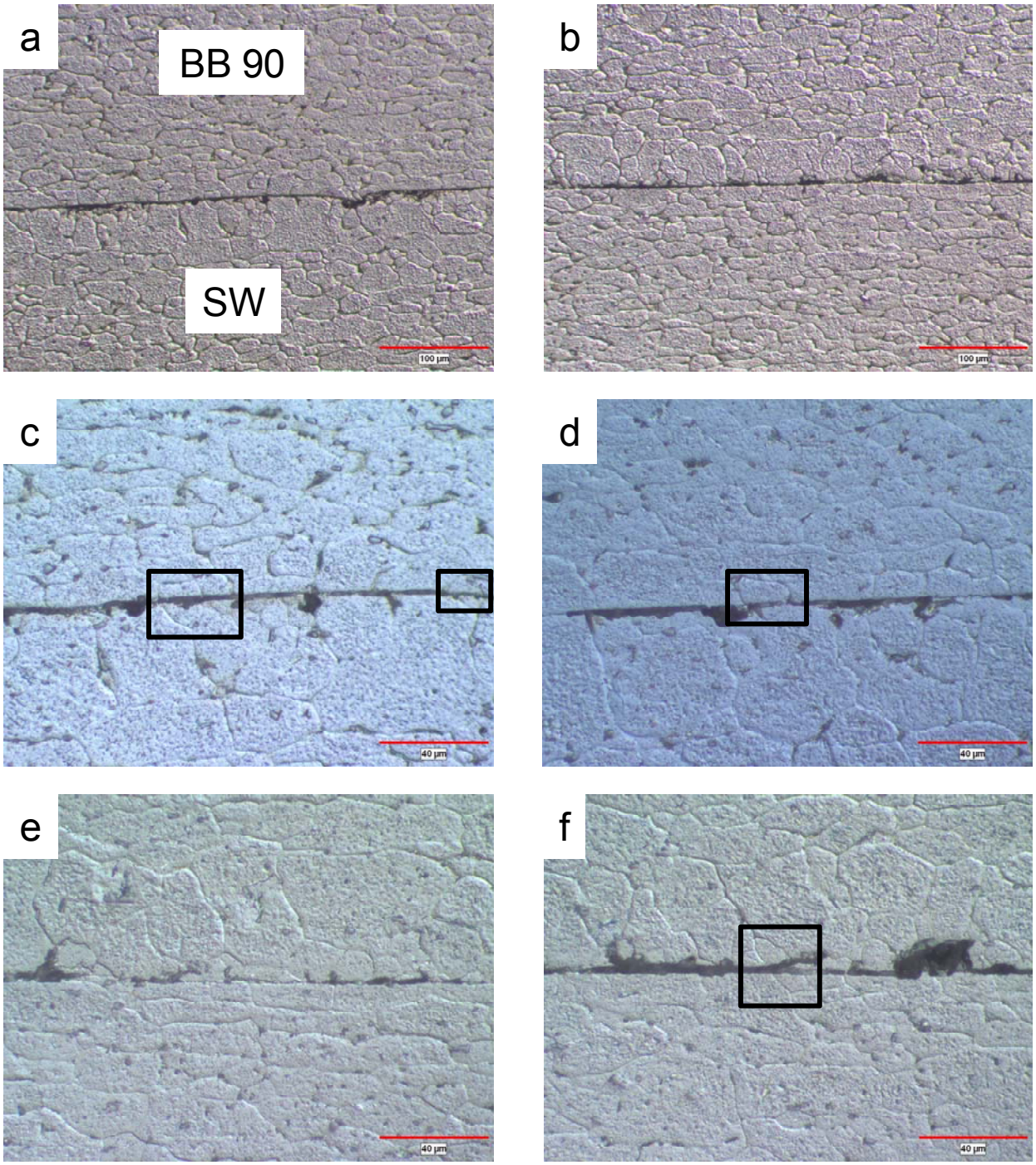

Figure 7.13. LOM images of sandwich 3b2b (bead blasted 90º /steel wool) in the caustic etched condition (1% NaOH immersion for 5 minutes + 1% NaOH at 4 V for 30 seconds). The boxed regions in (c)-(f) are areas of possible grain penetration (identified on the contact-angle criterion). Job 12761, east plane of polish.

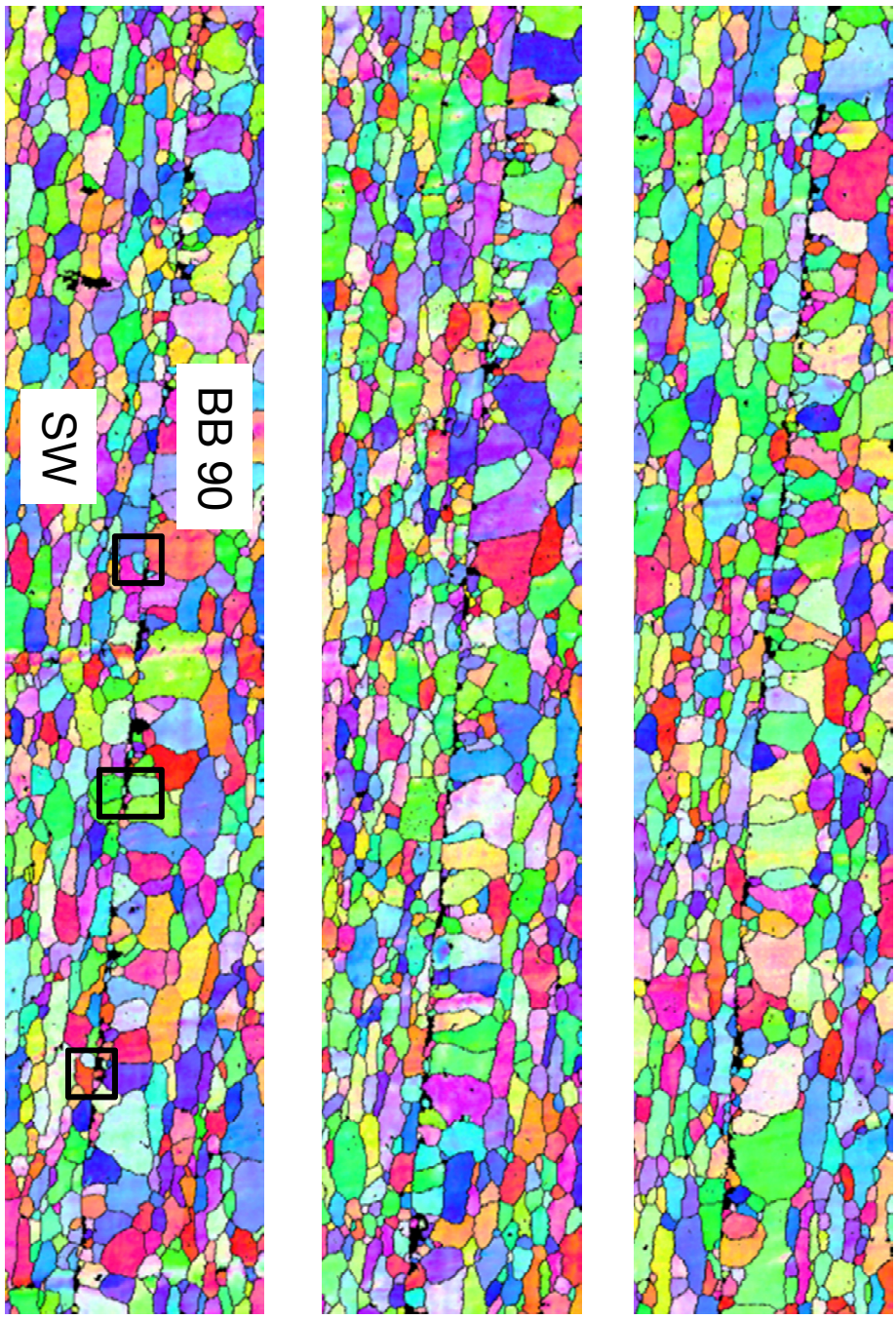

Figure 7.14. EBSD images of sandwich 3b2b (bead blasted 90º /steel wool). The boxed regions are areas of grain penetration (counted on the loose definition only). Images are 1000 × 200 micron. Job 12761, east plane of polish.

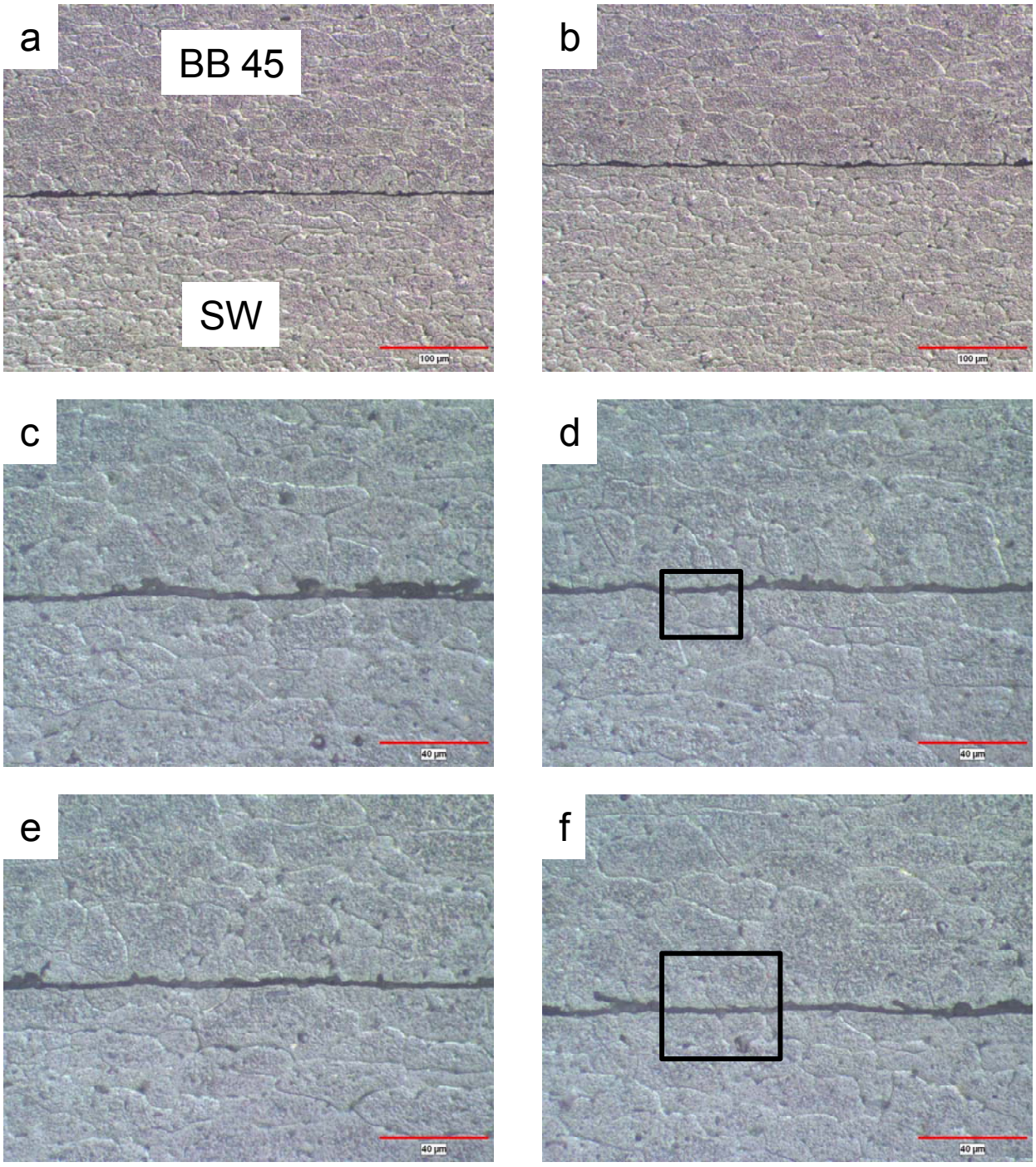

Figure 7.15. LOM images of sandwich 3c2b (bead blasted 45º /steel wool) in the caustic etched condition (1% NaOH immersion for 7 minutes + 1% NaOH at 4 V for 30 seconds). The boxed regions in (c)-(f) are areas of possible grain penetration (identified on the contact-angle criterion). Job 12761, east plane of polish.

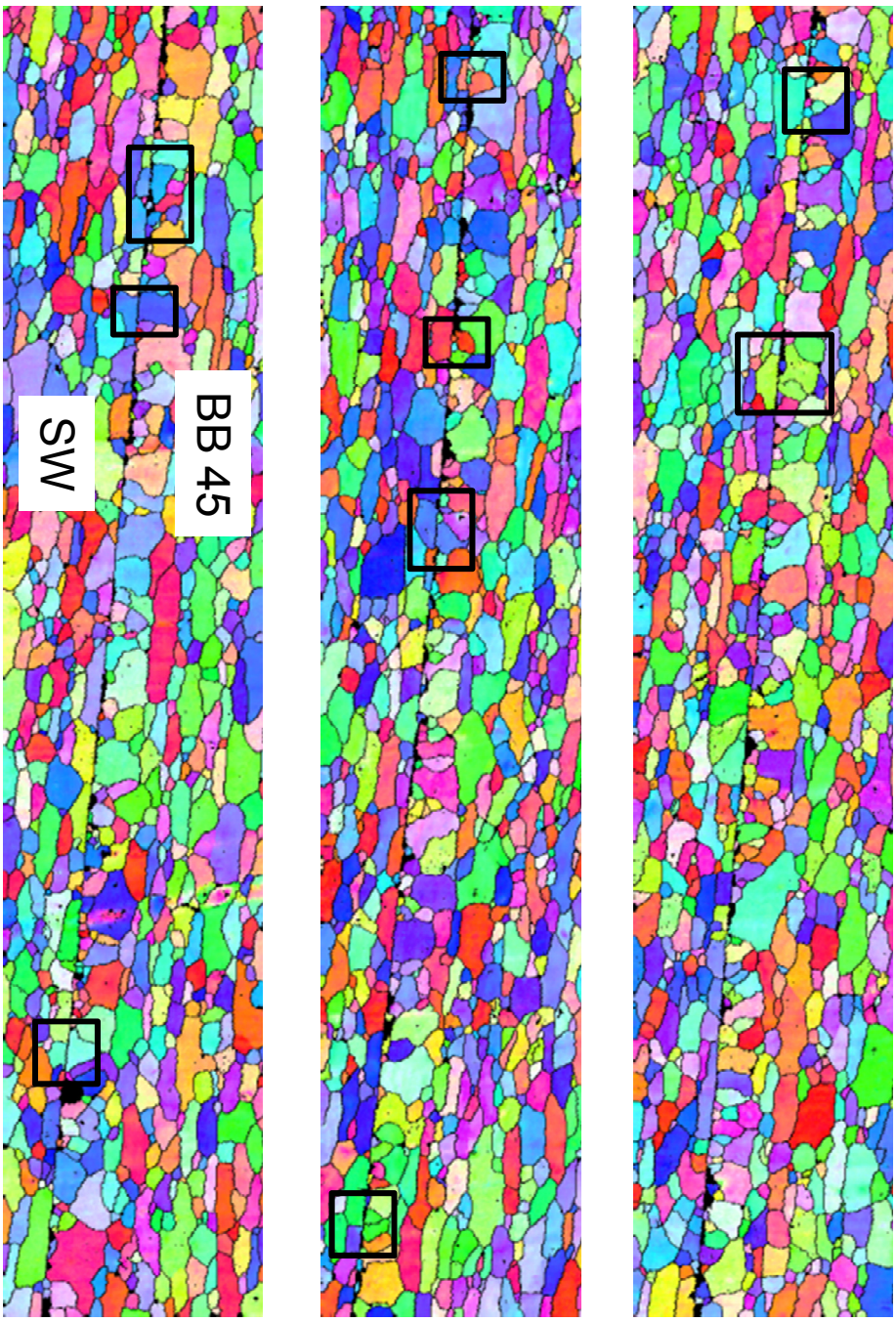

Figure 7.16. EBSD images of sandwich 3c2b (bead blasted 45º /steel wool). The boxed regions are areas of grain penetration (counted on the loose definition only). Images are 1000 × 200 micron. Job 12761, east plane of polish.

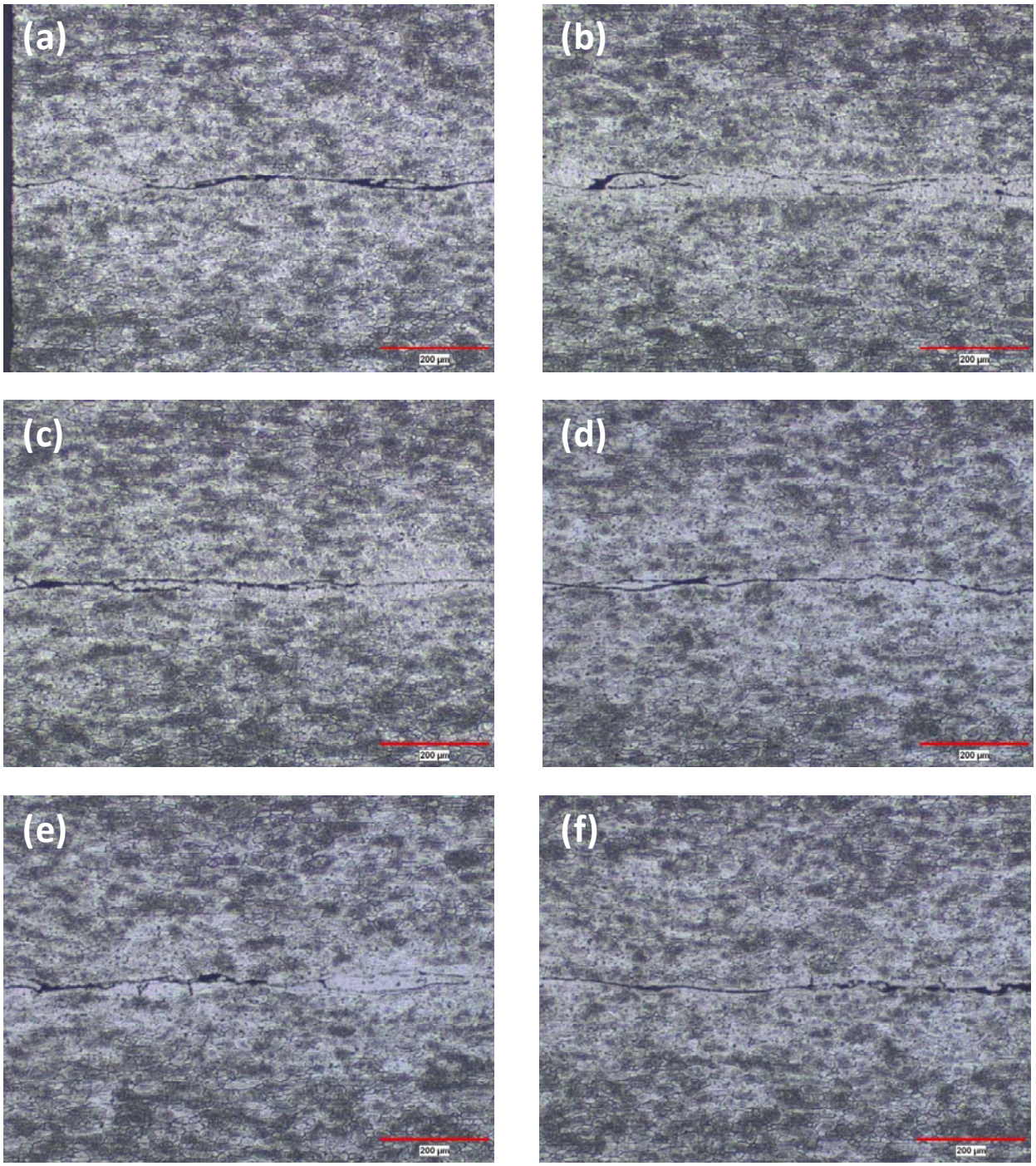

Figure 8.1. LOM image sequence (running left-right then top-bottom) of TA+ESD / TA+ESD (in argon, sandwich 3a2, job 12718-E.)

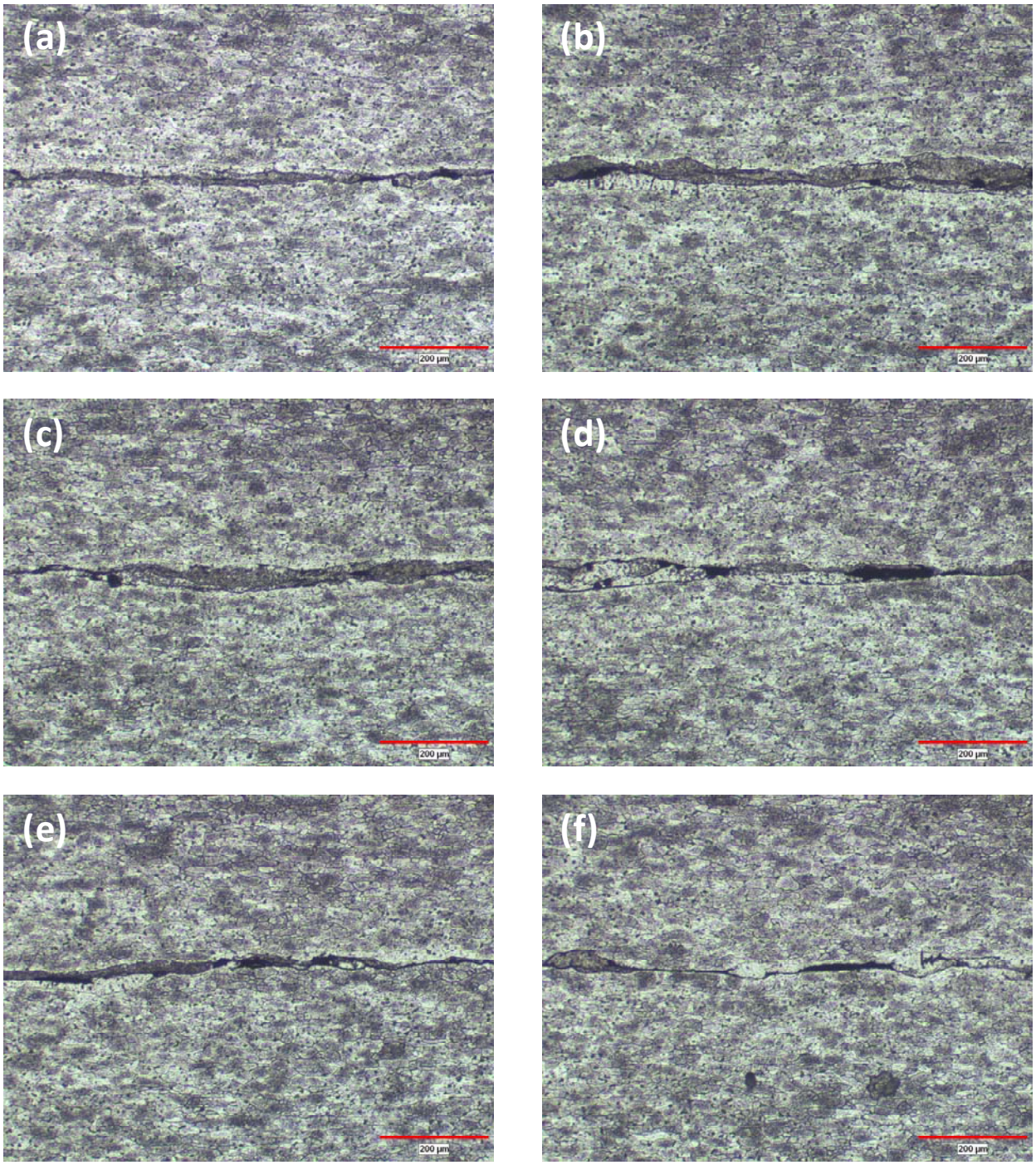

Figure 8.2. LOM image sequence (running left-right then top-bottom) of TA+ESD / TA+ESD (in nitrogen, sandwich 3a3, job 12719-E.)

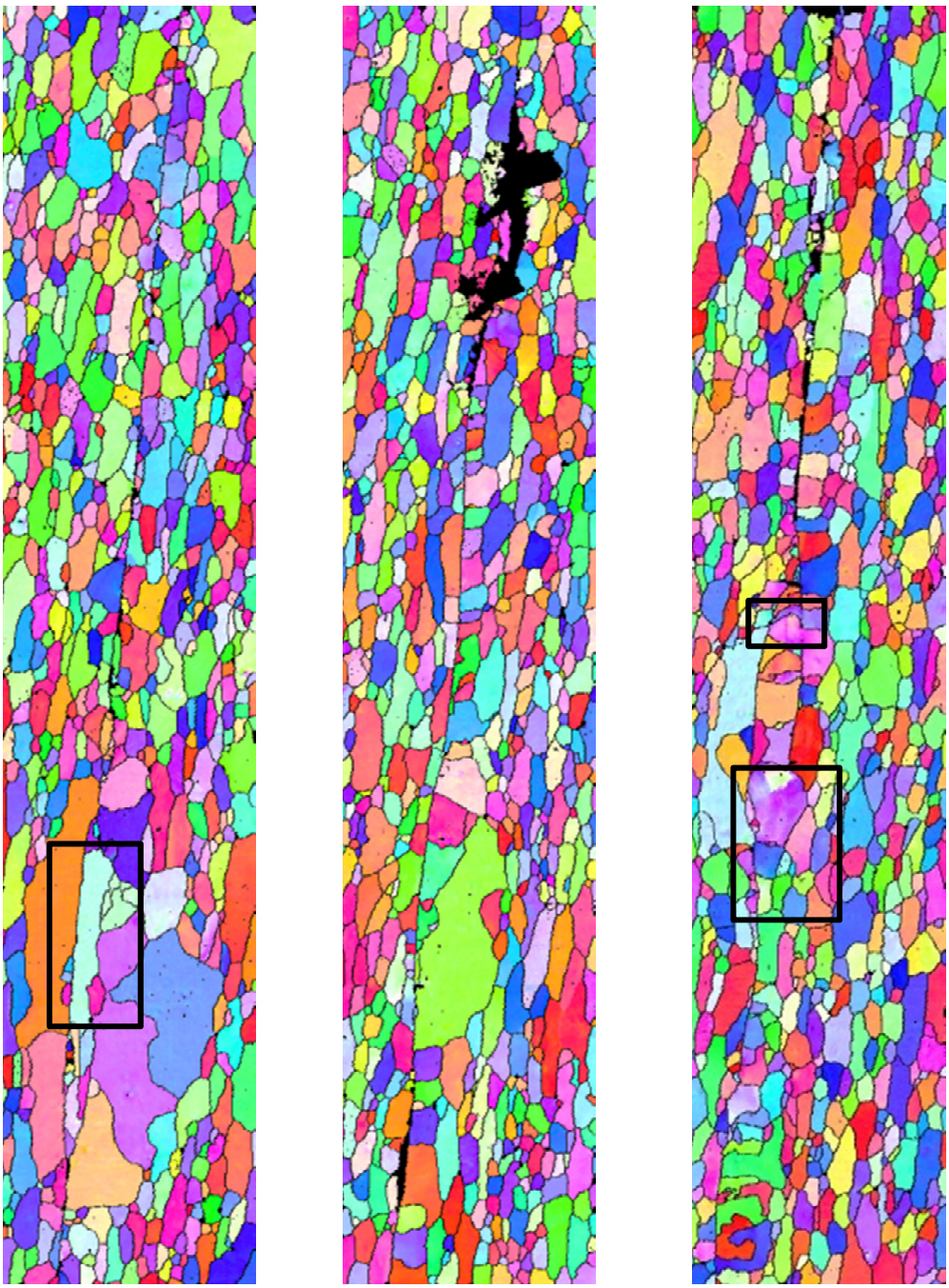

(a) *(b)* *(c)*

Figure 8.3. EBSD of TA+ESD / TA+ESD (in argon., sandwich 3a2, job 12718-E. The boxed regions are areas of grain penetration. Images are 1000 micron tall × 200 micron wide.

APPENDIX 1. COMPLETE SCANS OF LANL CLEANED BASELINE CONDITION

For the sake of completeness, the entire image set taken from one orientation (1L) of the LANL cleaned baseline condition is presented in Figures A1.1 and A1.2. A comparable LOM montage obtained in the other orientation (1T1) looked similar to that in the 1L orientation (Figure A1.1.)

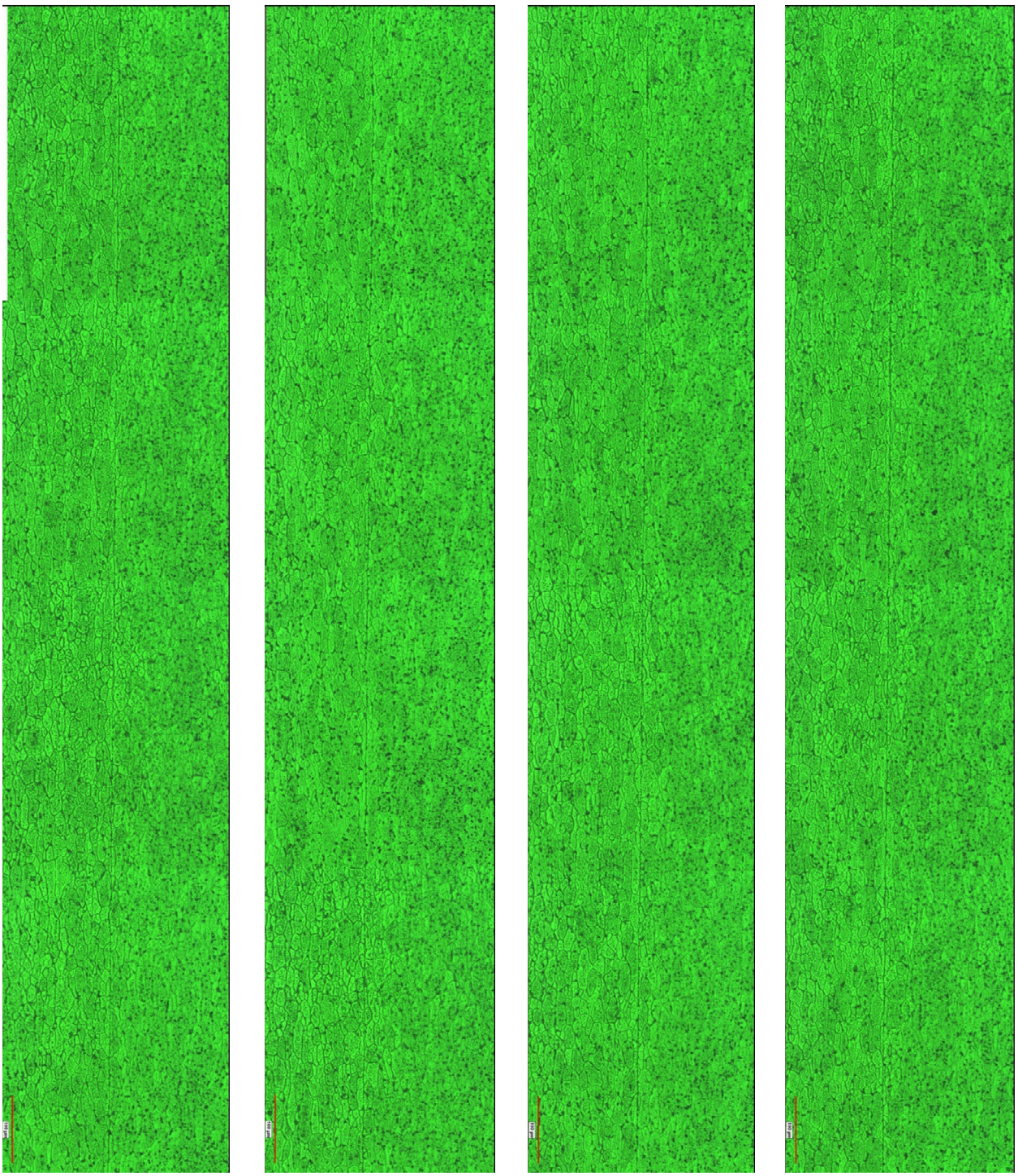

(a) *(b)* *(c)* *(d)*

Figure A1.1. LOM montage, job 12556-1yL. The image sequence runs top to bottom of each image foursome, and then left to right. Acid etched.

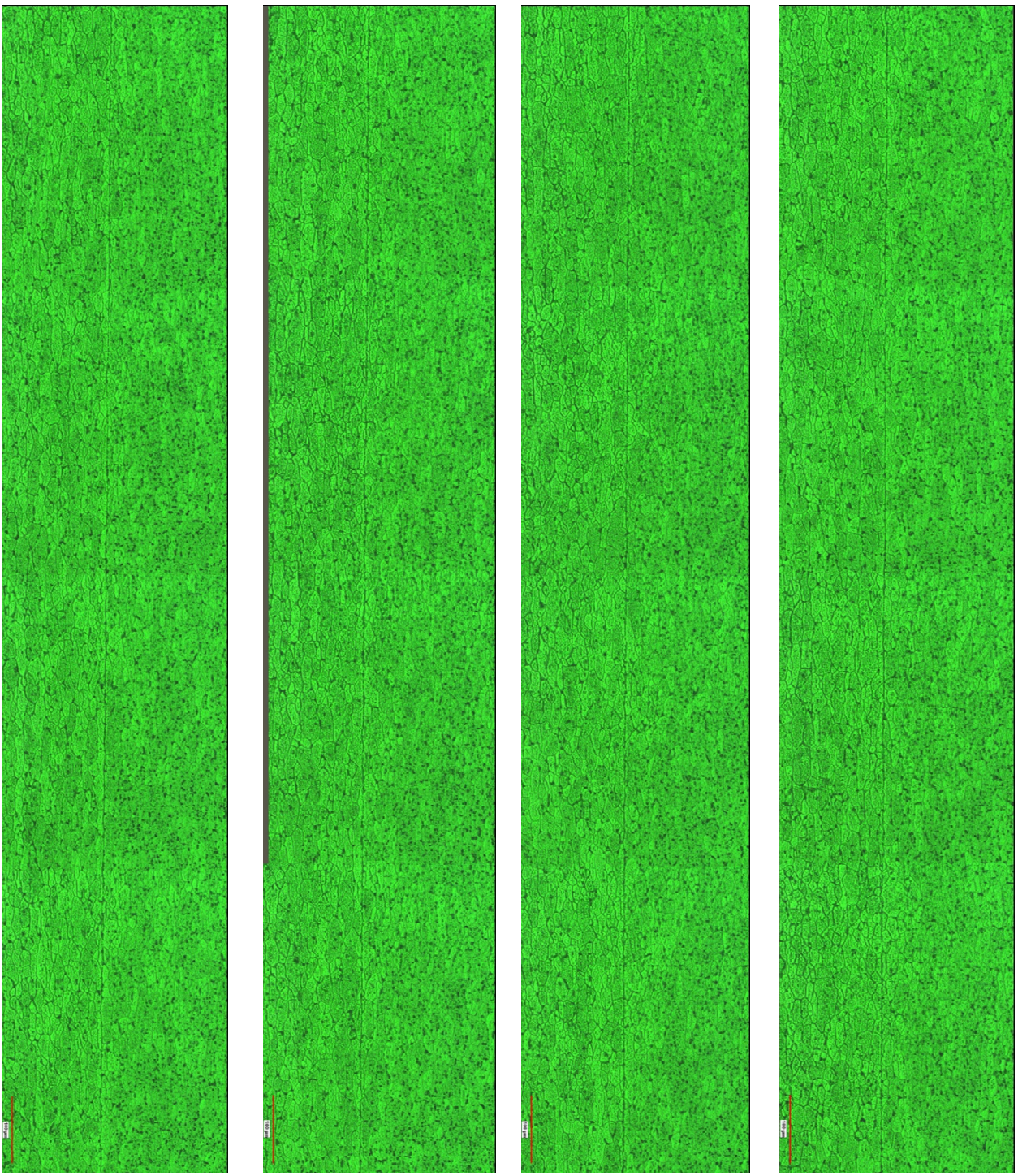

(e) *(f)* *(g)* *(h)*

Figure A1.1 (cont'd). LOM montage, job 12556-1yL.

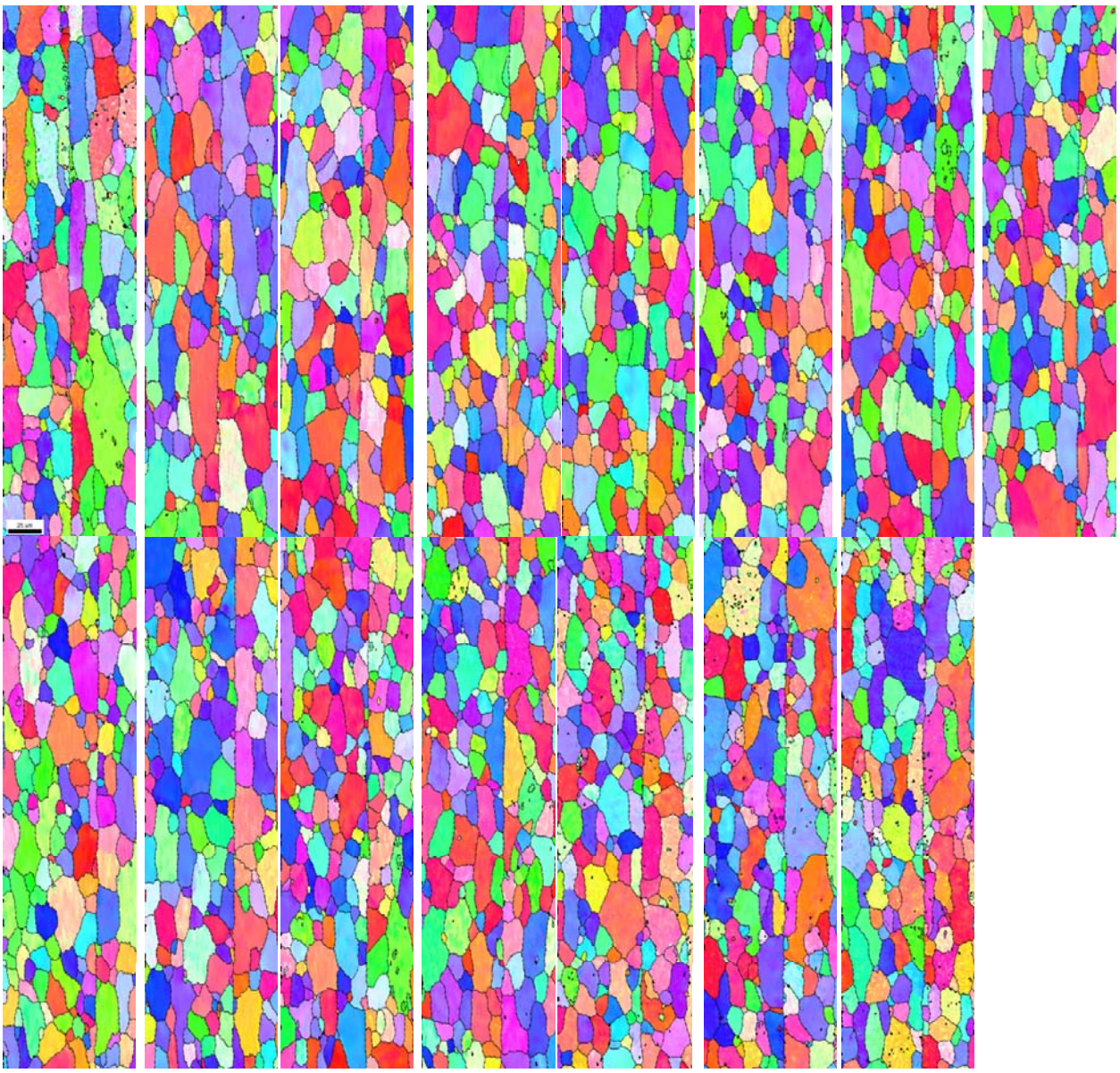

Figure A1.2. Complete EBSD scan, job 12556-1yL. Although this is not a montage since adjacent images do not overlap, the relative order of images along the bond line runs left to right and then top to bottom. Each image is 400 microns tall.

APPENDIX 2: FINITE-ELEMENT MODELING OF MACROSCOPICALLY GROOVED ALUMINUM DURING HIP

A2.1. Overview

Finite-element modeling (FEM) was used to examine material flow during the HIP cycle for variety of prospective macroscopically-grooved geometries. The top and bottom aluminum cladding geometries were modified to create lateral displacement between the surfaces. This displacement will aid in breaking up the surface oxide layers on each plate and promote grain penetration across the aluminum-aluminum interface. Finite element simulations were employed to evaluate geometry modifications and select geometries to be included in experiments.

To properly model the process at temperature, properties for aluminum 6061 and 304 stainless steel at the highest temperature available were used as shown in Table A.1.

Table A2.1. Room-temperature and elevated-temperature material properties for Al and stainless steel.

Material	Temp (^{o}C)	E (GPa)	Sy (MPa)	Su (MPa)	%el
304L SS	RT	193	186	482	42
304L SS	560	152	117	310	58
Al 6061-T6	RT	70	275	310	20
Al 6061-T6	371	47	12.4	20.6	98

The finite element simulation applies a 15 ksi load to the outside can to compress and bond the internal components. Because of the large number of contacts and gaps in the model, convergence is difficult at best. All simulations presented here were loaded to approximately 6.55ksi before the simulation failed due to numerical problems. While the simulations did not run to completion, the results at 6.55 ksi of loading can be used to help make an intelligent decision concerning which geometry configurations are best.

A2.2. Initial studies

The baseline case is two flat plates with the fuel meat sandwiched between. For every layer included in the fuel and cladding stackup additional contact surfaces are added to the simulation, increasing simulation nonlinearity and thus convergence difficulty. To simplify matters as much as possible, solid aluminum assemblies including the expected gaps are used in the simulation models. For instance, Figure A2.1 shows a schematic and two enlarged contour views of the baseline case which considered two flat aluminum plates with a fuel element sandwiched between creating a 0.01″ (=10 mil) gap between the plates. This is the simplest possible geometry for the fuel-cladding assembly.

Note that Figures A2.1-A2.7 show the half-plate in (a) and a zoomed-in area in (b) and (c).

Figure A2.2 shows an alternative geometry exploring a tapered geometry such that the cladding touches at the edge of the fuel and opens up to a gap of 0.01″ at the can interface. The intention of this geometry is to create space close to the outside edge of the cladding for material to flow into as the can and contents are compressed.

Figure A2.3 shows a modification to the geometry shown by Figure A2.2. In Figure A2.3, the bottom cladding plate is shortened to create more space for material flow and to create an asymmetric geometry to influence material flow in opposite directions.

Figure A2.4 shows another case investigating a tapered geometry. In this case, the cladding touches on the outside edges far from the fuel plates. The intention of this geometry is to influence material to flow toward the fuel giving good contact and bonding between the cladding layers around the edge of the fuel.

Figure A2.5 shows a variation of the tapered geometry case shown by Figure A2.4. An additional gap is created at the end of the bottom cladding plate in an effort to create some additional space for lateral extrusion of the bottom plate.

Figure A2.6 shows an iteration of the cladding geometries that considers a triangular shape with the apex of the upper and lower triangles touching at the midpoint between the edge of the fuel and the edge of the cladding. The intention of this geometry is to create material flow back toward the edge of the fuel and toward the outer edge of the cladding.

Figure A2.7 shows a modification to the geometry considered by Figure A2.6. In addition to a triangular shape for the upper and lower cladding surfaces, the lower cladding is trimmed leaving a gap between the edge of the cladding and the wall of the can.

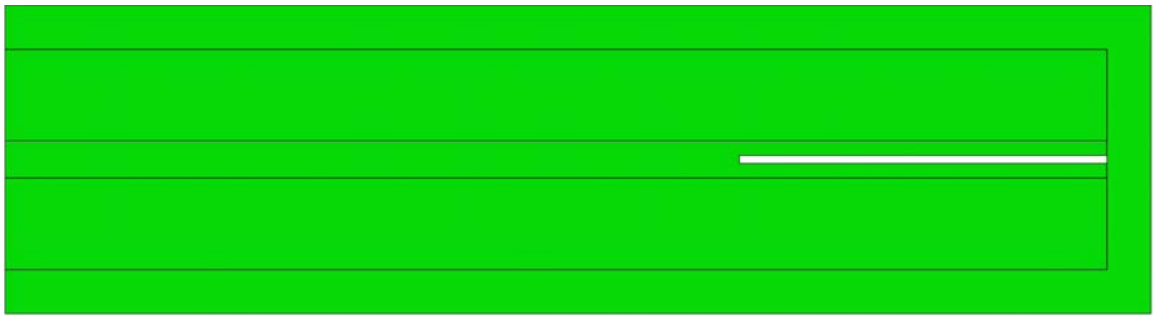

a.

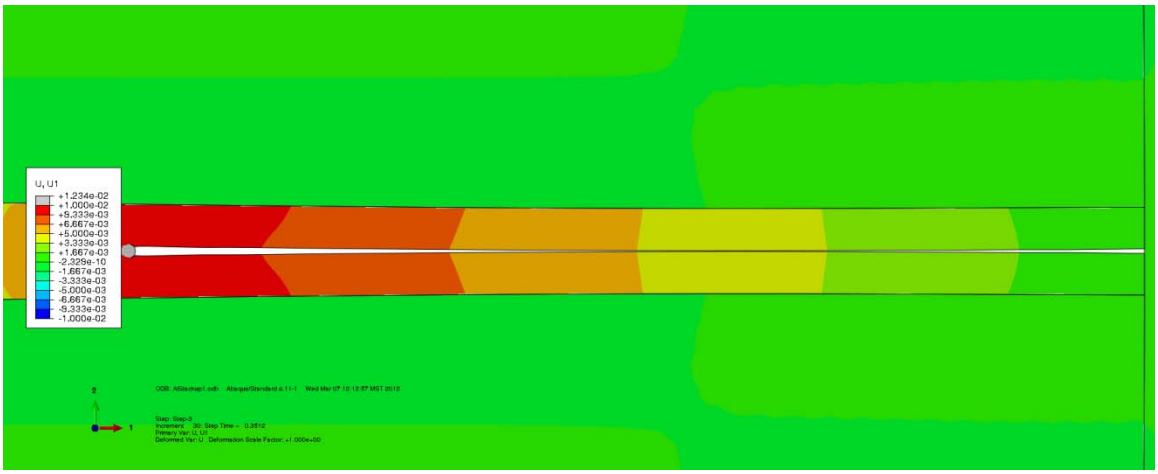

b.

c.

Figure A2.1. Baseline case considering flat plates. (a) shows a plan view of the entire plate geometry, (b) shows a closeup of the displacement profile at the ends of the plates after loading and (c) shows a closeup of the logarithmic shear strain profile at the ends of the plates after loading. Shear stains in the baseline case are small and the displacements are in the same direction.

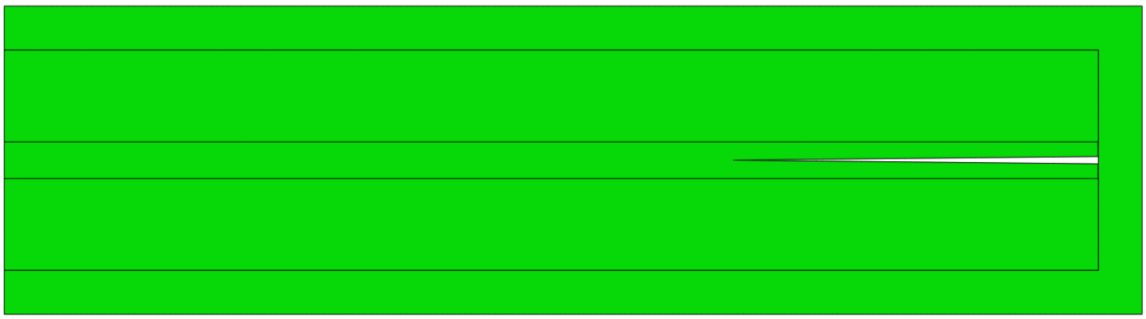

a.

b.

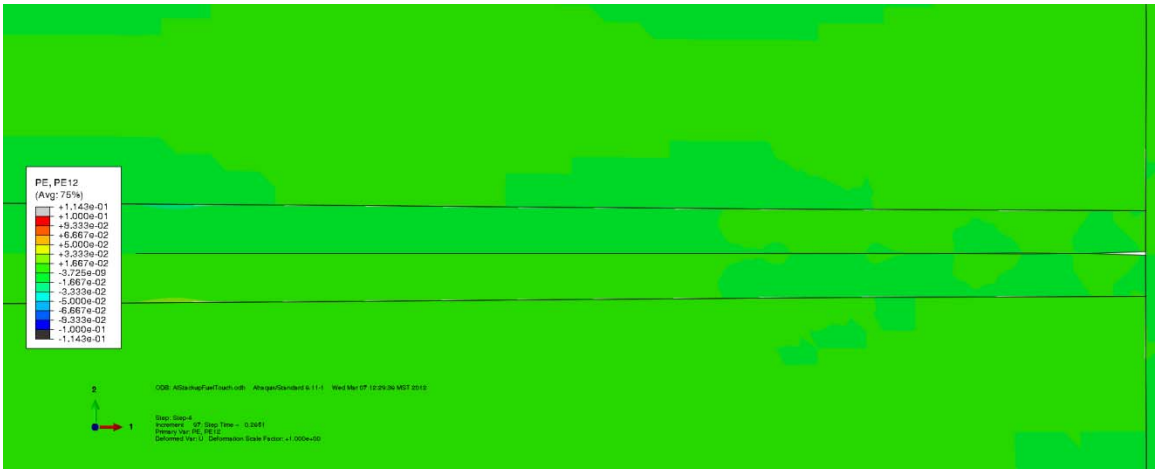

c.

Figure A2.2. Case considering a taper that touches at the fuel. (a) shows a plan view of the entire plate geometry, (b) shows a closeup of the displacement profile at the ends of the plates after loading and (c) shows a closeup of the equivalent plastic shear strain profile at the ends of the plates after loading. (b) shows that displacements in this case are small and (c) shows that shear strains are small for this geometry.

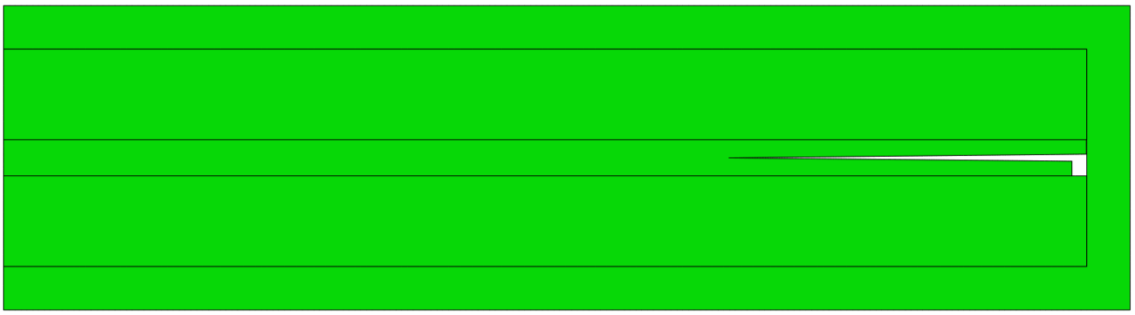

a.

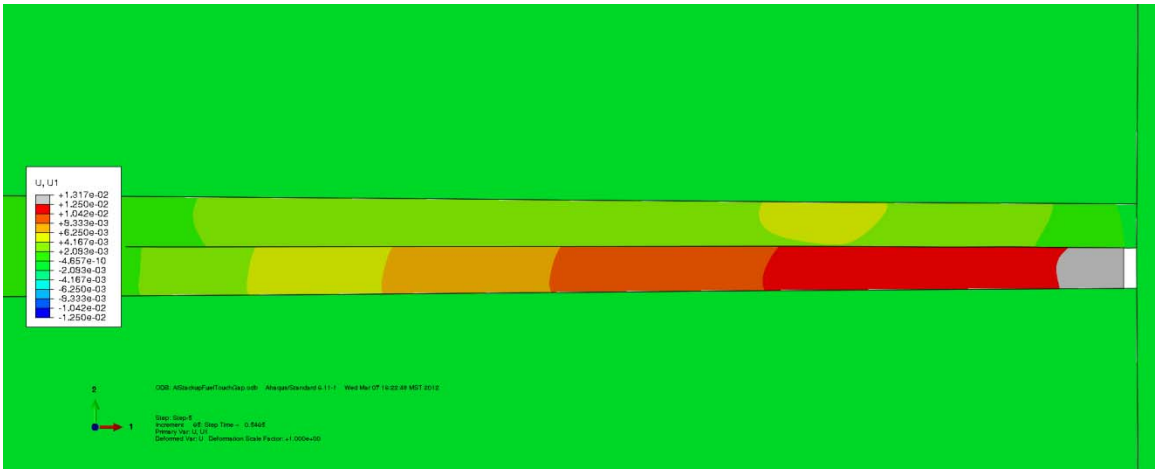

b.

c.

Figure A2.3. Case considering a taper that touches at the fuel with a gap at the right end of the bottom cladding. (a) shows a plan view of the entire plate geometry, (b) shows a closeup of the displacement profile at the ends of the plates after loading and (c) shows a closeup of the equivalent plastic shear strain profile at the ends of the plates after loading. (b) shows that adding the gap increased the displacements as the bottom plate extrudes into the open space (c) shows that shear strains are small for this geometry.

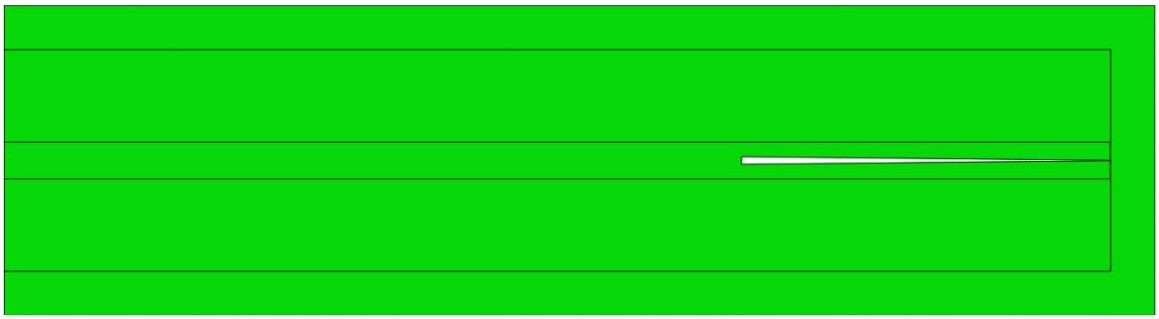

a.

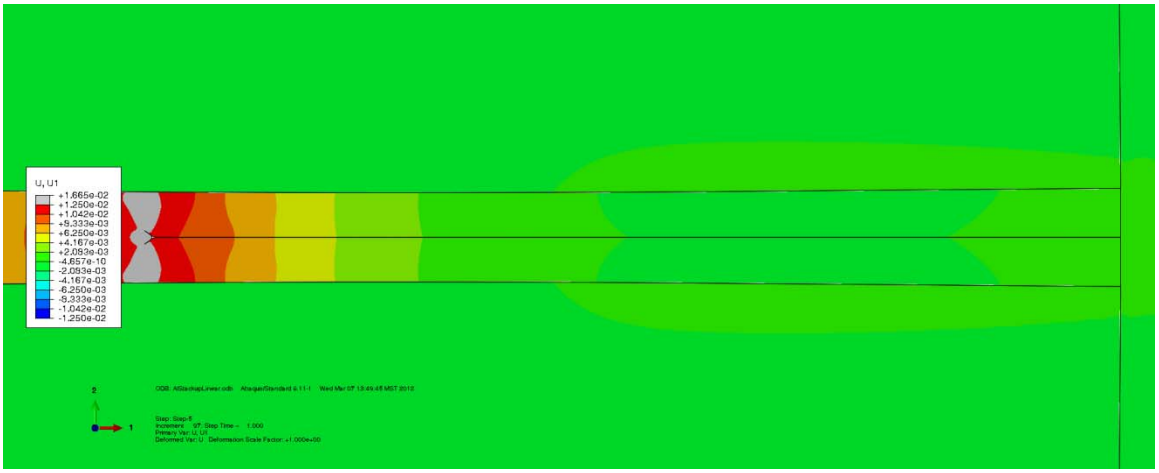

b.

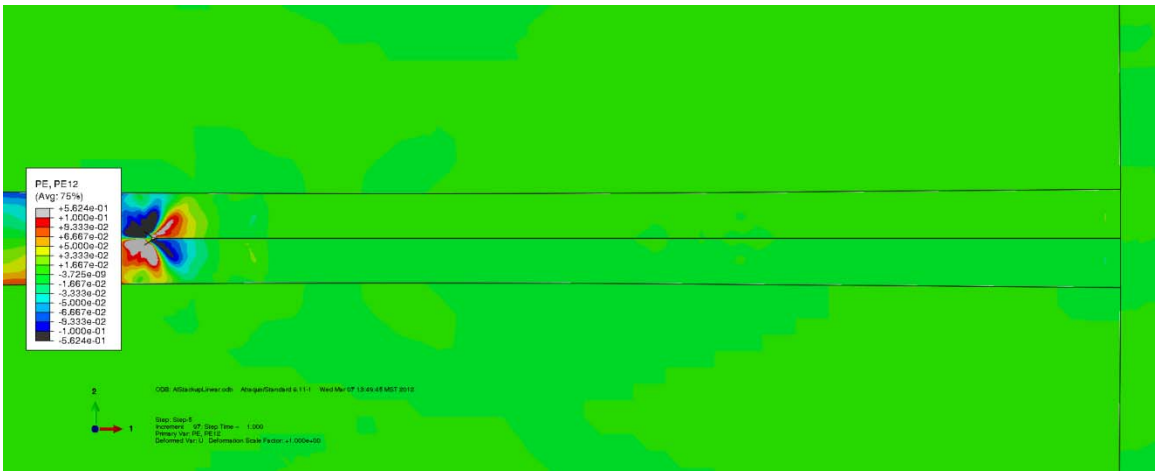

c.

Figure A2.4. Case considering a taper that touches at the fuel-cladding interface. (a) shows a plan view of the entire plate geometry, (b) shows enlarged view of the displacement profile at the ends of the plates after loading and (c) shows an enlarged view of the equivalent plastic shear strain profile at the ends of the plates after loading. (b) shows that for displacements along the fuel-cladding bond line are in the same direction (c) shows that shear strains are small for this geometry.

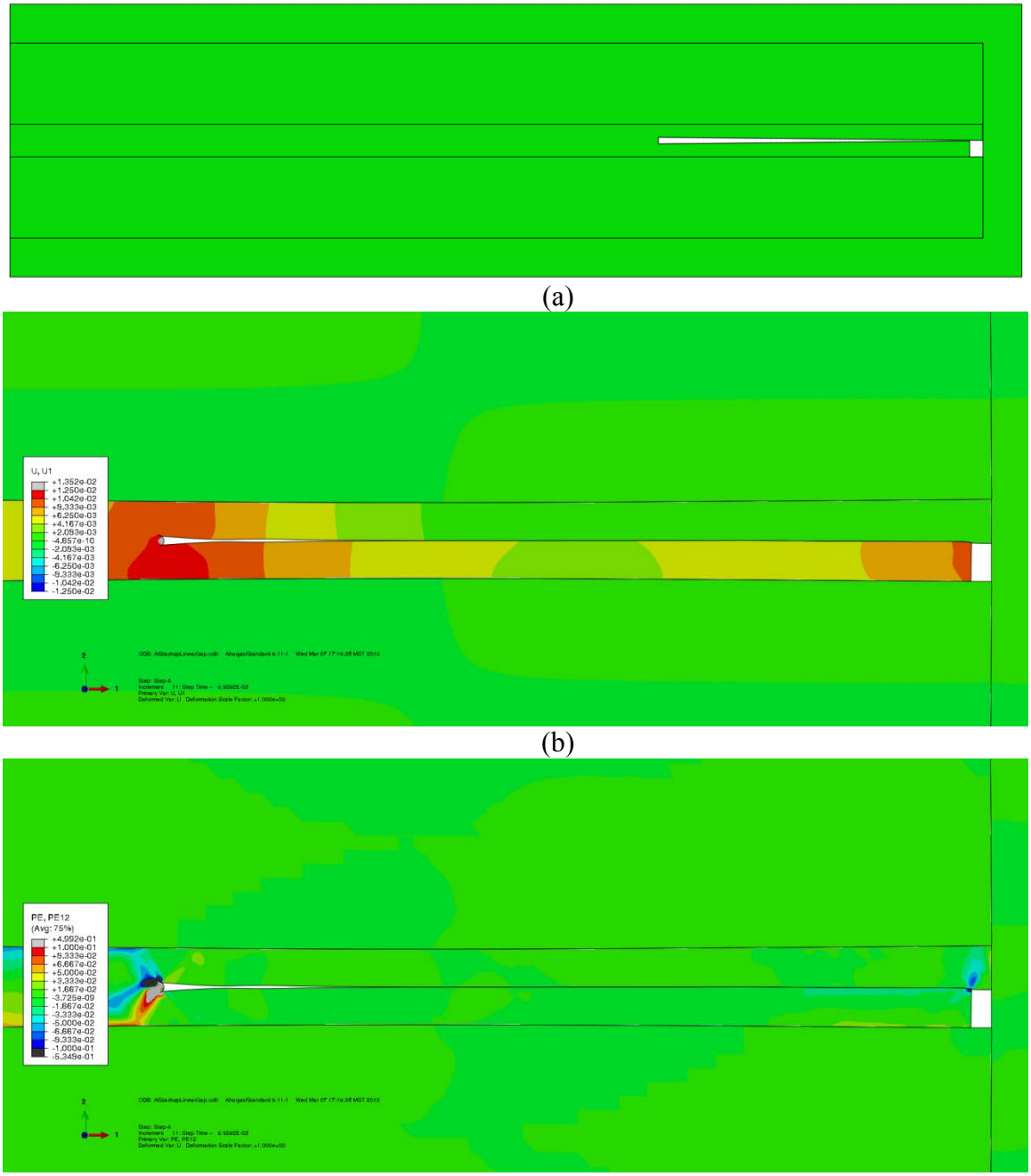

Figure A2.5. Case considering a taper that touches at the fuel-cladding interface. (a) shows a plan view of the entire plate geometry, (b) shows enlarged view of the displacement profile at the ends of the plates after loading and (c) shows an enlarged view of the equivalent plastic shear strain profile at the ends of the plates after loading. (b) shows that creating the gap at the end of the bottom cladding plate does increase displacements of the bottom plate and gives an asymmetric displacement profile (c) shows that although there is some improvement over case D, shear strains are small for this geometry.

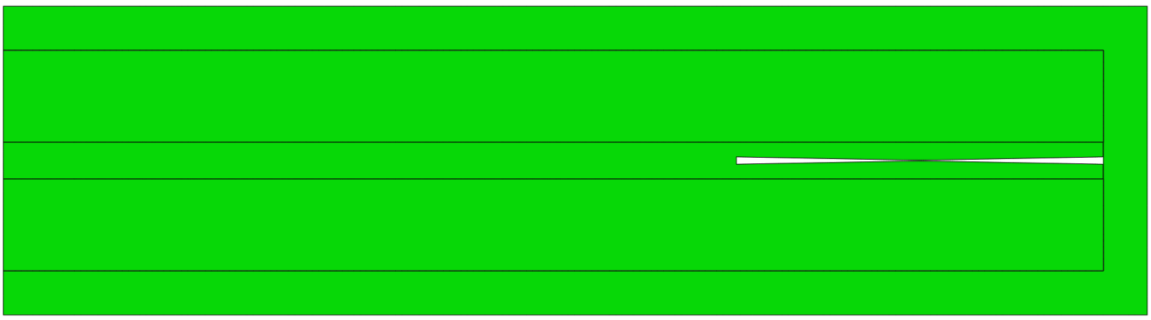

(a)

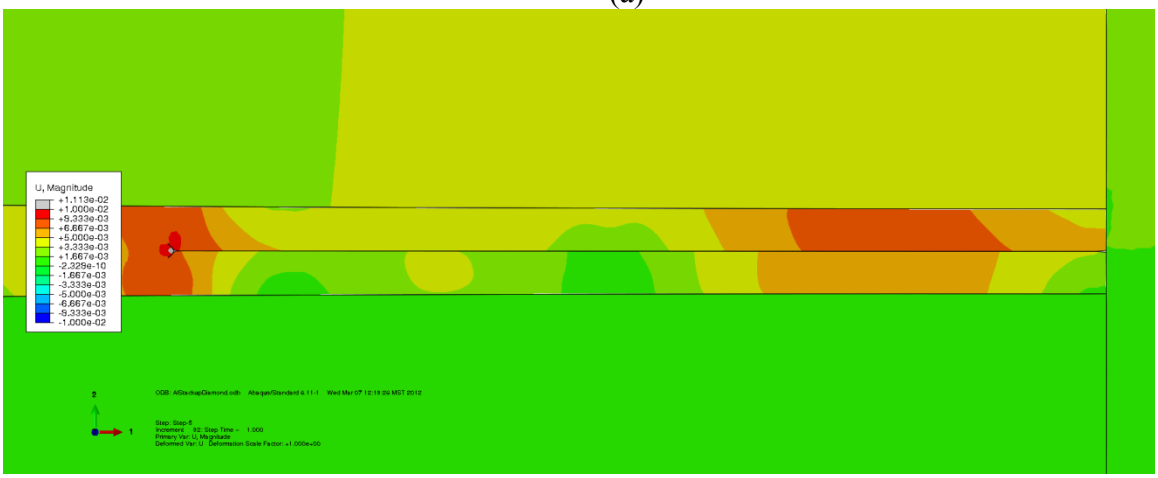

(b)

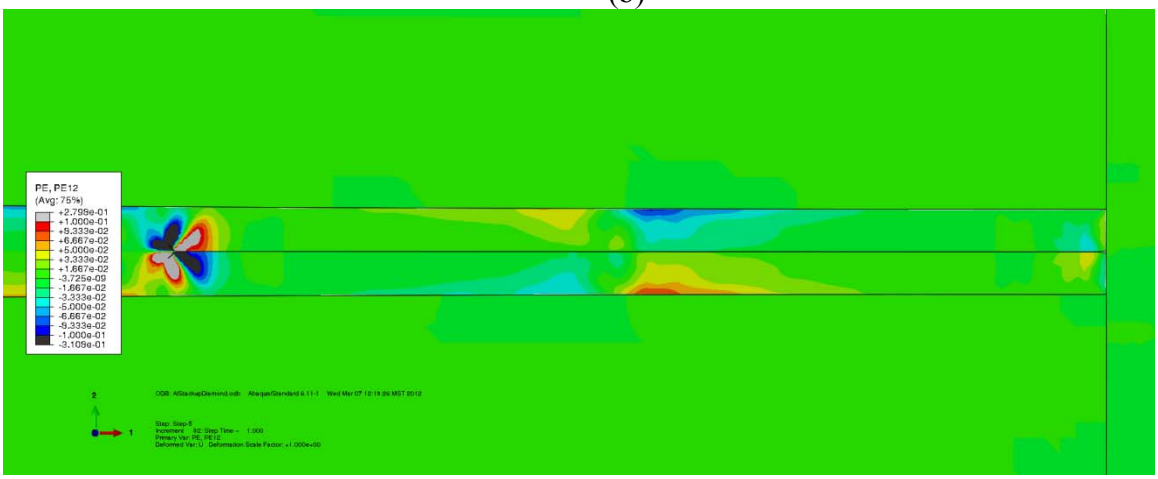

(c)

Figure A2.6. Case considering a triangular shape that touches at the apex of each triangle (a) shows a plan view of the entire plate geometry, (b) shows enlarged view of the displacement profile at the ends of the plates after loading and (c) shows an enlarged view of the equivalent plastic shear strain profile at the ends of the plates after loading. (b) shows that the triangular profile does create displacements in opposite directions for the cladding bonding surfaces (c) shows asymmetric shear strains forming during loading of the fuel assembly.

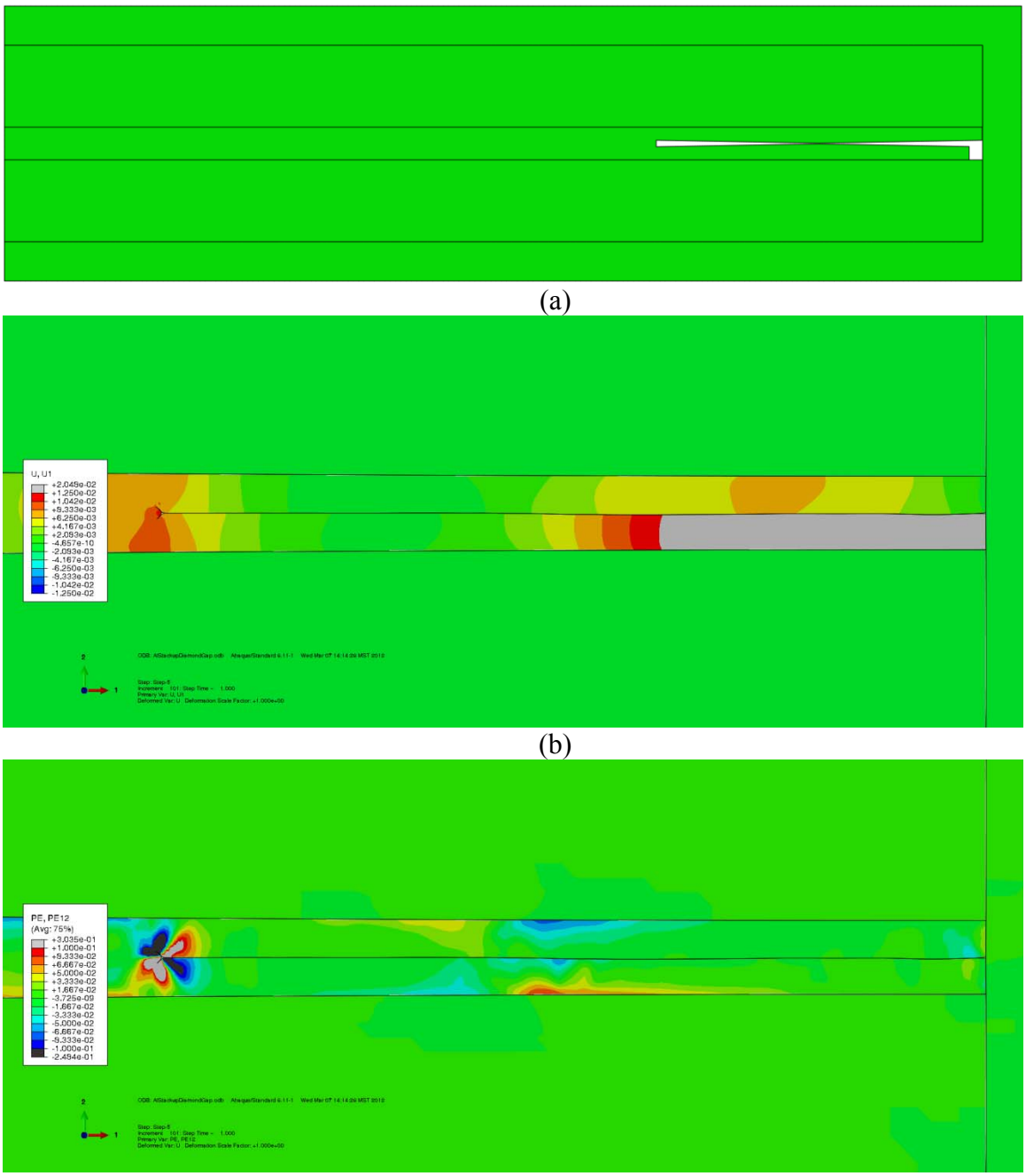

Figure A2.7. Case considering a triangular shape that touches at the apex of each triangle with an additional gap on the end of the bottom cladding (a) shows a plan view of the entire plate geometry, (b) shows enlarged view of the displacement profile at the ends of the plates after loading and (c) shows an enlarged view of the equivalent plastic shear strain profile at the ends of the plates after loading. (b) shows that the triangular profile does create displacements in opposite directions and the additional gap on the bottom plate increases the displacements for the cladding bonding surfaces (c) shows asymmetric shear strains forming during loading of the fuel assembly.

A2.3. Refinements of practical designs

After performing the studies shown by figures A2.1-A2.7 and considering the practicality of machining the types of profiles considered, we determined that the most effective geometries to consider in the experimental study should simply have grooves machined in the plates creating a step on the bottom plate with a gap on the fuel and HIP can side for material flow. The following discussion considers four geometries we designed via modeling for the aluminum grain penetration experimental study.

Figure A2.8. shows the shear plastic strain (PE12) and displacement contours (U1) for a HIP can containing two cladding geometries. The first geometry is a flat top plate and a bottom plate with a 0.1″ groove at the fuel interface and at the HIP can wall. The second geometry is simply two flat plates to serve as a baseline geometry.

Figure A2.9 shows the plastic shear strain and displacement contours for the case without a step between the plates. The displacement contours show that most of the displacement is in the same direction and will not produce much lateral sliding of the bonding faces against one another. Also, the plastic strain contours show a small gradient.

Figure A2.10 displays the plastic shear strain and displacement contours for the case considering a step with 0.1″ gap on either end between the plates. As can be seen in the contours, the plastic shear strain is much larger in this case with more variation. In addition, the displacement arrows show that some of the displacements of the top and bottom bonding surfaces are in opposite directions.

Figure A2.11 shows the plastic shear strain (PE12) and displacement contours for the entire model for a second HIP can simulation considering a flat plate and a plate with 0.05″ grooves at the fuel and can interface as well as flat plate with a plate with 0.02″ grooves a the fuel and can interface.

Figure A2.12 shows the plastic shear strain and displacement contours for the case with a 0.05″ groove machined in the bottom plate. The displacement contours show some reversal of the displacement direction, but less variation than the case considering a 0.1″ gap. The shear plastic strain contours also show some gradient, but again it is smaller than the case considering a 0.1″ gap.

Figure A2.13 shows the plastic shear strain and displacement contours for the case with a 0.02″ groove machined in the bottom plate. The displacement contours show some reversal of the displacement direction, but less variation than the case considering a 0.1″ gap. The shear plastic strain contours also show some gradient, but again it is smaller than the case considering a 0.1″ gap.

To further compare each geometry shown in figures A2.8 and A2.11, the final displacements from the nodes along the bond line were extracted. The difference in displacement for each set of initially adjacent nodes was calculated by subtracting the final displacement of the bottom node from the top node. This gives a measure of how much the nodes moved relative to one another. Figure A2.14 shows the relative displacement for every node along the initial bond line as a

function of their initial horizontal position. In the cases where a groove was machined into the plate, only the displacements along where the top of the step contacts the upper plate were calculated.

Figure A2.14 suggests that the cases with a larger gap will provide better lateral displacement of the bonding surfaces relative to one another. It is recommended that the cases considering no step, a step with 0.1″ gaps on either end, and a step with 0.05″ gaps on either end be considered in the experimental trials. It should be noted however that part of the displacements shown for the case without a step and the case with a gap of 0.1″ on either end are due to the fact that the plate without a step created a large volume of unfilled space in the HIP can. Because of this, the entire assembly deflects downward to fill the space as the gap closes.

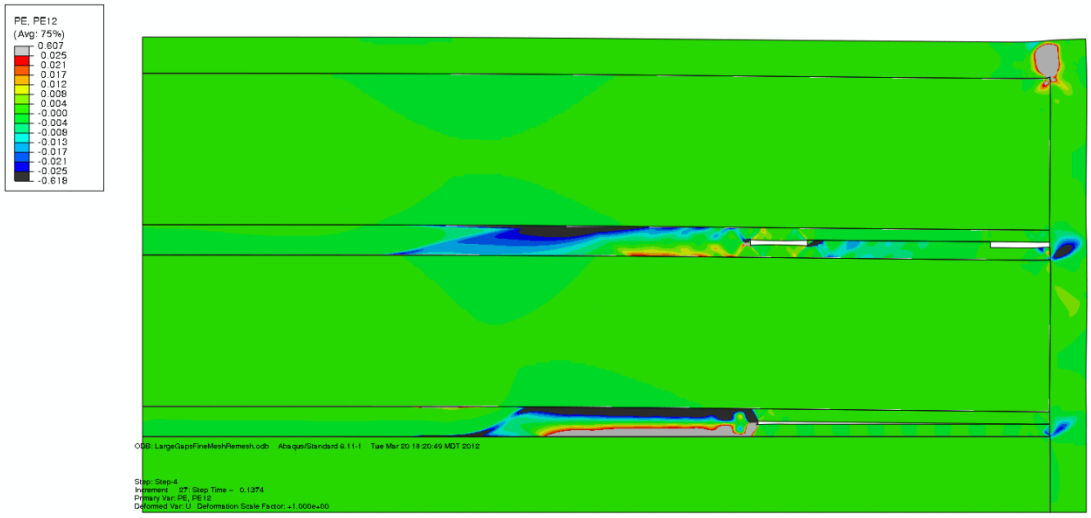

(a)

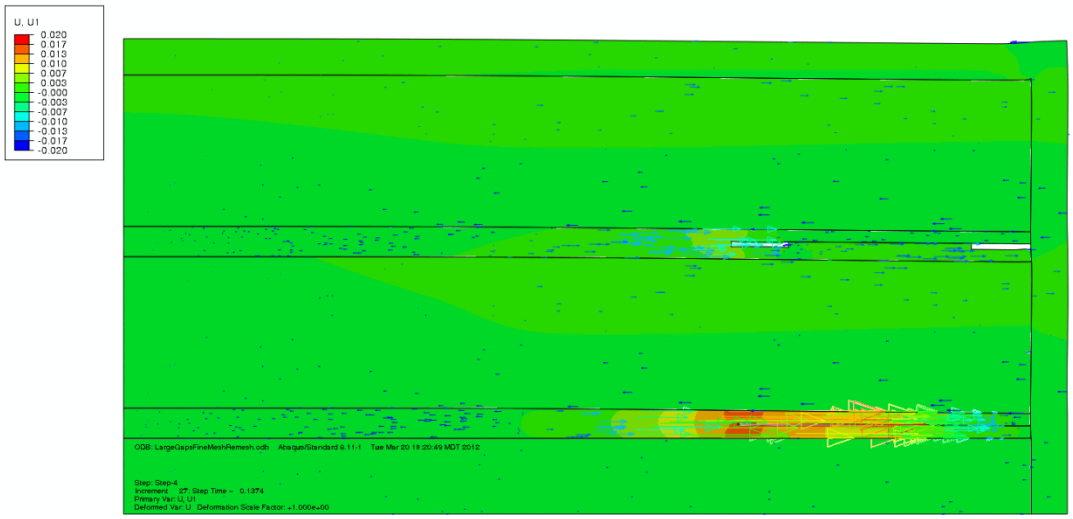

(b)

Figure A2.8. (a) Shear strain (PE12) and (b) displacement (U1) contours for a HIP can containing cladding with a top flat plate and a bottom plate with 0.1″ grooves machined at the fuel and HIP can interfaces (top) and two flat plates to serve as a baseline case (bottom). The arrows in (b) indicate the magnitude and direction of the displacements in the horizontal direction (U1).

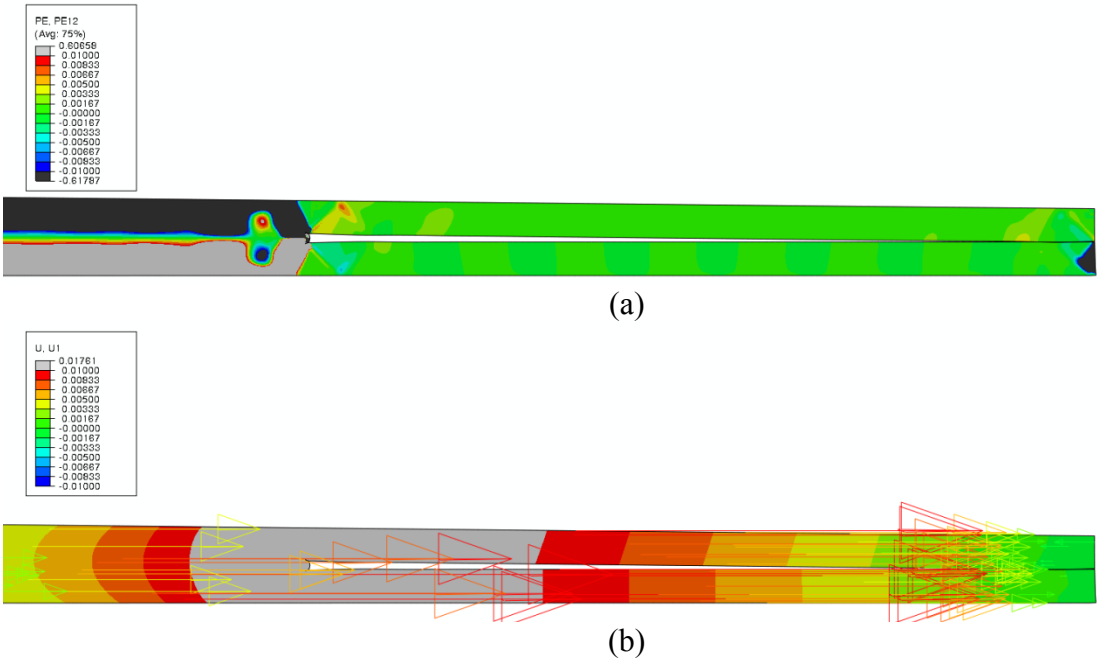

Figure A2.9. (a) Shear plastic strain (PE12) and (b) horizontal displacement (U1) contours for bonding area of flat plate. The shear strain shows little variation and the displacements are all towards the HIP can wall indicating that little lateral displacement is expected between the bonding surfaces.

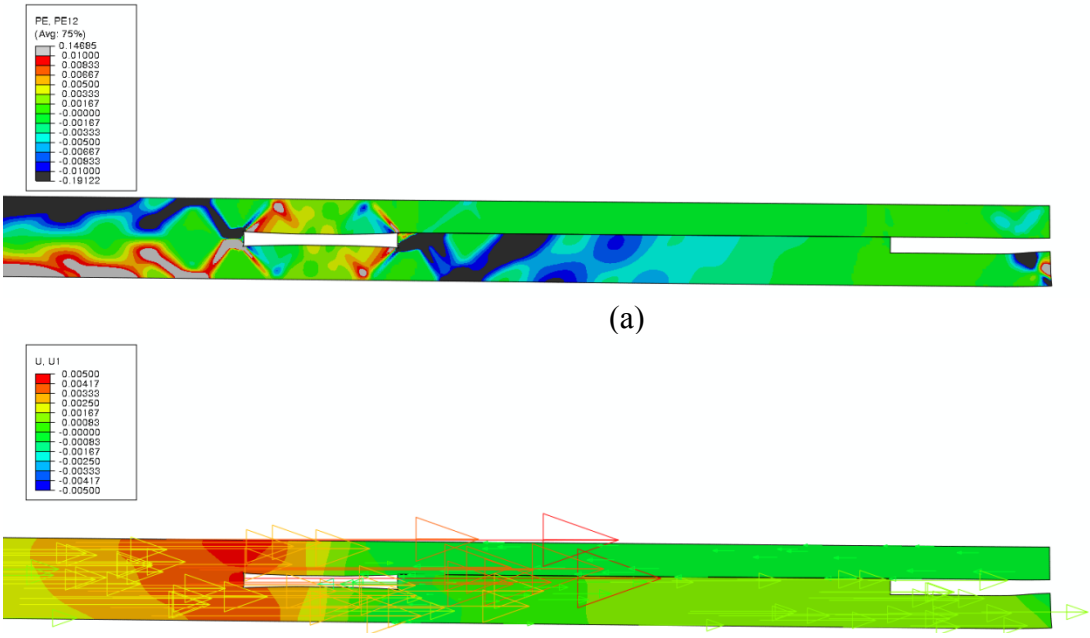

Figure A2.10. (a) Shear plastic strain (PE12) and (b) horizontal displacement (U1) contours for bonding area of flat plate and plate with 0.1″ gap at fuel and can interface. The shear strain in this case shows a considerable gradient and while displacements are mainly towards the can wall, some displacements have reversed directions, creating sliding along the bond line.

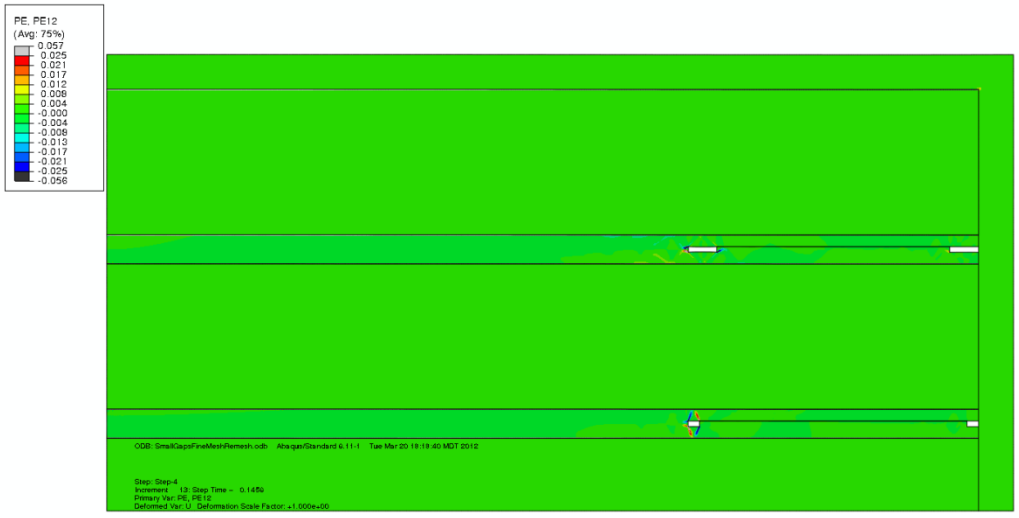

(a)

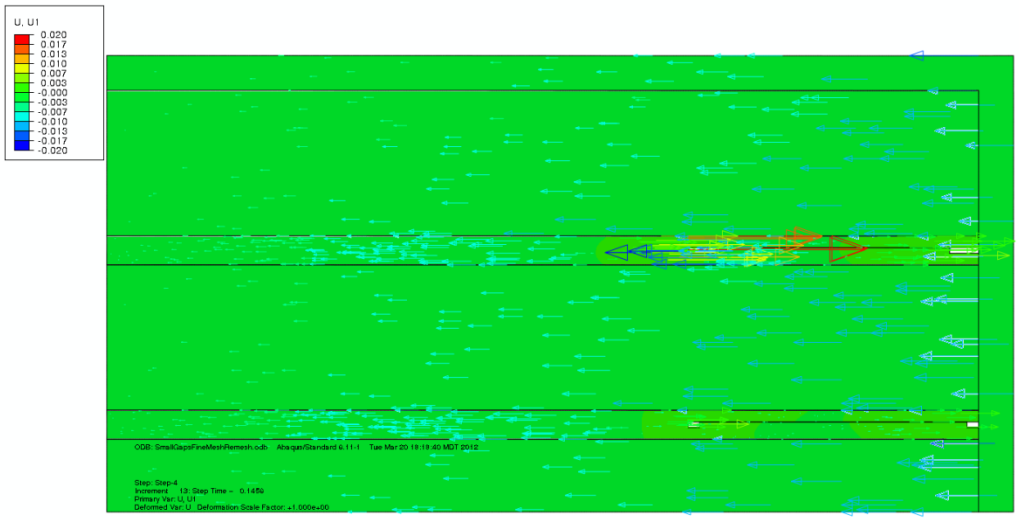

(b)

Figure A2.11. (a) Shear strain (PE12) and (b) displacement (U1) contours for a HIP can containing cladding with a top flat plate and a bottom plate with 0.05″ grooves machined at the fuel and HIP can interfaces (top) and a flat plate mated to a bottom plate with 0.02″ grooves at the fuel and can interfaces (bottom). The arrows in (b) indicate the magnitude and direction of the displacements in the horizontal direction (U1).

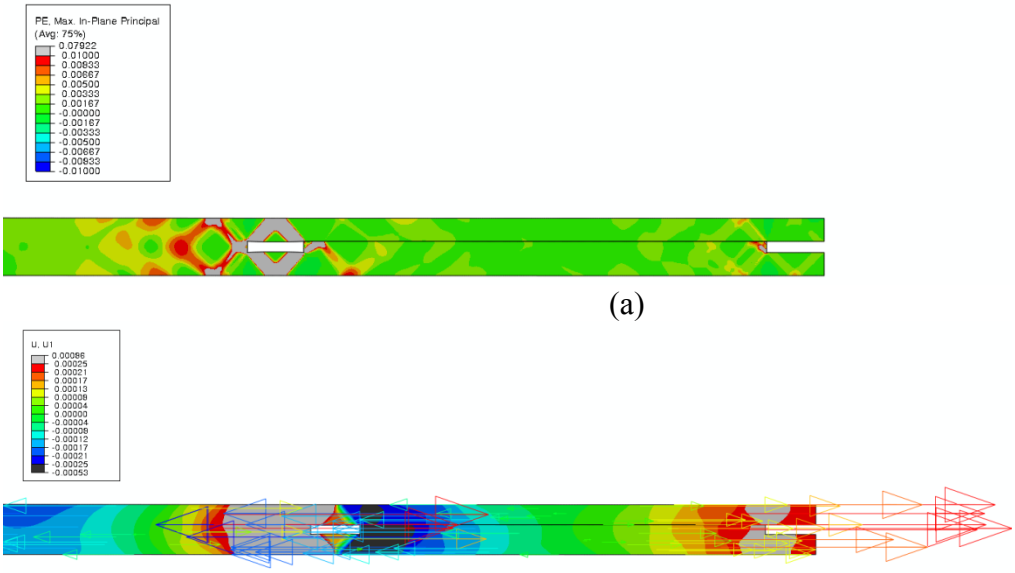

Figure A2.12. (a) Shear plastic strain (PE12) and (b) horizontal displacement (U1) contours for bonding area of flat plate. The displacement reversal is less than the case considering a 0.1″ gap at the fuel and can interface. In addition, the shear plastic strain gradients are smaller.

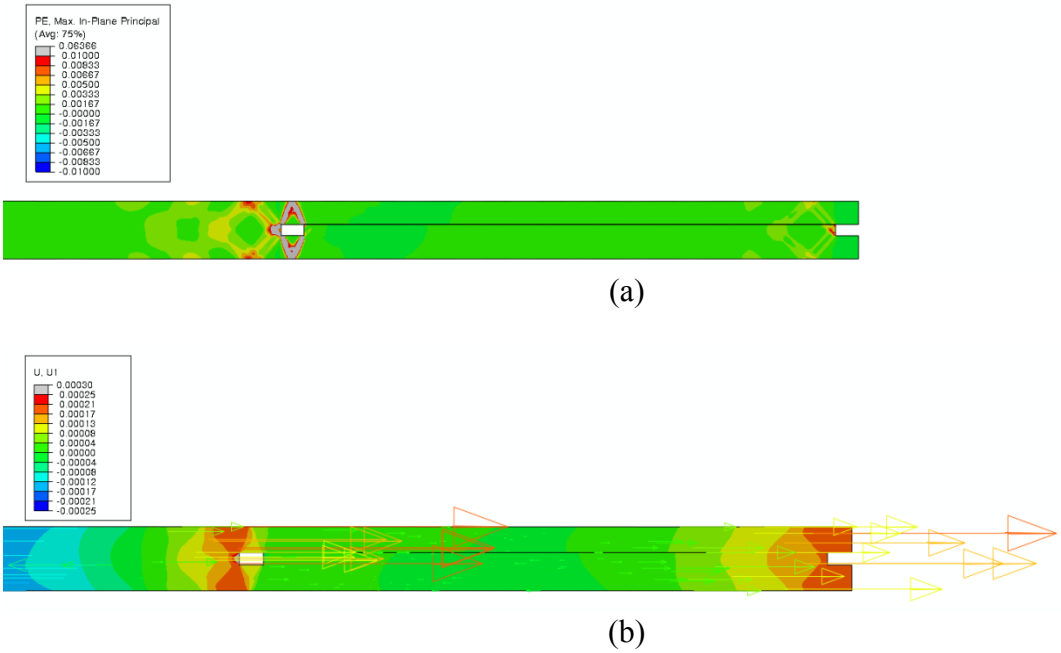

Figure A2.13. (a) Shear plastic strain (PE12) and (b) horizontal displacement (U1) contours for bonding area of flat plate. The displacement reversal is less than the case considering a 0.1″ gap at the fuel and can interface. In addition, the shear plastic strain gradients are smaller.

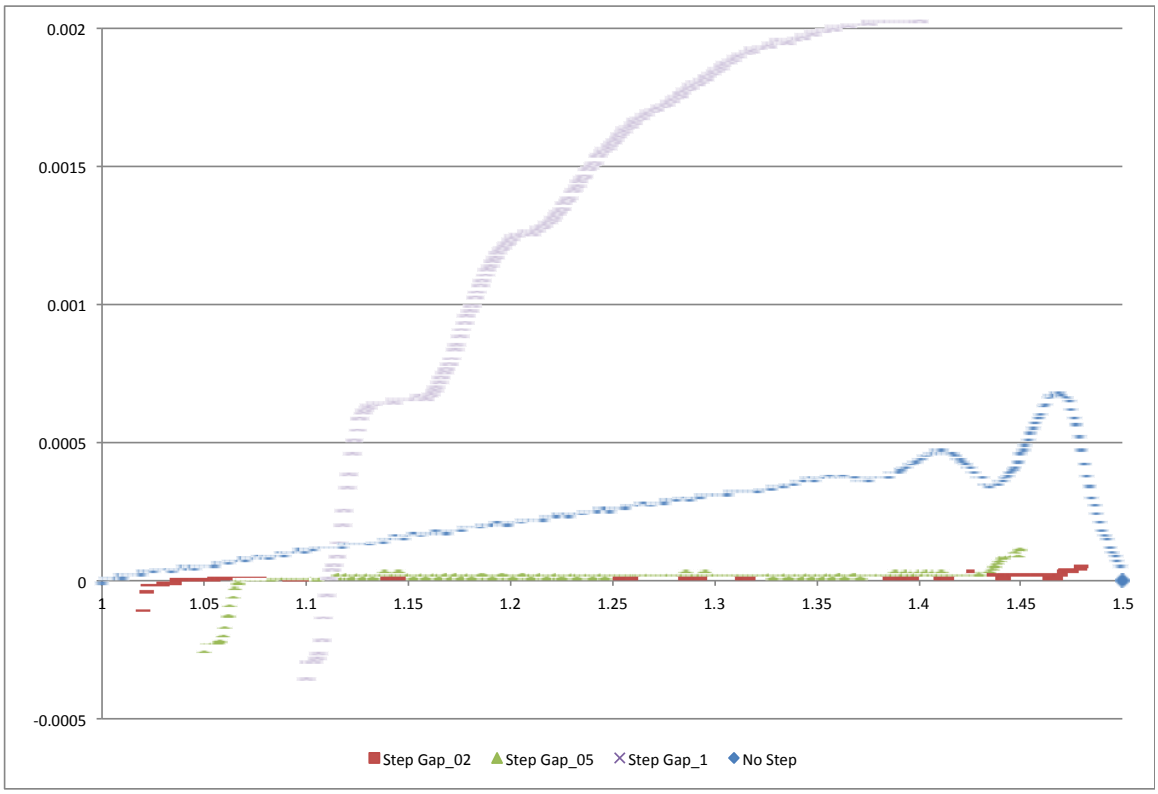

Figure A2.14. Relative displacements of initially adjacent nodes after loading. The case considering grooves of 0.1″ provides the most lateral displacement between the bonding surfaces.